Systematic Examination of the Impact of Pre-Stimulus Alpha-Mu and Gamma Band Oscillations on Perception: Correlative and Causal Manipulation in Mouse and Human

By

Dominique L. Pritchett

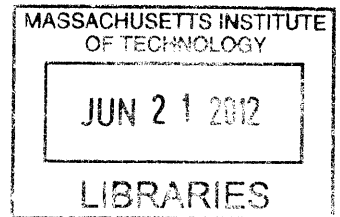B.S. - Chemistry, Virginia State University, 2002

Submitted to the Department of Brain & Cognitive Sciences in Partial Fulfillment of the Requirements for the Degree of
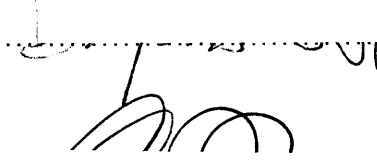
DOCTOR OF PHILOSOPHY IN NEUROSCIENCE AT THE MASSACHUSETTS INSTITUTE OF TECHNOLOGY

JUNE 2012
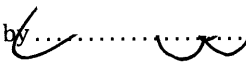
Author...

Department of Brain & Cognitive Sciences

April 26, 2012

Certified by... ....

Christopher I. Moore

Associate Professor of Neuroscience, Brown University

Thesis Supervisor

Accepted by...

Earl K. Miller

Picower Professor of Neuroscience

Director, Department of Brain & Cognitive Sciences Graduate Program

Systematic Examination of the Impact of Pre-Stimulus Alpha-Mu and Gamma Band Oscillations on Perception: Correlative and Causal Manipulation in Mouse and Human

By

Dominique L. Pritchett

ABSTRACT

The over-arching hypothesis that drives my work is that neural dynamics, fluctuating on millisecond to second time scales, powerfully impact perception. In this thesis, I employ correlative electrophysiological recording methods and causal optogenetic control of neural circuits to systematically test the importance of dynamics in the expression of pre-stimulus oscillations on perception. Specifically, I test the prediction that alpha oscillations expressed in a given sensory representation within a neocortical map predict diminished sensory capability in that region of sensory space, while gamma oscillations predict enhanced capacity. My model system throughout is primary somatosensory neocortex and tactile perception: I combine studies from human and mouse to benefit from the relative merits of each preparation.

Several prior studies support this more generally stated view of oscillatory dynamics— alpha predicting diminished and gamma predicting enhanced perceptual capacity. However, there is significant disagreement on even this broad assumption. Leading researchers have argued that alpha in fact predicts enhanced detection of tactile stimuli (e.g., Nicolelis and Fanselow, 2002). Further, there remains significant discord over whether gamma oscillations predict enhanced ability and, even if they do so, whether their expression is a causal contributor to this increased capacity or whether gamma is an epiphenomenal by-product of other beneficial shifts in neural dynamics. My thesis directly addresses these basic questions as to the predictive value of these oscillations, and favors the view that alpha and gamma are in general predictive of perception as stated. Further, I provide unique causal data showing that, under the conditions of our experiments, entrainment of a realistic and local gamma oscillation in neocortex can enhance stimulus detection.

I also address important questions as to the independence of different frequency bands expressed in pre-stimulus oscillatory dynamics. Specifically, in contrast to prior reports, I provide evidence in humans and mouse that alpha and beta are unique in their expression

and do not occur as a single coincident "mu" rhythm. I also provide direct evidence against the simplistic view—which has also been recently postulated—that alpha and gamma rhythms are inherently opposed in their expression (e.g., that increase in one is necessarily coincident with decrease in the other). Perhaps most importantly, while my data support the general view that alpha and gamma have opposing impacts on perception, I also show that there are more complex interactions between alpha and gamma in predicting perceptual success, suggesting that a simplistic view of each frequency as a 'state' is inappropriate, and that these oscillations are independent in their expression and potentially in their allocation to optimize perception, e.g., with selective attention.

Our MEG results support the hypothesis that the alpha band oscillation is negatively correlated with perception. Further, using LFP in the mouse we observe that this alpha oscillation is a disengaging rhythm in rodents as well, contrary to prior work in barrel cortex in rats. More, we show that increased gamma power is correlated with perception of a liminal tactile stimulus. Then using optogenetic control of the fast-spiking interneurons, we causally entrain a gamma oscillation to show enhancement of perception.

Thesis Supervisor: Christopher I. Moore

Title: Associate Professor of Neuroscience

Acknowledgements

Lastly, and most significantly, I would like to thank my wife, my love Tracy. Thanks for putting up with my irrational fits, and for loving me unconditionally. It was with your support I have made it through this process.

Table of Contents

Chapter 1

Introduction: Oscillations, of Mice and Humans

1.1 Outline of Thesis Work

My primary interest is in behavior—how neural circuits create action and perception. Building on my prior studies in monkey physiology when I was being introduced to neuroscience at the NIH, the goal of my thesis work has been to develop expertise at two other complimentary levels: In the human, which is my greatest interest and is the most clinically relevant preparation, and in the mouse, which is a particularly favorable model for studying the mammal because of the genetic control it allows. As described in **Chapter 2**, I obtained extensive training in human physiology (magnetoencephalography, MEG) and psychophysics in my thesis research. My focus, however, has been on rodent behavior and neurophysiology. I developed the head-posted behavioral preparation in the Moore laboratory, and later integrated chronic neurophysiology and optogenetic control in this preparation.

The over-arching hypothesis that drives my work is that neural dynamics, fluctuating on millisecond to second time scales, powerfully impacts perception. My initial interest was in attention: My participation in the human selective attention studies described in **Chapter 2** reflects this interest. To directly parallel that work, I developed a nearly identical rat preparation that required selective allocation of attention to one vibrissa versus another (Pritchett and Moore, SfN Abstracts, 2008; data not described here). However, when mouse optogenetic control became available, I adapted my rig to this work and employed a simpler detection task, and completed the studies described in **Chapters 3** and **4**.

In this **Introduction**, I first discuss my primary model system, rodent "barrel" neocortex, and prior studies of its frequency-dependent dynamics. I then discuss alpha and gamma oscillations and the existing debate regarding their roles in perception, and briefly discuss theories that have proposed necessary cross-frequency coupling, a topic my thesis research has significant bearing on.

1.2 Barrel Cortex: Advantages as a Model for Perceptually-Related Cortical Dynamics

The barrel system is an ideal model to investigate circuit-level mechanisms of cortical dynamics, as this system provides anatomical identification of columnar position, has high acuity for detection, frequency-dependent dynamics are robust, and many of the synaptic mechanisms underlying these dynamics have been identified.

Woosley and van der Loos ('70) discovered that there is a one-to-one correspondence between vibrissae in the periphery and clusters of neurons and neuropil in layer IV of primary somatosensory cortex (SI) in rodent ('barrels'). This anatomical representation

demarcates the center and peak of the sensory-evoked point-spread function (Simons and Carvell 89, Armstrong-James et al. 92). As a first advantage, then, barrels provide a rare opportunity for spatial map registration of a functional column with a fixed anatomy.

The vibrissa sensory system is also useful because it demonstrates high perceptual acuity. With regards to feature or input detection, the focus of my studies, freely-behaving rodents show exceptional sensitivity in detecting rough versus smooth surfaces (Carvell and Simons 90, Carvell and Simons 95). Further, the head-posted rat can detect discrete vibrissa deflections (Weist and Nicolelis 03, Stüttgen et al. 06). At amplitudes of motion < 1-3 degrees, a vibrissa stimulus can be detected at velocities above 750 degrees per second in this preparation. Above this amplitude, threshold velocities can be as low as 125 degrees per second (Stuttgen et al. 06).

Perhaps most important for my thesis, the barrel cortex also shows well-documented frequency-dependent dynamics. Vibrissa stimulation at frequencies above ~3 Hz leads to decreased gain of sensory responses in layer IV (Moore et al. 99, Moore 04, Simons 78, Castro-Alanmoncos 02, Castro-Alanmancos and Oldford 02, Katri and Simons 06, Chung et al. 02, Sheth et al. 99, Garabendian et al. 03). These findings from anesthetized animals are consistent with reports from awake animals during whisking and whisker twitching. During these behaviors, there is enhanced power in the alpha frequency range in SI, and suppressed sensory responses (Fanselow and Nicolelis 02, Chrochet and Pettersen 06).

This sensory-evoked, frequency-dependent suppression observed in barrel cortex is likely the product of a variety of mechanisms, a subset are listed here. First, adapting stimulation may cause sub-cortical suppression, leading to decreased transmission to SI (Higley and Contreras, 03, 05) Second, synaptic depression, reflecting a presynaptic depletion of neurotransmitter at the thalamocortical synapse, also likely decreases sensory gain (Castro-Alanmancos and Oldford 02, Chung et al. 02). Third, we have recently developed computational models showing that alpha rate thalamic bursting should prove an ideal stimulus for recruiting otherwise less active somatostatin-positive interneurons (Vierling-Classen et al., 2010). We further showed in that modeling that the impact of these dendrite targeting interneurons is to enhance lower frequency (alpha and beta range) oscillations.

These suppressive dynamics expressed in the barrel cortex suggest that one mechanism through which response gain can be modulated is by regulation of the frequency of activity in thalamocortical input. Consistent with this view, Moore and colleagues (Moore et al. 99, Moore 04) have hypothesized that activity in the thalamocortical pathway at > 3 Hz that produces response suppression should also impair detection of sensory stimuli. In agreement, as reviewed in the next section, recent studies have shown alpha rhythm, an intrinsically generated rhythmic behavior in the thalamocortical pathway in this frequency range, blocks detection.

1.3 Alpha Rhythm: 7-14 Hz 'Internal' Oscillations and Perceptual Capability

Phenomenology and Physiology of Alpha

One frequency band that is modulated with attention is the 'alpha' band, which is variously defined as occurring between 5-15 Hz, and has been identified as a prominent 'mu' rhythm expressed in SI (Nicolelis and Fanselow 02; Crunelli 05; see Chapter 2 for a more extensive discussion of mu and its components). One prominent form of alpha requires thalamocortical activity: Thalamic activity in this band is correlated with the cortical expression of alpha, and lesions in the thalamus suppress expression of alpha, reviewed in (Crunelli 05). Intracortical mechanisms may also contribute to alpha production, in part potentially through rhythmic corticothalamic drive (Jones et al. 00; Silva et al. 91; Castaro-Alanmancos and Connors 96).

Impact of Alpha on Detection

Alpha expression in humans typically shows an inverse correlation with detection, with increases in alpha predicting decreased detection probability. Schubert et al. (2009) found a linear relationship between alpha and beta amplitudes in EEG electrodes over SI and tactile detection probability. These results are consistent with the relationship between smaller alpha amplitudes and increased perception and decreased reaction times in the visual system (Thut et al., 2006; Hanslmayr et al., 2007; van Dijk et al., 2008; Kelly et al., 2009). Other studies in the somatosensory (Linkenkaer-Hansen et al., 2004; Zhang and Ding, 2010) and visual (Rajagovindan and Ding, 2010) systems have reported a mostly linear relationship between alpha power and detection probabilities, but with a decreased efficacy of detection at the highest alpha levels.

Spatial Distribution of Alpha During Task Performance Supports a Suppressive Role for this Dynamic

Initial theories of alpha suggested that high alpha power represented a 'drowsy' or sleep-like state (Crunelli 05). More recent research suggests that variations in alpha do not inherently represent a general 'turning off' of cognitive ability, but rather can reflect the selective suppression of activity in specific brain representations. For example, alpha in visual cortex increases as a subject has to remember a greater number of items in working memory (Jensen 02). These findings suggest that neural mechanisms that enhance alpha can also selectively decrease activity in a sensory modality (e.g., vision), allowing greater attention to be directed to other brain processes (e.g., working memory maintained in frontal cortex).

Recent studies have shown that alpha expression may be even more precise, providing a mechanism for regulating signal transmission within sub-regions of a sensory map (for an excellent recent review from originators of this hypothesis, please see Foxe 02, Jensen and

Mazaheri 2010). In tasks where subjects anticipated a stimulus in one of four quadrants of visual space, increases in alpha were seen over the representations in primary visual cortex of non-attended quadrants in which distractor stimuli were presented (Worden et al 02; Ergonoglu et al. 04). Similar findings have been reported with in monkey area V4 with local allocation of spatial attention (e.g., Fries et al., 2008) and a similar impact on motor initiation has been observed in sensorimotor cortex (Pfurtscheller et al. 97). In total, these findings suggest that neural mechanisms that enhance alpha oscillations can also block sensory input in non-attended representations, 'inactivating' cortical regions, and that this blockade is a key substrate for the selectivity of attention and not an indication of diminished behavioral state.

The Contrary Hypothesis: Enhanced Detection Capability with Alpha in Barrel Cortex

This line of reasoning regarding alpha is in direct contrast to arguments offered by Nicolelis and colleagues (Fanselow and Nicolelis 99; Nicolelis and Fanselow 02), who have emphasized that a brief period of enhanced excitability immediately precedes a burst, as the thalamic neuron is leaving its hyperpolarized state. These authors predict that this window provides a periodic enhancement in sensory transmission and hence detection:

> "As the oscillatory thalamic bursting activity provides periods of hypersensitivity to stimulation of the whiskers just before the burst onset, we propose that rats are primed during these periods to detect minute or slowly changing deflections of the whiskers better than during the quiet behavior when neither 7–12 Hz oscillations nor VPM bursting are present."

> -- Nicolelis and Fanselow, 2002

In support, these authors have shown that supramaximal deflection of several vibrissae can be detected during ongoing periods of alpha rhythmicity (Weist and Nicolelis 03). In contrast to this view, however, these same authors have shown net sensory suppression of the response to electrical shocks when animals are in a whisker twitching state (Fanselow and Nicolelis 99; Fanselow and Nicolelis 01), which they suggest is the period of greatest alpha prominence (Wiest and Nicolelis 03; Nicolelis and Fanselow 02).

1.4 Gamma Rhythm: 30Hz-80Hz 'Internal' Oscillations and Perceptual Capability

Gamma Oscillations: Evidence for Allocation with Attention

Extracellular electrophysiological techniques have revealed a second frequency band, the gamma band (30-80 Hz), that is believed by many to be causally involved in enhancement of perceptual ability. The experimental evidence in support of a role for gamma in *enhancing* perceptual capability comes almost entirely from studies of changes in the

allocation of this rhythm with shifts in attention in primate visual neocortex. A series of reports by Desimone, Fries and colleagues has shown enhanced phase locking of local multi-unit activity to gamma LFP in the representation of attended stimuli (e.g., Womelsdorf et al., 2006 and Fries et al., 2008), and increased pre-stimulus gamma LFP expression with attention (e.g., Fries et al., 2008).

Why Might Local Neocortical Gamma Enhance Perception?

The predominant hypothesis for generation of this local synchrony is from synchronous inhibition. A wealth of correlative (e.g., Buzsaki, 1983) and causal studies (e.g., Cardin et al., 2009) provide evidence that gamma oscillations are crucially dependent on the activity of fast-spiking (FS) interneurons. We have previously shown that driving Channelrhodopsin-2 activity in fast spiking interneurons generates increased power in the gamma band of the LFP. Further, this inhibition leads to a phasic suppression of spiking and phasic enhancement of spike timing (Cardin et al. 09, Cardin et al. 10, Carlen et al., 11, **Chapters 3** and **4**).

While specific models have variation in their precise predictions as to the role of FS in this process (see Tiesinga and Sejnowski, 2009, for a recent review), the rapid inhibitory post-synaptic potentials evoked by this cell class are believed to set the time constant for gamma at ~12-30 msec (~80 to 30 Hz). The synchronous inhibition generated by FS during gamma expression is believed to increase the synchronous firing of pyramidal neurons, thereby enhancing the downstream impact of activity in a given neocortical area (see Knoblich, Siegle, Pritchett and Moore, 2010 for a discussion and computational modeling in support of this basic presumption). In the case of stimulus driven synchrony, input (in layer 4 the input would be thalamic) stimulates both excitatory and inhibitory neurons. Then the large di-synaptic inhibition silences the local activity. The duration of this inhibition is controlled by the time constant of GABA A receptors, ~25ms (40Hz), and the release of this inhibition allows for increased excitatory activity. This then leads to a rebound inhibition. This is known as the PING model of gamma (Pyramidal-INterneuron Gamma) (Börgers et al. 08).

The hypothesis for gamma enhancement, in addition to external stimulus driven enhancement, is that internal activity, either from a top-down source or via from neuromodulation (e.g. ACh), would selectively enhance inhibition. This inhibition would then entrain the excitatory activity similar to the method above. This is known as the ING model of gamma (INterneuron Gamma) (Börgers et al. 08).

In either model of gamma enhancement, gamma allows for multiple "windows of opportunity" (Knoblich et al. 10) that are the only permissive periods in which spiking can occur. This limited window—during the period when inhibition has worn off--enforces

synchrony. More synchronous firing should lead to gain in the downstream areas due to the time course of synaptic integration and decreased effect from feed forward inhibition (Knoblich et al. 10).

Contrasting Views and Some of the Open Questions Regarding Gamma Oscillations

Recent studies in primary visual neocortex of the primate have challenged the view that gamma oscillations are a general neocortical dynamic that predicts and/or contributes to enhanced perceptual processing. Specifically, Ray and Maunsell (2010) have found that the frequency of gamma expression is dependent on the relative contrast of a given stimulus, and that different gamma oscillations can be expressed in neighboring columns in response to the same stimulus, leading these authors to argue against a role for gamma in "binding" the percept of stimuli. Similar arguments against a "clocking" function for gamma have recently been offered based on primate V1 data from Burns et al. (2011). Most important for the studies conducted here, Chalk et al. (2010) have found that allocation of attention *reduces* gamma LFP expression and spike-field coherence in the corresponding representation in monkey V1, and suggest that gamma modulation in this area is a "byproduct" of other attentional mechanisms and not a causal contributor to perceptual ability. In aggregate, these studies suggest that gamma allocation is not what is driving enhanced perceptual capability outside of higher visual neocortex.

To our knowledge only one study has examined expression of gamma in the barrel cortex of behaving rodents (Hamada et al., 1999). These authors found that gamma expression predicted subsequent onset of exploratory whisking, in apparent agreement with the more general view that this oscillation indicates the allocation of sensory attentional processes (which are also indicated by exploratory whisking). As described above, we found that, while natural gamma expression is under-explored in barrel cortex, gamma can be readily induced in this structure by optogenetic means (Cardin et al. 09, Cardin et al., 10, Carlen et al., 11, **Chapters 3** and **4**).

1.5 Are Distinct Frequency Bands Inherently Coupled in Neocortex?

A theme addressed in a few different ways in my thesis is whether distinct frequency bands are inherently coupled. While at first glance this idea appears wrong, several major theories have proposed precisely such a relationship. My thesis work directly addresses two of these views, described in the next few paragraphs.

Are Gamma and Alpha Intrinsically Opposed Oscillations

"This led us to propose that an increase in alpha activity is a consequence of an increase in the magnitude of inhibitory bouts, which serve to break the ongoing gamma activity. While it remains to be tested, it is possible that rhythmic GABAergic input from the interneuronal

network is a key mechanism for producing the pulsed inhibition. The stronger the alpha activity, the shorter the "duty-cycle" of gamma activity **(Figure 4)**. By this principle the alpha activity can provide graded inhibition by blocking the ongoing gamma activity in a phasic manner: If the alpha activity is strong, the time-window of processing is short (the duty-cycle). As alpha activ- ity decreases in magnitude, the time-windows become longer."

--   Jensen and Mazaheri 2010

Jensen and Mazaheri (2010) are two key leaders in the use of electrencephalography to define oscillatory states, having been, for example, leading proponents of the view that alpha can be flexibly applied to enhance attentional focus (please see above). As indicated by this quote, they have recently argued that alpha and gamma are inherently tied to one another in an inverse fashion. My data, primarily from **Chapter 3**, strongly argues against this idea.

Alpha-Beta as a Necessarily Coupled 'Mu" Rhythm

The mu rhythm measured with magnetoencephalography (MEG) over Rolandic cortex shows alpha and beta components (Hari and Salmelin 1997; Tiihonen et al. 1989). This finding is in contrast to the Rolandic mu rhythm measured with electroencephalography (EEG), in which only a dominant alpha component is typically observed (Kuhlman 1978; Zhang and Ding 2009). This historical distinction is likely attributable to differences in the recording techniques and has led to mixed usage of the term "mu" in the literature. This ambiguity in naming is indicative of the ongoing ambiguity with respect to the statistical characteristics and neural origins of the mu rhythm. Despite the fact that much research has been devoted to localizing the source of this rhythm in the brain—and to understanding the cellular-level neural mechanisms creating alpha and beta rhythms independently—the neural origin of the MEG mu complex remains unknown.

One prominent view of the origin of the MEG mu rhythm, based on source localization of sensor data from human studies, is that the mu-beta component is produced by the precentral motor cortex, whereas the mu-alpha component originates from the postcentral somatosensory cortex (Hari and Salmelin 1997; Salmelin and Hari 1994; Salmelin et al. 1995). These studies focused on localizing late event-related desynchronization (ERD) of the rhythm after movement. More recent work, focused on spontaneous activity and early ERD, has shown that both components can be expressed in a single area (Brovelli et al. 2004; Gaetz and Cheyne 2006; Kopell et al. 2000; Pinto et al. 2003; Szurhaj et al. 2003), with intracerebral recordings in humans suggesting a common source in primary somatosensory (SI) cortex (Szurhaj et al. 2003). Studies that have investigated the cellular-level neural mechanisms inducing ongoing cortical alpha and beta rhythms have focused on the origin of the two frequency bands separately. A large body of experimental and computational work suggests neocortical alpha emerges from an approximately 10-Hz

thalamocortical rhythm (Andersen and Andersson 1968; Contreras and Steriade 1995; Hughes and Crunelli 2005; Suffczynski et al. 2001; Traub et al. 2005). Other evidence suggests that neocortical alpha also depends on, or could emerge independently from, intrinsic properties in large layer V pyramidal neurons (Bollimunta et al. 2008; Jones et al. 2000; Pinto et al. 2003; Silva et al. 1991) and/or the local activity of low-threshold spiking interneurons (Fanselow et al. 2008).

Fewer studies of the neural origins of the cortical beta rhythm have been conducted. Slice recordings (Roopun et al. 2006; Whittington et al. 2000) and computational models (Jensen et al. 2002; Kopell et al. 2000; Pinto et al. 2003; Roopun et al. 2006) have shown a beta-frequency range oscillation in isolated cortex that depends on the kinetics of the M-type potassium current in excitatory neurons, combined with GABAergic inhibition. Roopun et al. (2006) further found that axonal gap junctions were critical to the maintenance of pharmacologically induced 20- to 30-Hz rhythms in slices from somatosensory cortex (referred to as a "beta 2" rhythm) and that lower-frequency beta rhythms (13–17 Hz; "beta 1") could be produced by period concatenation of higher-frequency beta (20–30 Hz) and gamma (30–50 Hz) oscillations (Kramer et al. 2008; Roopun et al. 2008). In all of these studies, the beta rhythm is argued to emerge from the activity of localized cells in a single cortical circuit that are spiking nearly synchronously and that the frequency of these rhythms depends on intrinsic membrane time constants.

Another body of research has suggested that beta activity mediates long-range communication between cortical areas, suggesting that intracortical projections may play a role in local beta expression (Buschman and Miller 2007; Hanslmayr et al. 2007; Roelfsema et al. 1997; Schubert et al. 2008; von Stein et al. 2000; Witham et al. 2007). For example, Von Stein et al. (2000) found coherence in beta-band activity between temporal and parietal EEG sensors during multimodel object representation in humans, and Buschman and Miller (2007) between parietal and frontal indwelling electrodes during selective attention in monkeys. In support for a role of interareal projections in the neocortex, Whitham et al. (2007) found interactions between 20-Hz activity in somatosensory and motor areas that did not depend on intrinsic spiking (Witham and Baker 2007) and claimed there was oscillatory coupling across the central sulcus. Brovelli et al. (2004) applied Granger causality analysis to 20-Hz oscillatory activity measured intracranially from multiple cortical sites in the monkey and claimed that the beta activity propagated from the primary somatosensory (SI) cortex to primary motor and parietal cortices. Nonlemniscal thalamic nuclei have also been proposed as relays for signal transmission between neocortical areas (Sherman 2005). Such thalamic nuclei are also ideally poised to generate oscillatory coherence across multiple cortical areas (Llinas and Ribary 2001). As such, beta activity related to long-range communication could also arise, at least in part, from these projections. Difficulty establishing the neural mechanisms generating the MEG

mu rhythm comes in part from the fact that the shared temporal dynamics of the mu-alpha and mu-beta components are not well characterized. Tiihonen et al. (1989) observed qualitatively that the mu-alpha and mu-beta components do not always overlap in time, suggesting they are not harmonics, but did not quantify this assertion (Palva et al. 2005b; Tiihonen et al. 1989). Evidence for cross-frequency coupling of these components has also been reported (Palva et al. 2005b). Quantifying the degree to which mu-alpha and mu-beta co-occur and co-vary in amplitude is crucial to understanding their relative interdependence and to constraining computational models of their origins. In **Chapter 2**, I provide evidence showing that while these two oscillations do co-vary at rates significantly above chance, they are independent in their expression and do not inherently co-occur.

1.6 References

Agmon, A. and B.W. Connors, Correlation between intrinsic firing patterns and thalamocortical synaptic responses of neurons in mouse barrel cortex. J Neurosci, 1992. 12(1): p. 319-29.

Andermann, M.L. and C.I. Moore, A somatotopic map of vibrissa motion direction within a barrel column. Nat Neurosci, 2006. 9(4): p. 543-51.

Andermann, M.L., et al., Neural correlates of vibrissa resonance; band-pass and somatotopic representation of high-frequency stimuli. Neuron, 2004. 42(3): p. 451-63.

Armstrong-James, M., K. Fox, and A. Das-Gupta, Flow of excitation within rat barrel cortex on striking a single vibrissa. J Neurophysiol, 1992. 68(4): p. 1345-58.

Börgers C, S. Epstein, N.J. Kopell. Gamma oscillations mediate stimulus competition and attentional selection in a cortical network model. Proc Natl Acad Sci U S A. 2008 Nov 18;105(46):18023-8.

Brecht, M. Barrell Cortex Spikes: Quantification and Psychophysics. in Computational and Systems Neuroscience (CoSyNe). 2007. Salt Lake City, UT.

Britten, K.H., M.N. Shadlen, W.T. Newsome and J.A. Movshon, Responses of neurons in macaque MT to stochastic motion signals. Vis. Neurosci., 10 (1993), pp. 1157–1169.

Buszaki G. Rhythms of the Brain. Oxford Press 2006.

Cardin J.A., M. Carlén, K. Meletis, U. Knoblich, F. Zhang, K. Deisseroth, L.H. Tsai, C.I. Moore. Driving fast-spiking cells induces gamma rhythm and controls sensory responses. Nature. 2009 Jun 4;459(7247):663-7.

Carvell, G.E. and D.J. Simons, Biometric analyses of vibrissal tactile discrimination in the rat. J Neurosci, 1990. 10(8): p. 2638-48.

Carvell, G.E. and D.J. Simons, Biometric analyses of vibrissal tactile discrimination in the rat. J. Neurosci., 10 (1990), pp. 2638–2648.

Carvell, G.E. and D.J. Simons, Task- and Subject-Related Differences in Sensorimotor Behavior during Active Touch. Somatosensory and Motor Research, 1995. 12(1): p. 1-9.

Castro-Alamancos, M.A. and B.W. Connors, Short-term synaptic enhancement and long-term potentiation in neocortex. Proc Natl Acad Sci U S A, 1996. 93(3): p. 1335-9.

Castro-Alamancos, M.A. and E. Oldford, Cortical sensory suppression during arousal is due to the activity-dependent depression of thalamocortical synapses. J Physiol, 2002. 541(Pt 1): p. 319-31.

Castro-Alamancos, M.A., Different temporal processing of sensory inputs in the rat thalamus during quiescent and information processing states in vivo. J Physiol, 2002. 539(Pt 2): p. 567-78.

Chung, S., X. Li, and S.B. Nelson, Short-term depression at thalamocortical synapses contributes to rapid adaptation of cortical sensory responses in vivo. Neuron, 2002. 34(3): p. 437-46.

Crochet S., Poulet J.F., Kremer Y., Petersen C.C. Synaptic mechanisms underlying sparse coding of active touch. Neuron. 2011 Mar 24;69(6):1160-75.Crochet, S. and C.C. Petersen, Correlating whisker behavior with membrane potential in barrel cortex of awake mice. Nat Neurosci, 2006. 9(5): p. 608-10.

Crunelli, V., et al., The 'window' T-type calcium current in brain dynamics of different behavioural states. J Physiol, 2005. 562(Pt 1): p. 121-9.

Dai, H., On measuring psychometric functions: a comparison of the constant-stimulus and adaptive up-down methods. J Acoust Soc Am, 1995. 98(6): p. 3135-9.

de Lafuente, V. and R. Romo, Neural correlate of subjective sensory experience gradually builds up across cortical areas. Proc Natl Acad Sci U S A, 2006. 103(39): p. 14266-71.

de Lafuente, V. and R. Romo, Neuronal correlates of subjective sensory experience. Nat Neurosci, 2005. 8(12): p. 1698-703.

Ergenoglu, T., et al., Alpha rhythm of the EEG modulates visual detection performance in humans. Brain Res Cogn Brain Res, 2004. 20(3): p. 376-83.

Fanselow, E.E. and M.A. Nicolelis, Behavioral modulation of tactile responses in the rat somatosensory system. J Neurosci, 1999. 19(17): p. 7603-16.

Fanselow, E.E., et al., Thalamic bursting in rats during different awake behavioral states. Proc Natl Acad Sci U S A, 2001. 98(26): p. 15330-5.

Ferezou I., Haiss F., Gentet L.J., Aronoff R., Weber B., Petersen C.C. Spatiotemporal dynamics of cortical sensorimotor integration in behaving mice. Neuron. 2007 Dec 6;56(5):907-23.

Fontanini, A. and D.B. Katz, 7 to 12 Hz activity in rat gustatory cortex reflects disengagement from a fluid self-administration task. J Neurophysiol, 2005. 93(5): p. 2832-40.

Fries P. Neuronal gamma-band synchronization as a fundamental process in cortical computation. Annu Rev Neurosci. 2009;32:209-24.

Fries P.,J.H. Reynolds, A.E. Rorie, and R. Desimone. Modulation of oscillatory neuronal synchronization by selective visual attention. Science. 2001 Feb 23;291(5508):1560-3.

Frostig R.D., Xiong Y., Chen-Bee C.H., Kvasnák E., Stehberg J. Large-scale organization of rat sensorimotor cortex based on a motif of large activation spreads. J Neurosci. 2008 Dec 3;28(49):13274-84.

Gao, P., R. Bermejo, and H.P. Zeigler, Whisker deafferentation and rodent whisking patterns: behavioral evidence for a central pattern generator. J Neurosci, 2001. 21(14): p. 5374-80.

Garabedian, C.E., et al., Band-pass response properties of rat SI neurons. J Neurophysiol, 2003.

Gentet L.J., Avermann M., Matyas F., Staiger J.F., Petersen C.C. Membrane potential dynamics of GABAergic neurons in the barrel cortex of behaving mice. Neuron. 2010 Feb 11;65(3):422-35.

Gentet L.J., M. Avermann, F. Matyas, J.F. Staiger, and C.C. Petersen. Membrane potential dynamics of GABAergic neurons in the barrel cortex of behaving mice. Neuron. 2010 Feb 11;65(3):422-35.

Gray C.M., and W Singer. Stimulus-specific neuronal oscillations in orientation columns of cat visual cortex. Proc Natl Acad Sci U S A. 1989 Mar;86(5):1698-702.

Hamada Y.,E. Miyashita, and H. Tanaka. Gamma-band oscillations in the "barrel cortex" precede rat's exploratory whisking. Neuroscience. 1999;88(3):667-71.

Harris K.D., Thiele A. Cortical state and attention. Nat Rev Neurosci. 2011 Aug 10;12(9):509-23.Haslinger, R., et al., Analysis of LFP phase predicts sensory response of barrel cortex. J Neurophysiol, 2006. 96(3): p. 1658-63.

Hayut I., Fanselow E.E., Connors B.W., Golomb D. LTS and FS inhibitory interneurons, short-term synaptic plasticity, and cortical circuit dynamics. PLoS Comput Biol. 2011 Oct;7(10):e1002248.

Higley, M.J. and D. Contreras, Integration of synaptic responses to neighboring whiskers in rat barrel cortex in vivo. J Neurophysiol, 2005. 93(4): p. 1920-34.

Higley, M.J. and D. Contreras, Nonlinear integration of sensory responses in the rat barrel cortex: an intracellular study in vivo. J Neurosci, 2003. 23(32): p. 10190-200.

Jensen, O., et al., Oscillations in the alpha band (9-12 Hz) increase with memory load during retention in a short-term memory task. Cereb Cortex, 2002. 12(8): p. 877-82.

Jones S.R., Kerr C.E., Wan Q., Pritchett D.L., Hämäläinen M., Moore C.I. Cued spatial attention drives functionally relevant modulation of the mu rhythm in primary somatosensory cortex. J. Neurosci. 2010 Oct 13;30(41):13760-5.

Jones S.R., Pritchett D.L., Stufflebeam S.M., Hämäläinen M., Moore C.I. Neural correlates of tactile detection: a combined magnetoencephalography and biophysically based computational modeling study. J. Neurosci. 2007 Oct 3;27(40):10751-64.

Jones, S.R., et al., Alpha-frequency rhythms desynchronize over long cortical distances: a modeling study. J Comput Neurosci, 2000. 9(3): p. 271-91.

Kandel, Schwartz, and Jessell, Principals of Neural Science. 3 ed. 1991, New York: Elsevier. 1135.Kelly, S.P., et al., Increases in alpha oscillatory power reflect an active retinotopic mechanism for distracter suppression during sustained visuospatial attention. J Neurophysiol, 2006. 95(6): p. 3844-51.

Khatri, V. and D.J. Simons, Angularly Nonspecific Response Suppression in Rat Barrel Cortex. Cereb Cortex, 2006.

Knoblich U., Siegle J.H., Pritchett D.L., and Moore C.I. What do we gain from gamma? Local dynamic gain modulation drives enhanced efficacy and efficiency of signal transmission. Front. Hum. Neurosci. 2010 4:185.

Kulics, A.T., Cortical neural evoked correlates of somatosensory stimulus detection in the rhesus monkey. Electroencephalogr Clin Neurophysiol, 1982. 53(1): p. 78-93.

Kvitsiani D., Ranade S., Hangya B., Taniguchi H., Huang J., Kepecs A. Functional specialization of identified interneuron classes in medial prefrontal cortex of behaving mice. Program No. 407.25. 2011 Neuroscience Meeting Planner. Washington, DC: Society for Neuroscience, 2011. Online.

Lee, A.C., et al., Regional brain activations differ for semantic features but not categories. Neuroreport, 2002. 13(12): p. 1497-501.

Linkenkaer-Hansen, K., et al., Prestimulus oscillations enhance psychophysical performance in humans. J Neurosci, 2004. 24(45): p. 10186-90.

Mitchell J.F., Sundberg K.A., Reynolds J.H. Differential attention-dependent response modulation across cell classes in macaque visual area V4. Neuron. 2007 Jul 5;55(1):131-41.

Moore, C.I. and M.L. Andermann, The vibrissa resonance hypothesis, in Neural Plasticity in Adult Somatic Sensory-Motor Systems, F.F. Ebner, Editor. 2005, Taylor & Francis Publishing Group, CRC Press. p. 21-59.

Moore, C.I. and S.B. Nelson, Spatio-temporal subthreshold receptive fields in the vibrissa representation of rat primary somatosensory cortex. J Neurophysiol, 1998. 80(6): p. 2882-92.

Moore, C.I., Frequency-dependent processing in the vibrissa sensory system. J Neurophysiol, 2004. 91(6): p. 2390-9.

Moore, C.I., S.B. Nelson, and M. Sur, Dynamics of neuronal processing in rat somatosensory cortex. Trends Neurosci, 1999. 22(11): p. 513-20.

Mountcastle, V.B., et al., Cortical neuronal mechanisms in flutter-vibration studied in unanesthetized monkeys. Neuronal periodicity and frequency discrimination. J Neurophysiol, 1969. 32(3): p. 452-84.

Nicolelis M.A., Fanselow E.E. Dynamic shifting in thalamocortical processing during different behavioural states. Philos Trans R Soc Lond B Biol Sci. 2002 Dec 29;357(1428):1753-8.

Nicolelis, M.A. and E.E. Fanselow, Thalamocortical [correction of Thalamcortical] optimization of tactile processing according to behavioral state. Nat Neurosci, 2002. 5(6): p. 517-23.

O'Connor D.H., N.G. Clack, D. Huber, T. Komiyama, E.W. Myers, and K. Svoboda. Vibrissa-based object localization in head-fixed mice. J Neurosci. 2010 Feb 3;30(5):1947-67.

Pfurtscheller, G., et al., Foot and hand area mu rhythms. Int J Psychophysiol, 1997. 26(1-3): p. 121-35.

Pikovsky, A., O. Popovych, and Y. Maistrenko, Resolving clusters in chaotic ensembles of globally coupled identical oscillators. Phys Rev Lett, 2001. 87(4): p. 044102.

Pouget A., and G.C. DeAngelis. Paying attention to correlated neural activity. Nat. Neurosci. 2008 Dec;11(12):1371-2.

Pritchett D.L., Siegle J.H., and Moore C.I. Optogenetic Gamma Entrainment in Primary Sensory Cortex Enhances Tactile Detection. [in prep].

Reynolds, J.H., L. Chelazzi, and R. Desimone, Competitive mechanisms subserve attention in macaque areas V2 and V4. J Neurosci, 1999. 19(5): p. 1736-53.

Shadlen M.N., K.H. Britten, W.T. Newsome, and J.A. Movshon. A computational analysis of the relationship between neuronal and behavioral responses to visual motion. J Neurosci. 1996 Feb 15;16(4):1486-510.

Sheth, B.R., C.I. Moore, and M. Sur, Temporal modulation of spatial borders in rat barrel cortex. J Neurophysiol, 1998. 79(1): p. 464-70.

Silva, L.R., Y. Amitai, and B.W. Connors, Intrinsic oscillations of neocortex generated by layer 5 pyramidal neurons. Science, 1991. 251(4992): p. 432-5.

Simons, D.J. and G.E. Carvell, Thalamocortical response transformation in the rat vibrissa/barrel system. J Neurophysiol, 1989. 61(2): p. 311-30.

Simons, D.J., Response properties of vibrissa units in rat SI somatosensory neocortex. J Neurophysiol, 1978. 41(3): p. 798-820.

Spitzer, H., Desimone R., and Moran J., Increased attention enhances both behavioral and neuronal performance. Science, 1988. 240(4850): p. 338-40.

Stüttgen, M.C., J. Ruter, and C. Schwarz, Two psychophysical channels of whisker deflection in rats align with two neuronal classes of primary afferents. J Neurosci, 2006. 26(30): p. 7933-41.

Swadlow, H.A., Efferent neurons and suspected interneurons in S-1 vibrissa cortex of the awake rabbit: receptive fields and axonal properties. J Neurophysiol, 1989. 62(1): p. 288-308.

Treue, S. and J.H. Maunsell, Attentional modulation of visual motion processing in cortical areas MT and MST. Nature, 1996. 382(6591): p. 539-41.

Wiest, M.C. and Nicolelis M.A., Behavioral detection of tactile stimuli during 7-12 Hz cortical oscillations in awake rats. Nat Neurosci, 2003. 6(9): p. 913-4.

Wilson, F.A., et al., Amelioration of dural granulation tissue growth for primate neurophysiology. J Neurosci Methods, 2005. 144(2): p. 203-5.

Woolsey, T.A. and H. Van der Loos, The structural organization of layer IV in the somatosensory region (SI) of mouse cerebral cortex. The description of a cortical field composed of discrete cytoarchitectonic units. Brain Res, 1970. 17(2): p. 205-42.

Worden, M.S., et al., Anticipatory biasing of visuospatial attention indexed by retinotopically specific alpha-band electroencephalography increases over occipital cortex. J Neurosci, 2000. 20(6): p. RC63.

Vierling-Claassen D, Cardin JA, Moore CI, Jones SR. Computational modeling of distinct neocortical oscillations driven by cell-type selective optogenetic drive: separable resonant circuits controlled by low-threshold spiking and fast-spiking interneurons. Front Hum Neurosci. 2010 Nov 22;4:198.

Zhang F, Aravanis AM, Adamantidis A, de Lecea L, Deisseroth K. Circuit-breakers: optical technologies for probing neural signals and systems. Nat Rev Neurosci. 2007 Aug;8(8):577-81.

Chapter 2

MEG analysis of the Relation Between Pre-Stimulus Alpha and Beta Oscillations and Perceptual Success and the Interaction of Alpha and Beta Oscillations in Expression of the Mu Rhythm

2.1 Author Contributions

This chapter is derived from three papers previously published as:

Jones S.R., **Pritchett D.L.**, Stufflebeam S.M., Hamalainen M., Moore C.I. (2007) Neural correlates of tactile detection: a combined MEG and biophysically based computational modeling study. J Neurosci 27:10751–10764.

Jones S.R., **Pritchett D.L.**, Sikora M.A., Stufflebeam S.M., Hämäläinen M., Moore C.I. Quantitative analysis and biophysically realistic neural modeling of the MEG mu rhythm: rhythmogenesis and modulation of sensory-evoked responses. J Neurophysiol. 2009 Dec;102(6):3554-72. Epub 2009 Oct 7.

Jones S.R., Kerr C.E., Wan Q., **Pritchett D.L.**, Hämäläinen M., Moore C.I. Cued spatial attention drives functionally relevant modulation of the mu rhythm in primary somatosensory cortex. J. Neurosci. 2010 Oct 13;30(41):13760-5.

I was responsible for construction of the MEG compatible tactile stimulator, the design of the behavioral task, data collection, aspects of data analysis and participated in the writing of the manuscripts.

2.2 Abstract

Cued spatial attention modulates functionally relevant alpha rhythms in visual cortices in humans. Here, I present evidence for analogous phenomena in primary somatosensory neocortex (SI). Using magnetoencephalography, we measured changes in the SI mu rhythm containing mu-alpha (7–14 Hz) and mu-beta (15–29 Hz) components. We found that cued attention impacted mu-alpha in the somatopically localized hand representation in SI, showing decreased power after attention was cued to the hand and increased power after attention was cued to the foot, with significant differences observed 500 –1100 ms after cue. Mu-beta showed differences in a time window 800–850 ms after cue. Analysis of a second dataset showed that, on a trial-by-trial basis, tactile detection probabilities decreased linearly with pre-stimulus mu-alpha and mu-beta power. These results support the growing consensus that cue-induced alpha modulation is a functionally relevant sensory gating mechanism deployed by attention. Further, while cued attention had a weaker effect on the allocation of mu-beta, oscillations in this band also predicted tactile detection.

Despite the prominence of the mu rhythm, a fundamental question regarding its manifestation has not been conclusively addressed. Specifically, mu is often considered the simultaneous occurrence of alpha and beta activity: The degree to which rolandic expression of either rhythm can occur alone has not been defined. We characterized the ongoing MEG mu rhythm from a localized source in the finger representation of primary somatosensory (SI) cortex. Subjects showed variation in the relative expression of mu-alpha or mu-beta, which were non-overlapping for roughly 50% of their respective durations on single trials.

These results provide correlative evidence that the mu, alpha and beta, oscillations expressed in human somatosensory cortex are involved in disengaging oscillation to impair perception. Moreover, our data show that the mu-alpha and mu-beta oscillations can and often do express as two distinct oscillations, indicating distinct mechanistic origins and possible roles in neural computation.

2.3 Background

Mu – Alpha and Beta Oscillations and Detection
The historical view of electroencephalography/magnetoencephalography (EEG/MEG)-measured alpha rhythms (7–14 Hz) as a "resting" brain state is being challenged by evidence that they are actively and topographically deployed to gate information processing. Cued spatial attention leads to decreased alpha amplitudes in parietal-occipital EEG sensors contralateral to the attended site in visual (Worden et al., 2000; Kelly et al., 2006, 2009; Thut et al., 2006) and intersensory visual–auditory (Foxe et al., 1998; Fu et al., 2001) tasks. Alpha decreases are accompanied by increases in opposing hemifields, and lateralized alpha amplitudes predict reaction times and visual discriminability (Worden et al., 2000; Kelly et al., 2006, 2009; Thut et al., 2006). Recent work has also shown that attentional biases are tied to changes in components of the broadband cue-induced evoked response (ER) in early visual cortices (Kelly et al., 2009).

In the somatosensory neocortex in humans, a spontaneous mu rhythm containing a complex of mu-alpha (7–14 Hz) and mu-beta (15–29 Hz) components is commonly observed above rolandic cortex (Tiihonen et al., 1989; Jones et al., 2009). These rhythms show an event-related desynchronization (ERD) with stimulation or movement (please see **Chapter 3**, **Figure 8** for an example of ERD in mouse neocortex), and in pre-movement periods, with a subsequent synchronization (ERS). There is an increase in alpha band ERS over the sensorimotor neocortex during visual processing, with a simultaneous alpha ERD over visual cortices, and vice versa during movement (Pfurtscheller, 1992) (see also Rougeul et al., 1979). Further, pre-movement alpha ERD is accentuated in elite athletes

over the entire brain, suggesting that this is a functionally relevant mechanism that can be enhanced with practice (Del Percio et al., 2009).

Several studies have shown that selective somatic attention impacts movement- or sensory-induced ERD and ERS changes in sensorimotor mu-alpha and mu-beta activity (Bauer et al., 2006; Babiloni et al., 2008; Dockstader et al., 2010). However, allocation of these rhythms following an attentional cue, in anticipation of tactile sensory processing, has not been investigated.

Is Mu Monolithic? The Relation between Alpha and Beta in Mu

While the mu rhythm is one of the most robust in macroscopic electrophysiological measures and has been widely studies, the shared temporal dynamics of the mu-alpha and mu-beta components are not well characterized. Tiihonen et al. (1989) observed qualitatively that the mu-alpha and mu-beta components do not always overlap in time, suggesting they are not harmonics, but did not quantify this assertion (Palva et al. 2005; Tiihonen et al. 1989). Evidence for cross-frequency coupling of these components has also been reported (Palva et al. 2005). Quantifying the degree to which mu-alpha and mu-beta co-occur and co-vary in amplitude is crucial to understanding their relative interdependence and to constraining computational models of their origins.

To investigate these two questions—whether alpha and beta are allocated with attention, and whether these rhythms are independently we recorded whole-head 306-channel MEG data and applied an equivalent current dipole inverse solution technique to look at activity from the hand area of SI, a technique that has been found to consistently localize signals discretely to the anterior bank of the postcentral gyrus, area 3b (Jones et al. 2007). In the present study, we used MEG imaging to investigate whether similar effects to those observed in the visual system are also present in somatosensation, using the well localized hand representation in SI as our substrate (Jones et al., 2007, 2009). We investigated whether spatial attention directed to or away from the hand impacted allocation of mu-alpha and mu-beta, the predictive value of these rhythms for detection, and the impact of cued attention on evoked responses. We observed an impact in each of these dimensions, indicating that the decreased expression of localized alpha oscillations could be causally beneficial to attentional regulation employed across neocortical areas.

On single trials, we further observed that during the prestimulus time period high-power epochs of mu-alpha and mu-beta were not simultaneous in their emergence, but did co-occur at rates greater than chance. These findings suggest that mu-alpha and mu-beta emerge from separable generators within SI that share common elements. The data indicated these rhythms are not simple harmonics.

2.4 Materials and Methods

Subjects

MEG data were collected from 12 neurologically healthy (exclusion criteria included musculoskeletal diseases, arthritis, lupus, multiple sclerosis, scleroderma, and diagnosed current psychiatric disorder), right-handed, 18- to 50-year-old adults (mean age 31.6 years, SD 7 years, 1 male and 11 female). Subjects were medication free or on stable doses of selective serotonin reuptake inhibitor medication. The experimental protocol was approved by the Massachusetts General Hospital Internal Review Board, and each subject gave informed consent before data acquisition.

Stimuli

Subjects' hand and foot rested on solid plastic frames through which tactile stimuli were delivered. The stimulus (single cycle of a 100 Hz sine wave, 10 ms duration) was generated by fused multilayer piezoelectric benders, which provide more favorable force and higher-frequency resonance characteristics than typical ceramic wafers (Noliac) (see Jones et al., 2007). Stimuli were applied to the distal pads of the third digit of the left hand and first digit of the left foot via a Delrin contactor affixed to the piezoelectric bender (7 mm diameter presented within a 1 cm circular rigid surround). The device was not glued to the skin. Instead, matched intensity of stimulation, relative to perceptual threshold, was maintained individually for each subject using a parameter estimation sequential testing (PEST) convergence procedure (Dai, 1995; Leek, 2001). During the cued detection runs described below, stimulus strength was maintained at 66% detection threshold with suprathreshold (100% detected) and null stimuli randomly interleaved for 10% and 20% of the trials, respectively. The PEST procedure and the hand stimulation device and protocol were as used by Jones et al. (2007, 2009).

Experimental procedure

Localization runs. To aid localization of primary equivalent current dipoles (ECDs) in contralateral SI, each experiment began with presentation of suprathreshold stimuli to the left hand third digit for 3 min with an interstimulus interval of 3 s (60 trials per subject). Separate localization runs were also performed on the first digit of the foot, as an original goal of our study was to look at the somatotopic precision of attention allocation by comparing hand and foot activity. However, consistent dipoles could not be reconstructed from the foot localization data using the standard ECD localization techniques described below. Thus, only hand area activity is presented, as its precise position in the SI map could be confirmed.

Cued detection runs. Subjects were instructed to fixate on a cross on a projection screen. PEST procedure was used for 3 min at the beginning to determine subjects' initial detection

28

thresholds. This run was followed by at least 5 cued detection runs, described in Figure 1, consisting of a 3.5 s trial that began with the fixation cross changing into a visual word cue on a projection screen directing the participant to attend to the "Hand" (the attend-in condition), the "Foot" (the attend-out condition), or "Either" location. The visual cue was accompanied by a 60 dB, 2 kHz tone delivered to both ears to mask audible clicks created by the tactile stimulator and remained constant for 2.5 s. At a randomized time between 1.1 and 2.1 s (fixed 100 ms intervals) after the visual cue, the piezoelectric stimulator delivered a brief tactile stimulus to either the finger or toe. At the end of the 2.5 s visual cue, and at least 400 ms after tactile stimulus, subjects reported detection or nondetection of the stimulus at the cued location with button presses using the second and third digits of the right hand, respectively. The next trial began 1 s after cessation of the visual cue. There were 120 trials per run, 40 of each attention condition, totaling at least 200 trials of 3 stimulus strengths in each condition.

MEG data acquisition and source analysis. The MEG signals were recorded using a 306-channel whole-head planar dc-SQUID Neuromag Vectorview system. Data were acquired at 601 Hz and filtered from 0.1 to 200 Hz. Four head position coils recorded head position in the Dewar for coregistration with structural MR images. Vertical and horizontal electro-oculogram (EOG) signals were recorded with electrodes placed close to the left eye. Epochs with EOG peak-to-peak amplitude exceeding 100 V were excluded from analysis.

The contribution from the left third digit representation in SI to the measured fields was estimated using a least-squares fit with a dipole forward solution calculated using a spherically symmetric conductor model of the head (Ha¨ma¨la¨inen and Sarvas, 1989). Averaged data from the localization runs described above were used to find an ECD (Elekta- Neuromag software) at the time of peak activity (mean peak activity 66.8 ms, SD6.4 ms) in the mean signal from the suprathreshold stimuli (minimum n 50 runs per subject). The goodness of fit of this single dipole model was larger than 70% in all fit data during peak responses.

Coregistration of the SI source localization with the individual's anatomical MRIs confirmed that the source emerged from the anterior band of the postcentral gyrus finger representation of area 3b in SI (Moore et al., 2000) in all subjects. All analysis considered the forward solution from this SI source.

Analysis

Time evolution of spectral power
This metric was calculated using a complex wavelet analysis, from which time–frequency representations (TFRs) of near instantaneous changes were determined. The TFRs were

calculated from 1 to 40 Hz on the SI ECD time courses by convolving signals with a complex Morlet wavelet of the form w(t, f0)= A exp(-t 2/2[t2])exp(2iπf0t), for each frequency of interest f0, where $σ_t$ = m/2πf0, and i is the imaginary unit. The normalization factor was A = 1/(σ_t√2pi), and the constant m defining the compromise between time and frequency resolution was 7, as in the Jones et al. (2009) study. Time–frequency representations of mu-alpha and mu-beta power were calculated as the squared magnitude of the complex wavelet-transformed data averaged across the range of interest. For the postcue analysis, baseline was calculated as averaged power [-200, 0] ms relative to the cue—averaged across attend-in and attend-out trials separately. For the prestimulus analysis, baseline was calculated as average power [-500, 0] ms relative to the stimulus.

Data were analyzed using the last 100 trials of each condition. This choice reflects analysis across multiple studies in our laboratory (see Wang et al., 2011, for a full explication of these data) indicating that the initial 100 trials provide less stable and consistent neurophysiological activity patterns across individuals.

Visual cue and tactile stimulus broadband evoked responses

SI evoked responses were calculated across an equal number of attend-in and attend-out trials per subject from threshold-level tactile stimulation to the finger (number of trials mean 88 trials; SD 10). Averages were baseline normalized by subtracting the mean over [-100, 0] ms from the cue or stimulus, for each subject. Impact of mu-alpha and mu-beta on detection probabilities. We could not use the current data to assess the impact of mu-alpha and mu-beta on detection probabilities because the subset of relevant data was a statistically small sample.

The relevant data consisted of the "hit" and "miss" trials in the attend-hand condition, and there were only a small number of miss trials per subject in this sub-condition (number of miss trials: mean = 11, SD = 6; number of hit trials: mean = 83, SD = 11). Therefore, we conducted analysis using a second dataset where the statistics were tractable. As in the present study, subjects detected taps applied to the third digit fingertip (of the right hand) using the same stimulator, and signals were localized to the hand dipole using identical means. Because foot trials and "either" trials were not interleaved—subjects attended to the hand throughout—we had a more extensive trial base for comparing hit and miss trials (last 100 trials analyzed). Details of data collection were described in detail in prior reports by our group (Jones et al., 2007, 2009; Ziegler et al., 2010).

Analysis methods were as in the Linkenkaer-Hansen et al. (2004) study. In brief, for each subject mu-alpha and mu-beta power was averaged over a 1 s prestimulus time window for each of the last 100 threshold-level stimulus trials, and binned into 10 power percentile bins (10 averages per bin) sorted from low to high. The probability of detection in each bin

was calculated as a percentage change in hit rate (number of detected trials/total number of trials) from the mean.

Statistical analyses. Nonparametric Wilcoxon sign-rank tests were used to assess the statistical significance of differences in attend-in and attend-out conditions across subjects at every time point. The Wilcoxon test was preferred over ANOVA because the data were non-normally distributed (Shapiro– Wilks test). Linear regression on the mean percentage change in hit rate across subjects was used to assess the impact of mu-alpha and mu-beta power on detection.

2.5 Results

Consistent with previous studies, the ongoing mu rhythm recorded here expressed peaks of activity in the mu-alpha (7–14 Hz) and mu-beta (15–29 Hz) frequency bands. The dual peak in mu can be observed in the mean and SE across subjects of the PSD calculated from the frequency range 1–60 Hz (**Figure 1**, blue curve; n = 10 Ss, mean of 200 1-s prestimulus trials per subject, calculated with Welch's periodogram; see Methods).

Peaks in the mu-alpha and mu-beta range are evident in this analysis and the relative mu-alpha and mu-beta expressions vary across subjects. The gray curve in **Figure 1A** shows the corresponding results when the data from the three subjects—whose SI dipole localizations were not determined by standard methods—were removed (see **Methods**) and their individual subject data are shown in black in **Figure 1B**. Although the overall power of the oscillations is smaller without these subjects, the overall shape is preserved and the dual-peak mu phenomenon is still present.

The spectrograms from these subjects show clear bands of mu-alpha and mu-beta activity in the average data. We subsequently show that, although the relative mu-alpha and mu-beta expressions across subjects are not the same, the existence of separable activity in both frequency ranges persists in all subjects and in single trials.

Performance in Mu-Alpha and Mu-Beta on Detection

We investigated the temporal evolution of changes in mu-alpha and mu- power in a localized dipole source in the right hand area of SI after a cue to attend to tactile finger stimulation to the contralateral left hand (attend-in condition), or to tactile toe-stimulation to the left foot (attend-out condition). These were uniformly observed in the SI hand representation in the anterior bank of the postcentral gyrus (area 3b), confirmed by proximity to the -shaped bend in the central sulcus (Moore et al., 2000). **Figure 2B** shows the corresponding average percentage change from baseline [n = 12 subjects (Ss)] in SI mu-

31

alpha and mu-beta power during the time period [-100, 1100] ms relative to the cue in attend-in and attend-out conditions. A significant difference across subjects was observed between the conditions in the mu-alpha band during the anticipatory postcue time period [500, 1100] ms relative to the cue (p = 0.05 marked with asterisks, Wilcoxon sign-rank test). Significant differences in the mu-beta band were observed for a time window of [800, 850] ms.

Aligning trials to the tactile stimulus onset ([-1000, 200] ms), rather than visual cue, also showed a dominant effect of cued attention on prestimulus mu-alpha activity (**Figure 2C**). Significant differences between attend-in and attend-out conditions are seen in the mu-alpha across the entire prestimulus time period, and in the [-200, 0] ms time window for mu-beta, with another period of significance around -800 ms.

We assessed trial-by-trial impact of prestimulus mu-alpha and mu-beta in our SI signal on tactile detection probabilities, using a second dataset that used analogous MEG and tactile detection methods, but with sustained attention to the finger (Jones et al., 2007, 2009; Ziegler et al., 2010). This previously collected dataset gave greater statistical power than the current data, where the relevant hit and miss trials represented a statistically small sample (see Materials and Methods). Following prior convention (Linkenkaer-Hansen et al., 2004), on individual trials average prestimulus mu-alpha and mu-beta power was calculated (1 s before stimulus) and sorted from high to low power into 10 equally sized percentile bins. Detection probabilities in each bin were calculated as the percentage change in hit rate from the mean (see Materials and Methods). We found a linear relationship between tactile detect on probabilities and mu-alpha and mu-beta power (p < 0.05, F test, R^2 = 0.65 and R^2 = 0.85, respectively) such that the hit probability was greater during trials with lower prestimulus mu-alpha and mu-beta power (**Figure 3**).

Conjoint Analysis of Alpha and Beta

To investigate the relation between these bands, we analyzed the spontaneous SI signal in individual trials. **Figure 4** shows two examples of SI frequency distributions and corresponding waveforms during the 1-s prestimulus epochs for four subjects. These spectrograms are different from the average responses (**Figure 1**). In single trials, periods of high mu-alpha and mu-beta power often have non-overlapping time courses. We note that subjects 3 and 4 had nonstandard dipole localizations and larger overall power (**Figure 1B**). However, these subjects still showed the characteristic periods of non-overlapping high mu-alpha and mu-beta power.

This feature implies that these rhythms are not simple harmonics, further indicating separable neural generators. To quantify this observation, we calculated the probability that high power in mu-alpha and mu-beta was expressed simultaneously in the

spontaneous mu rhythm. We sorted the relative power of mu-alpha and mu-beta in each 100-ms window. We then calculated the probability that bins in the top third of the mu-alpha and mu-beta power distributions were identical. If these rhythms were generated from an identical neural process, they would be predicted to correlate perfectly. A completely random association would predict overlap on roughly 10% of bins. We found overlap on 50% of bins (**Figure 5** inset, 50.31% mean, SD = 0.056% n = 10 Ss, calculated from 2,000 100-ms time windows per subject). This finding implies a degree of independence for the two rhythms, but also that they co-occurred at greater than chance levels, suggesting they share components of neural mechanism.

To further characterize the relation between alpha and beta occurrence, we plotted a histogram of the ratio of alpha to beta power calculated in the same 100-ms time windows (**Figure 5**, n = 2,000 trials, 10 Ss, 1,000 bins). The mean and median of the histogram were 2.4 and 1.3, respectively. The normalization applied to the TFR data in our analysis favors the observation of higher-frequency bands (see Methods). As such, the dominance of alpha power in this analysis, despite the normalization applied, underscores the relative prevalence of this oscillation in the mu signal.

2.6 Conclusions

Alpha and Beta Oscillations and Perception
Both parts of mu, but differently, have a negative relationship to detection. This is n agreement (with subtle disagreements perhaps) with other findings in the human field (Klimesch 07, Jensen 10, Palva 06, Rajagovindan 10). Consistent with findings in visual cortices, we observed that cued attention modulates anticipatory post-cue mu-alpha activity and early peaks in the broadband visual cue- and tactile stimulus-induced ERs in the SI hand representation. We found a significant difference in the post-cue change from baseline of mu-alpha power between attend-in and attend-out conditions. Detection probabilities were greater during lower prestimulus mu-alpha and mu-beta power. These results are consistent with the theory that attentionally induced focal alpha changes are an active mechanism for modulation of sensory information processing (Foxe et al., 1998; Worden et al., 2000; Kelly et al., 2006, 2009; Thut et al., 2006; Klimesch et al., 2007). Further, our results show that although attentional cuing has a weaker impact on SI mu-beta rhythms, they also predict tactile detection.

Our finding of a linear relationship between mu-alpha and mu-beta power and tactile detection agrees with Schubert et al. (2009), who found a linear relationship between alpha and beta amplitudes in EEG electrodes over SI and tactile detection probability. These results also are consistent with the relationship between smaller alpha amplitudes and increased perception and decreased reaction times in the visual system (Thut et al., 2006;

Hanslmayr et al., 2007; van Dijk et al., 2008; Kelly et al., 2009). Other studies in the somatosensory (Linkenkaer-Hansen et al., 2004; Zhang and Ding, 2010) and visual (Rajagovindan and Ding, 2010) systems have reported an inverted-U relationship between alpha power and detection probabilities. We also found that, on trials with the lowest values of mu-alpha power, detection probability diminished compared to slightly higher values (compare 10th and 20th percentiles in **Figure 3**), suggesting that a minimal baseline of alpha activity is necessary for optimal signal propagation. These results imply that the reduction of mu-alpha and mu-beta activity in SI with cued attention is an active cortical gating mechanism that increases the perceptual salience of tactile signals.

Prior research connecting low-frequency oscillations and cued attention in somatosensory cortex in humans has focused on sensory-stimulus- and movement-induced ERD and subsequent ERS in alpha and beta frequencies (Bauer et al., 2006; Babiloni et al., 2008; Dockstader et al., 2010) (see also Pfurtscheller, 1992). These studies also investigated attentional modulation of somatosensory gamma (35–80 Hz) activity. Gamma was not a focus of our study because it is not robust in our spontaneous SI signal (see Jones et al., 2009).

Is Mu Monolithic?
The MEG recordings revealed an SI mu rhythm with mu-alpha and mu-beta components, whose relative expression was subject dependent. On single trials, the mu-alpha and mu-beta components were not simultaneous in their emergence, but did co-occur at rates greater than chance. Our results showed that the mutual generation of the mu-alpha and mu-beta components of the prestimulus rhythm, as well as the relative separation of these components in time. The data indicated these rhythms are not simple harmonics.

2.7 References

Babiloni C, Capotosto P, Brancucci A, Del Percio C, Petrini L, Buttiglione M, Cibelli G, Romani GL, Rossini PM, Arendt-Nielsen L (2008) Cortical alpha rhythms are related to the anticipation of sensorimotor interaction between painful stimuli and movements: a high-resolution EEG study. J Pain 9:902–911.

Bauer M, Oostenveld R, Peeters M, Fries P (2006) Tactile spatial attention enhances gamma-band activity in somatosensory cortex and reduces low frequency activity in parieto-occipital areas. J Neurosci 26:490 –501.

Dai H (1995) On measuring psychometric functions: a comparison of the constant-stimulus and adaptive up-down methods. J Acoust Soc Am 98:3135–3139.

Del Percio C, Babiloni C, Bertollo M, Marzano N, Iacoboni M, Infarinato F, Lizio R, Stocchi M, Robazza C, Cibelli G, Comani S, Eusebi F (2009) Visuo-attentional and sensorimotor alpha rhythms are related to visuomotor performance in athletes. Hum Brain Mapp 30:3527–3540.

Dockstader C, Cheyne D, Tannock R (2010) Cortical dynamics of selective attention to somatosensory events. Neuroimage 49:1777–1785.

Foxe JJ, Simpson GV, Ahlfors SP (1998) Parieto-occipital approximately 10 Hz activity reflects anticipatory state of visual attention mechanisms. Neuroreport 9:3929 – 3933.

Fu KM, Foxe JJ, Murray MM, Higgins BA, Javitt DC, Schroeder CE (2001) Attention-dependent suppression of distracter visual input can be crossmodally cued as indexed by anticipatory parieto-occipital alpha-band oscillations. Brain Res Cogn Brain Res 12:145–152.

Hämäläinen MS, Sarvas J (1989) Realistic conductivity geometry model of the human head for interpretation of neuromagnetic data. IEEE Trans Biomed Eng 36:165–171.

Hanslmayr S, Aslan A, Staudigl T, Klimesch W, Herrmann CS, Bäuml KH (2007) Prestimulus oscillations predict visual perception performance between and within subjects. Neuroimage 37:1465–1473.

Jones SR, Pritchett DL, Stufflebeam SM, Hämäläinen M, Moore CI (2007) Neural correlates of tactile detection: a combined MEG and biophysically based computational modeling study. J Neurosci 27:10751–10764.

Jones SR, Pritchett DL, Sikora MA, Stufflebeam SM, Hämäläinen M, Moore CI (2009) Quantitative analysis and biophysically realistic neural modeling of the MEG mu rhythm: rhythmogenesis and modulation of sensory-evoked responses. J Neurophysiol 102:3554 –3572.

Kelly SP, Lalor EC, Reilly RB, Foxe JJ (2006) Increases in alpha oscillatory power reflect an active retinotopic mechanism for distracter suppression during sustained visuospatial attention. J Neurophysiol 95:3844 –3851.

Kelly SP, Gomez-Ramirez M, Foxe JJ (2009) The strength of anticipatory spatial biasing predicts target discrimination at attended locations: a high density EEG study. Eur J Neurosci 30:2224 –2234.

Klimesch W, Sauseng P, Hanslmayr S (2007) EEG alpha oscillations: the inhibition-timing hypothesis. Brain Res Rev 53:63– 88.

Leek MR (2001) Adaptive procedures in psychophysical research. Percept Psychophys 63:1279 –1292.

Linkenkaer-Hansen K, Nikulin VV, Palva S, Ilmoniemi RJ, Palva JM (2004) Prestimulus oscillations enhance psychophysical performance in humans. J Neurosci 24:10186 – 10190.

Moore CI, Stern CE, Corkin S, Fischl B, Gray AC, Rosen BR, Dale AM (2000) Segregation of somatosensory activation in the human rolandic cortex using fMRI. J Neurophysiol 84:558 –569.

Palva S, Linkenkaer-Hansen K, Naatanen R, Palva JM. (2005) Early neural correlates of conscious somatosensory perception. J Neurosci 25: 5248– 5258.

Pfurtscheller G (1992) Event-related synchronization (ERS): an electrophysiological correlate of cortical areas at rest. Electroencephalogr Clin Neurophysiol 83:62– 69.

Rajagovindan R, Ding M (2010) From prestimulus alpha oscillation to visual-evoked response: an inverted-U function and its attentional modulation. J Cogn Neurosci. 2010. doi:10.1162/jocn.2010.21478.

Rougeul A, Bouyer JJ, Dedet L, Debray O (1979) Fast somato-parietal rhythms during combined focal attention and immobility in baboon and squirrel monkey. Electroencephalogr Clin Neurophysiol 46:310 –319.

Schubert R, Haufe S, Blankenburg F, Villringer A, Curio G (2009) Now you'll feel it, now you won't: EEG rhythms predict the effectiveness of perceptual masking. J Cogn Neurosci 21:2407–2419.

Thut G, Nietzel A, Brandt SA, Pascual-Leone A (2006) Alpha-band electroencephalographic activity over occipital cortex indexes visuospatial attention bias and predicts visual target detection. J Neurosci 26:9494 –9502.

Tiihonen J, Kajola M, Hari R (1989) Magnetic mu rhythm in man. Neuroscience 32:793–800.

van Dijk H, Schoffelen JM, Oostenveld R, Jensen O (2008) Prestimulus oscillatory activity in the alpha band predicts visual discrimination ability. J Neurosci 28:1816 –1823.

Wan Q, Kerr C, Pritchett D, Hämäläinen M, Moore C, Jones S. Dynamics of dynamics within a single data acquisition session: variation in neocortical alpha oscillations in human MEG. PLoS One. 2011;6(9):e24941. Epub 2011 Sep 22.

Worden MS, Foxe JJ, Wang N, Simpson GV (2000) Anticipatory biasing of visuospatial attention indexed by retinotopically specific alpha-band electroencephalography increases over occipital cortex. J Neurosci 20:RC63.

Zhang Y, Ding M (2010) Detection of a weak somatosensory stimulus: role of the prestimulus mu rhythm and its top-down modulation. J Cogn Neurosci 22:307–322.

Ziegler DA, Pritchett DL, Hosseini-Varnamkhasti P, Corkin S, Ha¨ma¨la¨inen M, Moore CI, Jones SR (2010) Transformations in oscillatory activity and evoked responses in primary somatosensory cortex in middle age: a combined computational neural modeling and MEG study. Neuroimage 52:897–912.

2.8 Figures

A MEG SI Mu-Rhythm

B Individual Subjects

C Subject 1
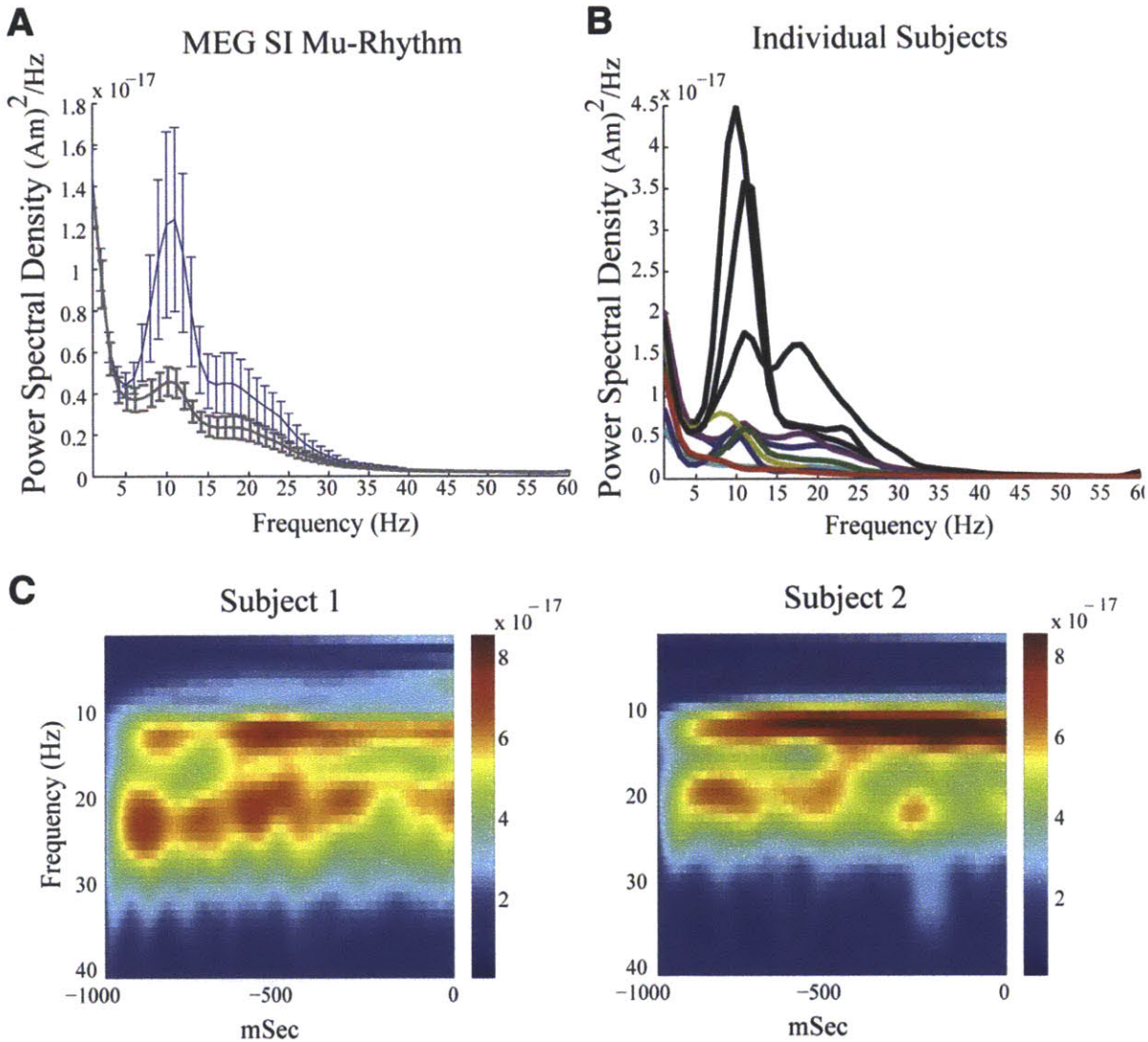
Subject 2

Figure 1 | Magnetoencephalographic (MEG) SI mu rhythms A, blue curve: grand mean power spectral density (PSD) vs. frequency averaged across 10 subjects, 200 trials each (SE bars) showing 2 peaks of activity in the mu-band between 7 and 29 Hz. Gray curve: analogous curve with removal of data from 3 subjects with nonstandard SI dipole localization methods. B: PSD vs. frequency in each subject; subjects with nonstandard dipole localization are shown in black. C: example frequency vs. time spectrograms averaged over 100 trials (1-s prestimulus time period) from 2 subjects, emphasizing that the SI mu rhythm is a 2-component rhythm containing separate bands of mu-alpha and mu-beta activity. The unit of power is (Am)2. (Figure 3, Jones 09)
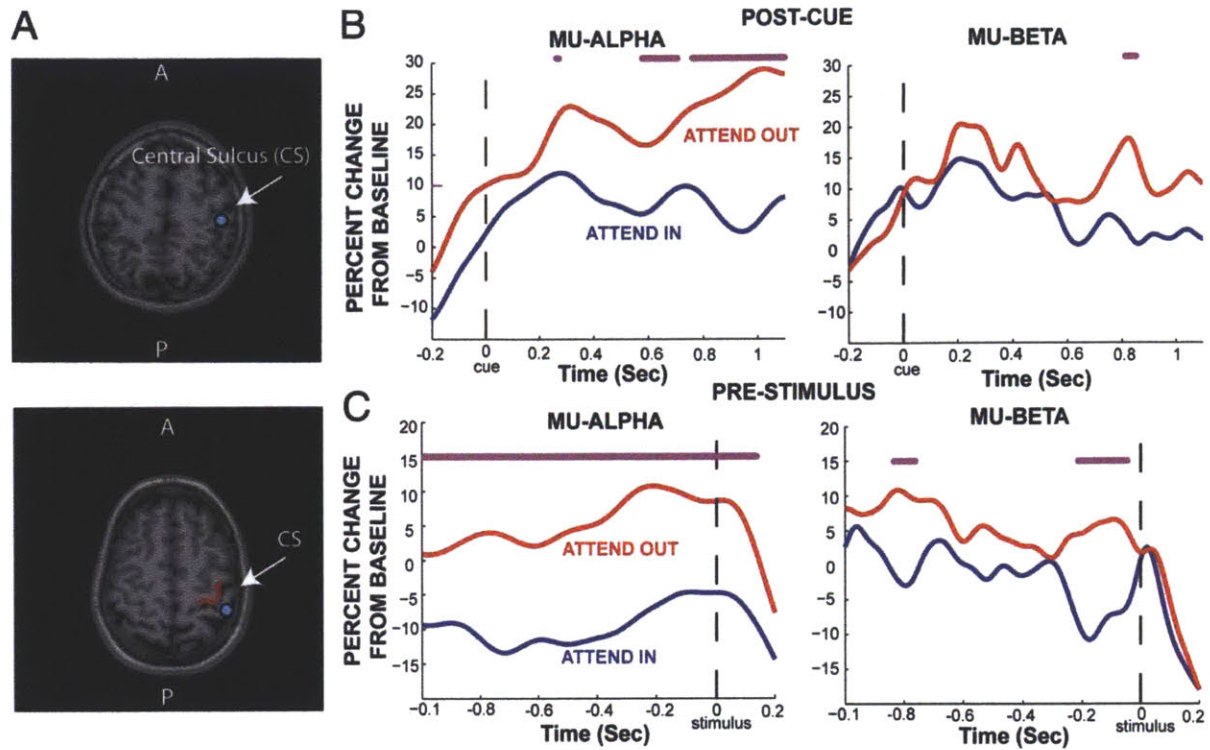
Figure 2 | Impact of cued attention on SI mu-alpha and mu-beta A, Two examples of the estimated SI ECD localizations (blue dots) overlaid on the subjects' structural MRI brain images. Response evoked by a suprathreshold tactile stimulus to the left hand, third digit, was localized to the SI hand representation in area 3b, confirmed by proximity to the Ω shape (marked in red bottom panel), in the anterior bank of the contralateral postcentral gyrus. B, Continuous postcue temporal evolution of the hand area SI mu-alpha (7–14 Hz) and mu-beta (15–29 Hz) activity in attend-in and attend-out conditions (avg. n12 Ss). C, Corresponding continuous prestimulus evolution of mu-alpha mu-beta. Asterisks, Significant difference between conditions (p < 0.05).
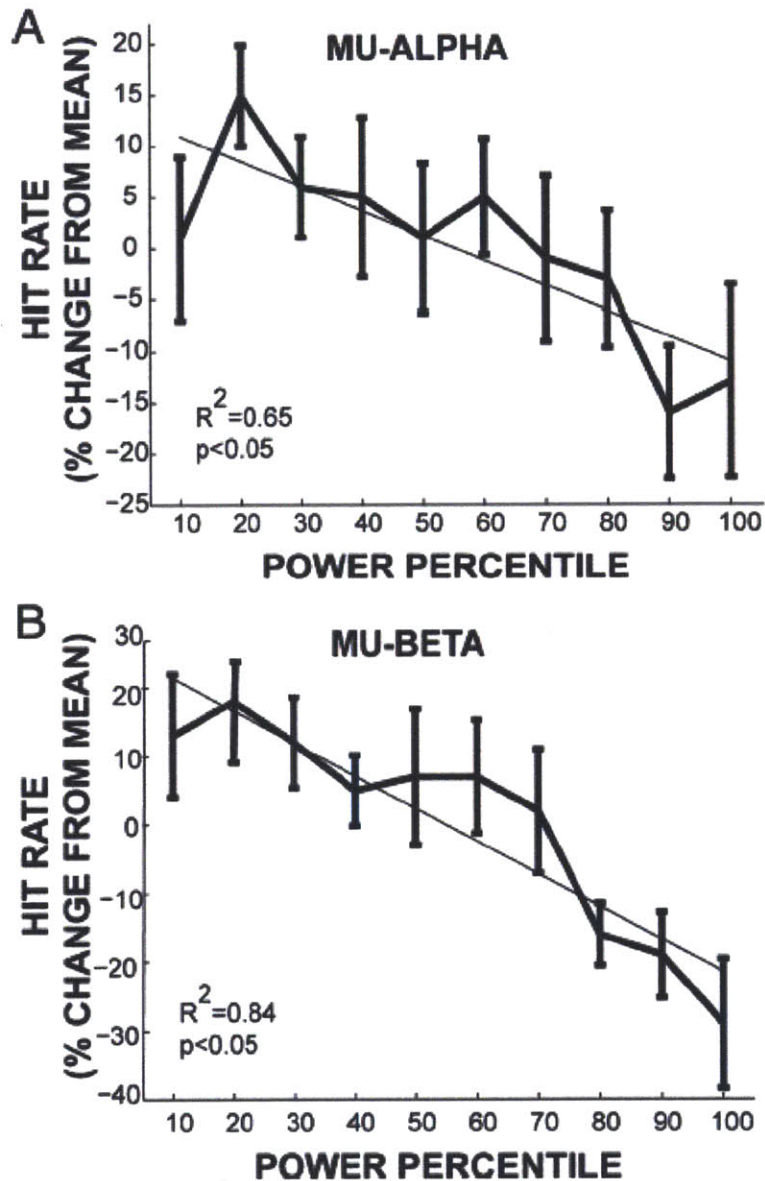
Figure 3 | Impact of prestimulus mu-alpha and mu-beta power on detection probabilities. A, Tactile detection probabilities, measured as percentage change in hit rate from the mean, as a function mu-alpha power sorted into 10 power percentile bins. Bold traces, Mean and SE across subjects (n10 Ss); thin traces, linear fit from linear regression analysis (R 20.65, p0.05). B, Analogous traces as a function of mu-beta power (R 20.84, p0.05). This analysis was performed on data from the Jones et al. (2007, 2009) studies (see Materials and Methods). (Figure 4, Jones, 10)
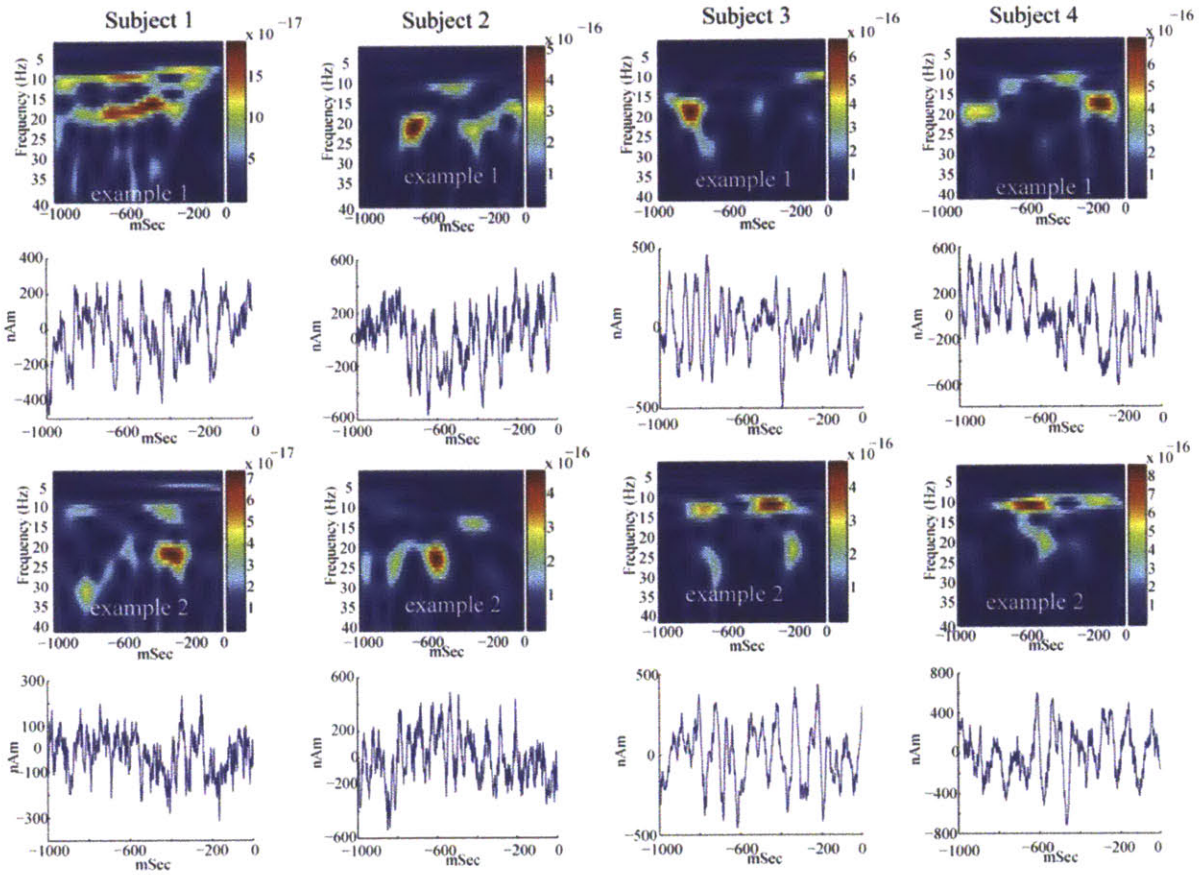
Figure 4 | Single-trial mu rhythms. Two examples of single-trial SI frequency spectrograms and waveforms from 4 subjects. The unit of power is (Am)2. On a single-trial basis, peaks in mu-alpha and mu-beta power often occur at different points in time, indicating that the rhythms are not harmonics of each other and may have different neural sources. The corresponding waveforms oscillation around zero polarity. (figure 4, Jones, 09)
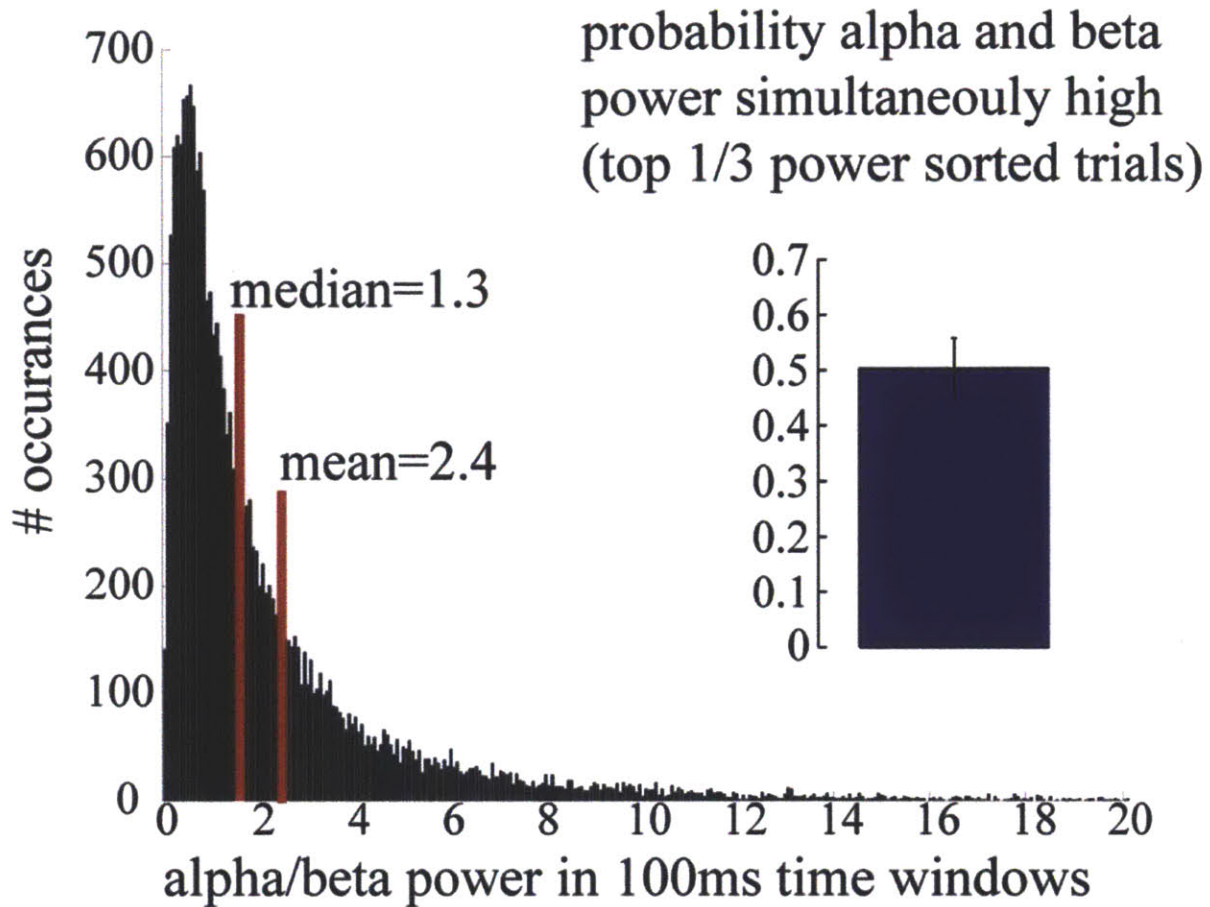
Figure 5 | Mu-alpha and mu-beta components of the MEG SI mu rhythm are nonoverlapping MEG data showing a histogram of the ratio of alpha to beta power over 100-ms time bins (n = 2,000 trials, 10 Ss). The mean (2.4) and median (1.3) of this histogram are > 1, underscoring the relative prevalence of alpha power in the mu signal. Inset: MEG data showing probability that high mu-alpha and mu-beta power (top 33% of all power) occur simultaneously roughly 50% of the time (mean = 50.31%; SD = 0.056%). (Figure 5, Jones 09)

Chapter 3

Analysis of the Relation Between Alpha and Gamma Pre-Stimulus Oscillations in the Mouse Local Field Potential and Perceptual Success in a Detection Task

3.1 Authorship Contributions

D.L.P., J.H.S., and C.I.M. designed the experiments. D.L.P. designed the behavioral rig and oversaw behavioral training. D.L.P., R.C.C., J.F., and H.F. ran the behavioral experiments. J.H.S. designed the implants and performed the viral injections.

D.L.P. conducted all data analysis and made all figures shown in this **Chapter**.

Pritchett DL*, Siegle JH*, Clary RC, Feather J, Farrow H, Moore CI, [Manuscript in Prep.]

3.2-3.3 Abstract/Background

The prior chapter reported studies of the relation between alpha expression and attention and perception in the human using MEG. While such studies are of high clinical relevance, and can be interpreted in more mechanistic circuit terms using computational modeling (e.g., Jones et al., 2007; Jones et al., 2009), they do not permit the kind of invasive data collection and causal control of circuits possible in an animal model. The following 2 Chapters reflect, therefore, my studies using similar paradigms to those in a mammalian model, the mouse, where invasive recording and causal control of neural circuits during perceptual task performance is possible.

Alpha Oscillations and Detection: Contrasting Views

The alpha oscillation (7-14 Hz) is arguably the most prominent in the human brain, as reflected by its being the first oscillation discovered by Berger upon the invention of the EEG (Berger, 1929). In human somatomotor cortex, alpha oscillations are typically considered part of a "mu" rhythm that also includes expression of beta (15-29Hz) (Jones et al. 09, 10, Linkenkaer-Hansen et al. 04, Palva et al. 05). As described in **Chapter 2**, the 'mu' rhythm is not a monolithic construct, as alpha and beta can show unique independent expression patterns though they do often co-occur. Studies using macroscopic recording methods in humans have repeatedly found that decreased power in these frequency bands predicts enhanced perceptual capability in various behavioral tasks, suggesting that the mu rhythm could have a role in the suppression of distracting information (please see **Introduction** and **Chapter 2** for our data in support of this view and a more extensive discussion).

In contrast, based on local field potential recordings (LFP) recorded with invasive electrodes in rodents, Nicolelis and colleagues (Nicolelis 02, Fanselow and Nicolelis 01; Fanselow and Nicolelis 99) have argued that alpha band oscillations in primary sensory "barrel" neocortex favor increased probability of tactile detection. Specifically, these authors argue that the thalamic bursting typical of observation of this state will enhance the probability of post-synaptic spiking in neocortex, potentiating detection (Nicolelis and Fanselow 02; Fanselow and Nicolelis 01). In general support of this view, Wiest and Nicolelis (2003) showed that presence of high power in the alpha band did not prevent detection of stimulation applied simultaneously to several vibrissae in a head-posted rat.

This study did not, however, test threshold level stimuli: It is already well established that supramaximal sensory drive can be detected even during the presence of sleep spindles in

slow wave sleep if strong enough (Ellenbogen 2010). Put colloquially, a gun going off next to a sleeping person will still wake them, even if they are in a state that might not favor sensory transmission. Further, Wiest and Nicolelis (2003) did *not* show enhanced perception with alpha—the original hypothesis—but rather simply that perception was possible during the expression of high alpha power. One of the key goals of the studies reported in **Chapter 3** was to directly test the prediction that alpha oscillations predict *decreased* probability of detection, in contrast to the theories of Nicolelis and colleagues, in exactly the preparation they employed—multi-vibrissal stimulation in the head posted rodent with LFP recordings used to define state. Our data, while replicating the findings of Nicolelis and colleagues when we employed supramaximal sensory stimuli, strongly support the view of alpha as a *suppressive* oscillation when threshold stimuli are applied, in opposition to their hypothesis.

Gamma Oscillations: Enhanced Processing?

Gamma oscillations crucially involve activity of fast-spiking (FS) interneurons, this has been shown using both correlative (e.g., Buzsaki, 1983) and causal studies (e.g., Cardin et al., 2009). While specific models have variation in their precise predictions as to the role of FS in this process (see Tiesinga and Sejnowski, 2009, for a recent review), the rapid inhibitory post-synaptic potentials evoked by this cell class are believed to set the time constant for gamma at ~12-30 msec (~80 to 30 Hz). The synchronous inhibition generated by FS during gamma expression is believed to increase the synchronous firing of pyramidal neurons, thereby enhancing the downstream impact of activity in a given neocortical area (see Knoblich, Siegle, Pritchett and Moore, 2010 for a discussion and computational modeling in support of this basic presumption). Other views have also been offered for the utility of this oscillation in enhancing perception, including beneficial lateral inhibition of non-dominant inputs by FS (e.g., Borgers and Kopell, 2008).

The experimental evidence in support of a role for gamma in *enhancing* perceptual capability comes almost entirely from studies of changes in the allocation of this rhythm with shifts in attention in primate visual neocortex. A series of key studies by Desimone, Fries and colleagues has shown enhanced phase locking of local multi-unit activity to gamma LFP in the representation of attended stimuli (e.g., Womelsdorf et al., 2006 and Fries et al., 2008), and increased pre-stimulus gamma LFP expression with attention (e.g., Fries et al., 2008).

Contrasting Views and Some of the Open Questions Regarding Gamma Oscillations

Recent studies in primary visual neocortex of the primate have challenged the view that gamma oscillations are a general neocortical dynamic that predicts and/or contributes to enhanced perceptual processing. Specifically, Ray and Maunsell (2010) have found that the frequency of gamma expression is dependent on the relative contrast of a given stimulus, and that different gamma oscillations can be expressed in neighboring columns in response to the same stimulus, leading these authors to argue against a role for gamma in "binding" the percept of stimuli. Similar arguments against a "clocking" function for gamma have recently been offered based on primate V1 data from Burns et al. (2011). Most important for the studies conducted here, Chalk et al. (2010) have found that allocation of attention *reduces* gamma LFP expression and spike-field coherence in monkey V1, and suggest that

gamma modulation in this area is a "byproduct" of other attentional mechanisms and not a causal contributor to perceptual ability.

These studies suggest that gamma allocation is not related to perceptual capability outside of higher visual neocortex. Similarly, almost no studies have been conducted of gamma expression in other high performance sensory neocortices. Specifically, to our knowledge only one study has examined expression of gamma in the barrel cortex of behaving rodents (Hamada et al., 1999). These authors found that gamma expression predicted subsequent onset of exploratory whisking, in apparent agreement with the more general view that this oscillation indicates the allocation of sensory attentional processes (which are also indicated by exploratory whisking). No study, to our knowledge, has systematically examined whether natural variations in gamma oscillations predict perceptual success in any neocortical area, and specifically not in barrel cortex.

The studies reported in this Chapter and the next directly address several of the questions central to the ongoing debate as to the meaning of neocortical gamma for perception. Specifically, we tested whether neocortical gamma in a primary sensory neocortex, and specifically in barrel cortex, predicts perception. In contrast to the recent findings in monkey V1, our data show that gamma expression predicts enhanced sensory processing, in favor of the more general view that this dynamic could play a role in information processing. This finding is supported in the following Chapter, where we further found that gamma *induction* can lead to enhanced perceptual success.

Inverse Relations between Alpha and Gamma: A Single State or Dissociable Dynamics?

The proposed perceptual roles for alpha and gamma suggest, in broad terms, an inverse relationship between these neocortical dynamics: Increased alpha should predict decreased gamma and vice versa. Jensen and colleagues have recently argued that these two rhythms are explicitly opposed, with expression of one decreasing expression of the other (see the **Introduction** for an extensive quote describing their view). A further goal of the proposed studies was to understand whether these oscillations are inherently interdependent, or whether their expression should be considered independent. Evidence from analysis of their perceptual impact, their pattern of electrophysiological co-expression and the absence of coincident changes with causal circuit control using optogenetics all favor the *independence* of these dynamics, despite their generally opposed relationship as regards to perceptual success.

3.4 Methods

Animals

All mice were male parvalbumin-Cre (PV-Cre) heterozygotes, derived from PV-Cre knock-in mice back-crossed into a C57BL/6J line (gift from S. Arber, now available as Jackson Laboratory strain B6;129P2-Pvalbtm1(cre)Arbr). Mice were 8-10 weeks old at the time of initial surgery. Animals were individually housed and maintained on a 12-hour light/dark cycle (lights out at 9:00 PM). All experimental procedures and animal care protocols were approved by the Massachusetts Institute of Technology Institutional Animal Care and Use Committee and were in accordance with NIH guidelines.

Fiber-optic–electrode implants

Implants (Siegle 12) were constructed around a custom plastic base, designed in SolidWorks (Dassault Systems, Waltham, MA) and printed via stereolithography in Accura 55 plastic (American Precision Prototyping, Tulsa, OK). The plastic base held 8 electrodes around a central fiber optic cable (Doric Lenses, Quebec, Canada). Electrodes were made from 12.5 μm polyimide-coated nichrome wire (Kanthal, Halstahammar, Sweden), twisted and heated to form tetrodes or stereotrodes (Nguyen et. al, 09). In three animals, the electrodes were stationary. In two animals, electrodes were fixed to laser-cut plastic springs (Pololu, Las Vegas, NV) individually driven by miniature screws. Electrodes were attached to a custom electrode interface board (Sunstone, Mulino, OR) with gold pins (Neuralynx, Bozeman, MT). Individual electrodes were gold plated to an impedance of 200-400 kΩ. The fiber optic cable had an inner diameter of 200 μm and a cladding diameter of 260 μm, and was terminated with a 1.25 mm metal ferrule.

AAV vectors

ChR2 fused to the fluorescent protein mCherry was cloned in the antisense direction into pAAV-MCS (Stratagene) to create AAV DIO ChR2-mCherry. ChR2-mCherry was flanked by a pair of canonical loxP sites and a pair of mutated lox2272 sites. A woodchuck hepatitis B virus post-transcriptional element was placed in sense direction 5′ of the poly(A). Adeno-associated viral particles of serotype 2 were produced by the Vector Core Facility at UNC Chapel Hill.

Surgical procedure

Mice were anesthetized with isofluorane gas anesthesia (0.75-1.25% in 1 L/min oxygen) and secured in a stereotaxic apparatus. The scalp was shaved, wiped with hair removal cream, and cleaned with iodine solution and alcohol. Following IP injection of Buprenex (0.1 mg /kg, as an analgesic) and dexamethasone (4 mg/kg, to prevent tissue swelling) and local injection of lidocaine, the skull was exposed with an incision along the midline. After the skull was cleaned, two small stainless steel watch screws were implanted in the frontal skull plates, one of which served as ground. Next, a ~1.5 mm-diameter craniotomy was drilled over barrel cortex of the left hemisphere (1.5 mm posterior to bregma and 3.5 mm lateral to the midline). Virus was delivered through a glass micropipette attached to a Quintessential Stereotaxic Injector (Stoelting). The glass micropipette was lowered through the dura to a depth of 450 μm below the cortical surface. A bolus of 1 μl of virus (AAV DIO ChR2-mCherry; 2×10^{12} viral molecules per ml) was injected into the cortex at 0.05 μl/min. After the injection, the pipette was held in place for 10 min at the injection depth and 10 min at a depth of 200 μm before being fully retracted from the brain. The fiber-optic–electrode implant (Fig. S3a) was aligned with the craniotomy at an angle of 15º from vertical and lowered to the surface of the cortex, centered approximately 200 μm anterior to the injection site. If anything more than a small amount of bleeding resulted from electrode implantation, the surgery was cancelled. Once the implant was stable, a small ring of dental acrylic was placed around its base. A drop of surgical lubricant (Surgilube) prevented dental acrylic from contacting the cortical surface. A custom head post made from durable plastic (APProto) was then affixed to the skull with adhesive luting cement (C&B Metabond). Once the cement was dry, the scalp incision was closed with

46

VetBond (3M), and mice were removed from isoflurane. Mice were given 3-10 days to recover prior to the start of water restriction.

Stimulus delivery and behavioral control

Vibrissae were stimulated by computer-controlled movements of piezoelectric wafers (Noliac, Kvistgård, Denmark). Stimulations consisted of high-speed deflections in the dorsal direction with a raised cosine velocity profile (5 ms duration). Vibrissae were held with a silk suture loop fed through a 4 mm, 21-gauge stainless steel cannula, which was attached to the piezoelectric wafer via a glass capillary tube (0.8 mm outer diameter). As many vibrissae as possible were secured, centered around the C2 vibrissa, and gripped approximately 5 mm from the mystacial pad. Mice were photographed from above at the start of each session to confirm which vibrissae were being stimulated. For maximum-amplitude deflections, vibrissae moved approximately 1 mm at the point of contact. Water delivery was based on gravitational flow controlled by a solenoid valve (Lee Co., Westbrook, CT) connected with Tygon tubing. Mice received distilled water through a plastic tube mounted on a piezoelectric wafer with epoxy. This "lick tube" was positioned near the animal's mouth using a micromanipulator. The water volume was controlled by the duration of valve opening (30-60 ms), calibrated to give ~8 μl per opening. Individual licks were detected by amplifying and thresholding the output of the piezoelectric wafer using a custom circuit board.

The light stimulus was delivered through a jacketed fiber-optic cable 200 μm in diameter and 2.5 m long (Doric Lenses, Quebec, Canada) connected to a 473 nm laser (Opto Engine, Salt Lake City, UT). Laser light passed through an adjustable neutral-density filter and a collimator (Thorlabs PAF-X-15-PC-A) before entering the fiber. The 2.5 m fiber was connected to the animal's head via two mating metal ferrules sheathed in a zirconia sleeve. Light loss for this connection was measured for each implant prior to surgery, and was usually around 50%. The amplitude of the light stimulus was calibrated daily with an optical power meter (Thorlabs PM100D with S120C sensor). Light power at the surface of the cortex was estimated to be ~1 mW, or 30 mW/mm2.

All behavioral events, piezoelectric control, reward delivery, laser stimulation, and lick measurements were monitored and controlled by custom software written in LabVIEW and interfaced with a PCI DIO board (National Instruments, Austin, TX).

Trial structure

On each trial, vibrissae were stimulated for 400 ms at a single amplitude, varying between 0 ("blank" trials) and 1 mm ("maximal" trials). Amplitude did not vary within a given trial. For any given session, all stimuli consisted of either 40 Hz, 20 Hz, or "naturalistic" deflections. On laser-stimulation trials, 1 ms light pulses were delivered at 40 Hz for 600 ms. Vibrissae deflections began after the fourth light pulse. The precise timing of the vibrissae deflections relative to the light pulses was varied across five phases, but remained consistent within individual trials. For all sessions, inter-trial intervals were uniformly distributed between 4 and 6 s.

If mice licked the reward spout at any point up to 500 ms after the onset of the vibrissae stimulus, a drop of water was delivered. After a slight delay, any remaining water was removed via vacuum suction. This prevented mice from receiving reward that was not immediately preceded by a vibrissae stimulus.

Behavioral training
Mice were trained to a simple whisker deflection task. Training began after at least 3 days of post-operative recovery and at least 7 days of water restriction (1 ml/d). At the beginning of each session, mice were secured to the head post apparatus with their bodies placed inside a Falcon tube. Initial training sessions lasted approximately 5 minutes, to allow mice to accommodate to head fixation. At first, all trials were maximal, with no blank trials. On successive days, training time was gradually increased to 45 minutes. Blank stimuli (up to 10%) were randomly interleaved and the probability of non-maximal stimuli was increased to 30%. Before moving to the next stage of training, each mouse had to perform two sessions in which it performed with an overall d' of 1.25.

After reaching criterion on the training task, laser light stimulation was added on a subset of trials. Laser stimulation was given ~100 ms preceding tactile stimulation for a duration of 600 ms (100 ms post stimulation) at ~1 mW power on the cortical surface. 50% of trials were at a single threshold value ranging from 20-40% of the maximum stimulus amplitude, with the same duration to peak amplitude (5 ms). 30% of trials were blank, with the remaining 20% of trials at max amplitude, to keep the animals engaged. On half of all trials, laser stimulation was presented at one of 5 temporal offsets (Figure 3a).

Mice that did not consume 1 ml of water during the training sessions were supplemented with water in their home cage several hours after the experiment finished.

Electrophysiology
Spikes and local field potentials were recorded using stereotrodes or tetrodes integrated into a custom implant (Siegle 12). Recording electrodes were either implanted 300–400 μm from the surface of the cortex during surgery, or lowered to the same depth over the course of several days. Throughout the recording session, broadband signals referenced to ground and digitized at 40 kHz (Recorder/64, Plexon, Dallas, TX). Electrophysiology data was synchronized with behavioral data via TTL pulses at the start of each trial.

Histology
At the end of training, electrodes sites were lesioned with 15 μA of current for 10 s. Mice were transcardially perfused with 100 mM PBS followed by 4% formaldehyde in PBS. Brains were post-fixed for at least 18 h at 4 °C. 60 μm sections were mounted on glass slides with Vectashield (Vector Laboratories), coverslipped, and imaged with an upright fluorescent microscope. Viral expression was confirmed in all animals. Expression was generally limited to the upper layers of barrel cortex (II-IV). In one animal, expression was also observed in the lower layers (V and VI). Ventral/medial and anterior/posterior spread of the virus ranged between 0.5 and 1.5 mm, encompassing 1-3 barrel columns.

48

Data analysis

Data analysis was performed in Matlab (Mathworks, Natick, MA). Raw data from LabVIEW was converted to event times for behavioral analysis. Trials were first filtered based on d' according to the following procedure: (1) hit rate and false alarm rates were calculated for blocks of 50 trials, slid in 1-trial intervals. A negative offset was added to the hit rate and an equal-but-opposite offset was added to false alarms, to prevent d' saturation. An offset of 0.04 was used for all analyses, except the natural stimulation condition, where an offset of 0.025 was used to include more trials. Hit rate was capped at a minimum value equivalent to the offset and false alarm rate was capped at a maximum value equivalent to 1 minus the offset. (2) d' was calculated as Z(hit rate) – Z(false alarm rate), where Z stands for the inverse of the Gaussian distribution function. (3) For any blocks with d' above a threshold value of 1.25, the middle trial (trial 25) was included in the analysis. After d' filtering, trials with pre-stimulus licks within one second of trial onset were also eliminated. Trials were selected from the remaining subset based on the parameters of the vibrissae and laser stimuli. Hit rate, d', and median reaction time were calculated for each animal for each set of parameters.

Continuous electrophysiological data from the Plexon system was either low-pass filtered (3rd-order Butterworth) and downsampled to 2 kHz or filtered between 600 and 6000 Hz (acausal FIR filter) and thresholded to extract spikes. Stimulus-evoked potential statistics were calculated on the mean SEP for each animal, taken from an electrode with clear vibrissae and laser responses. One animal had electrophysiology that was contaminated with 60 Hz line noise, and was therefore not included in the analysis.

Time evolution of spectral power This metric was calculated using a complex wavelet analysis, from which time–frequency representations (TFRs) of near instantaneous changes were determined. The TFRs were calculated from 1 to 100 Hz on the LFP time courses by convolving signals with a complex Morlet wavelet of the form w(t, f0)= A exp(-t 2/2[t2])exp(2i*pi*f0t), for each frequency of interest f0, where sigma (t) = m/2*pi*f0, and i is the imaginary unit. The normalization factor was A = 1/(sigma(t)* sqrt(2*pi), and the constant m defining the compromise between time and frequency resolution was 7, consistent with the Jones et al. (2009) study. Time–frequency representations of mu-alpha and mu-beta and gamma power were calculated as the squared magnitude of the complex wavelet-transformed data averaged across the range of interest. For the prestimulus analysis, baseline was calculated as average power [-250, 0] ms relative to the stimulus. This time period was chosen to because of short time scale of gamma rhythm, all analysis for alpha and beta was repeated on a 1000 ms window, consistent with Jones et al., 2009, and was shown to have a similar result (data not shown).

3.5 Results

General Analysis of the Relationship of Oscillatory Power and Detection Probability

Figure 1 shows the power spectral density of the LFP in SI during 1 second prior to vibrissa deflection across all electrodes that were driven by sensory stimulation. Each line represents data from a single mouse (N = 3 mice, F1, F2 and F5). In mouse F1, 6 electrodes

out of 8 implanted in SI showed a significant evoked response to multi-vibrissal stimulation; In F2, 6 of 8; in F5, 8 of 8. Consistent with the well-described 1/f relationship typical of brain oscillations (Buzsaki, 06), and parallel to similar data from human (please see **Chapter 2, Figure 1**), each animal showed highest relative power at lowest frequencies.

The spectrograms in **Figure 2** show the relationship between oscillatory power and probability of detection. **Figure 2Ai** shows the mean across animals for hit trials, **Figure 2Aii** shows the mean for miss trials. **Figure 2B** shows the subtraction of these two plots (hotter colors indicate higher activity on hit trials). **Figure 2B** shows that prior to stimulus onset, lower frequencies in the alpha range showed *decreased* power (cold colors) in SI when the animal was going to be successful, whereas there was increased power in the gamma range for hits (warm colors).

Figure 3A shows the relative power across frequencies on hits – misses for the pre-stimulus period 250 msec prior to vibrissa deflection in each mouse. As reflected in the color spectrograms in **Figure 2**, all individual animals showed lower relative power in alpha (7-14 Hz) for hits, and higher relative power in gamma (30-80 Hz) for hits. This pattern is also evident in the mean (**Figure 3B**, SEM is plotted across animals). For comparison with prior primate studies of the impact of attentional allocation on such LFP measures, we included Figure 5A from Fries et al. (2008 *J Neuroscience*). In agreement with our findings regarding perceptual success, these authors found that attentional allocation predicted decreased alpha band power and increased gamma power. The magnitude of these effects in the gamma range is similar, with peak effects of ~10% change.

Relation Between Pre-Stimulus Alpha Power and Perceptual Success

To systematically examine the relationship between alpha power and perceptual success, we divided the expression of alpha oscillations for each animal into quartiles, and then plotted the hit rate for each quartile (for an identical approach applied to human MEG data, please see the decile segmented plots in **Chapter 2, Figure 3**). **Figure 4A** shows the systematic relationship between alpha power and detection probability for threshold level stimuli, with increasing power predicting decreased likelihood of success. This impact was statistically significant (p < .002, r=-0.80, Pearson's Correlation Coefficient).

To directly compare our data to the prior reports of Wiest and Nicolelis (2003), we further analyzed these data more crudely, as the relative probability of obtaining a hit as a function of either high alpha (top 50% of observations) or low alpha (lower 50%). As shown in **Figure 4B**, in agreement with their results, variation in alpha power did not significantly impact detection of a supramaximal stimulus. However, as indicated in **Figure 4A**, threshold stimulus detection was lower during higher alpha expression, with a ~40% difference in hit rate between conditions. This relationship was present in all three animals (**Figure 2**). These findings replicate the main finding of Wiest and Nicolelis (2003) with regards to supramaximal stimuli and directly contradict their hypothesis that alpha enhances detection of threshold level stimuli.

Relation Between Pre-Stimulus Gamma Power and Perceptual Success

We similarly plotted the relation between gamma power broken into quartiles and hit rate (**Figure 5A**). While these effects were in general weaker than those observed for alpha, a significant relationship was observed ($r = -.80$, $p < .002$, Pearson's correlation coefficient). Similarly, when these data were plotted as in **Figure 4**, we found that higher gamma levels predicted ~7% increase in hit probability relative to low gamma (**Figure 5B**). Although all three animals showed higher power in the gamma range (**Figure 3A**) and although the quartile-based analysis was significant (**Figure 5A**), this simpler binary analysis did not prove significant ($p = .11$, 2-tailed t-test), underpowered due to the treatment of sampling as across animal ($N = 3$). We conducted this binary analysis for all electrodes that showed a vibrissa evoked response. This analysis across electrodes ($N = 15$, not plotted) showed significantly higher hit rates during higher gamma epochs, revealing a mean increase in the probability of detection at high gamma of 8.4% [8.9% SEM; $p = .009$ 2-tailed t-test], with 15 of 20 electrodes showing this effect ($p = .04$, 2-tailed Sign Test).

Conjoint Analysis of Alpha and Gamma

Our data in mice support the prediction that alpha negatively predicts perceptual outcome and gamma positively predicts it. To understand their conjoint impact in greater detail and to assess whether alpha and gamma are in a simple antagonistic relationship as recently postulated by Jensen and Mazaheri (2010) we conducted the following further analyses.

Figure 6A shows as a color map the hit rate as a function of the expression of alpha and gamma, broken into quartiles. To make this plot, the values required for membership in each quartile were first calculated (as in **Figures 4A** and **5A**). The hit rate was then calculated for those trials whose conjoint expression of these values fell into these bins. Note that this analysis is uneven with respect to the number of trials in each bin, a relationship examined in greater detail below in **Figure 7**.

As can be seen from this plot, while a general relationship of lower gamma predicting lower hit rate is evident, this prediction varied as a function of alpha co-expression. Specifically, under conditions of higher alpha power (top 2 rows), gamma showed the predicted systematic increase in hit rate with increased power. In contrast, however, at lower alpha power (bottom two rows), an inverted U relation was evident, with the 3rd quartile showing highest rates. These relations between gamma power and hit rate as a function of alpha co-expression are plotted in **Figure 6B**. As shown in **Figures 6A** and **6C**, the correlation of pre-stimulus alpha power with hit rate showed greater relative independence from gamma variation, though at highest gamma levels (rightmost column of **Figure 6A**), a less systematic correspondence was observed.

This analysis shows that the relation between alpha and gamma with regard to perceptual success is not a simple interdependent progression. Most notably, at low alpha levels, gamma power did not show the same systematic increase as seen in the mean (**Figure 5A**) or as seen at higher alpha levels (**Figure 6A, top rows**).

A further prediction of the dependent inverse relationship postulated by Jensen and Mazaheri (2010) is that a preponderance of the trials showing high alpha power should

show low gamma power. **Figure 7** shows the distribution of trials demonstrating conjoint participation in the two rhythms in each of the quartile bins plotted in **Figure 6A**. If alpha and gamma are negatively related in their expression probability, highest values should be observed extending from the upper left to the lower right of this plot (a line of warmer colors should extend this way). In contrast, the opposite is observed, with a trend towards co-expression of these two rhythms. While this finding might be explained for highest alpha and gamma levels by overall increase in power for sharp "delta" spike events (upper right corner), this justification does not explain co-expression of the lowest values of each rhythm (warm colors in the lower left). While our analyses to date have not attempted to provide a mechanistic explanation for this pattern, the simple point that we take from this plot here is that these are <u>not</u> inherently antagonistic rhythms in their mechanisms of origin, in contrast to the Jensen and Mazaheri (2010) prediction.

In further support of this idea, causal evidence that expression of gamma does not negatively impact alpha expression is provided in **Figure 8**, where we examine the impact of optogenetic activation of FS on alpha expression and compare its impact to other trial types. In this figure, the power in alpha is plotted for blank trials (*green line* no stimulus presented and no optogenetic drive of FS applied), for trials in which no stimulus was presented but robust gamma oscillations were induced by optogenetic drive of FS (*red line*), and on trials in which a threshold-level sensory stimulus was presented but no optical stimulus presented and the animal failed to detect the stimulus (*blue line*). This third category was chosen because the lick response to hit trials interferes with the post-event calculation in alpha fluctuations, so we chose miss trials on which no licking was present. The three electrodes selected for this analysis were those that showed strongest gamma induction in each animal, respectively.

What **Figure 8** reveals is that even an entirely subliminal sensory stimulus—present on 'miss' trials—was robust enough to generate the well-characterized event related desynchronization of alpha power (see **Background** in **Chapter 2**, Pfurtscheller 92; 97). This decrease in power can be seen in the *blue* trace. In contrast, almost no decrease in ongoing alpha power was observed with optical drive of FS (*red*). Further, this small effect was observed only in the mean (averaged across the 3 animals): 2 of 3 of the animals showed no negative impact of gamma induction on alpha power (data not shown). This lack of an impact of selective FS recruitment, which drives robust gamma expression (Cardin et al., 2009), on alpha expression underscores the mechanistic independence and the lack of cross-frequency contamination in the LFP recording of these two rhythms.

3.6 Discussion

In contrast to the hypotheses of Nicolelis and colleagues, our data confirm the view that alpha power predicts failed tactile detection of threshold level stimuli (**Figures 2-4 and 6**). These findings using LFP in mouse barrel cortex are in agreement with the view from human work, including our own (**Chapter 2**). The primary point of logic in the Nicolelis view is that thalamic bursting should enhance sensory transmission to the neocortex, a view shared by many (e.g., Swaldow et al. 01). One possible explanation for the difference in the EEG/MEG alpha phenomena and that which is predicted from work on bursting in

the thalamus is that the thalamocortical rhythmic bursting characteristic of alpha may be different from localized single neuron bursting. If the burst event was local and expressed by single neurons in an active network, one may observe that this single neuron was more effective at driving a downstream response (Swadlow et al. 01).

In agreement with the view that gamma oscillations could make a beneficial contribution to the transmission of information through sensory neocortex, our data show that higher pre-stimulus gamma power predicts tactile detection (**Figures 2, 3, 5** and **6**). These positive effects were weaker than the negative effects observed in alpha, and were found to be dependent on the relative level of alpha expression (e.g., **Figure 6A-B**). In particular to find significance in a simple binary test, we had to analyze single electrodes, which assumes independence across electrodes. This may be a problem in particular when we are using a simple go/no-go task, where performance is correlated within animals. However, the trend of power positively correlated with behavioral performance, when the power was divided into quartiles, was significant with N=3, animals used. This suggests that more animals may be necessary to solidify this result.

This finding is important for several reasons. First, outside of work in the rodent hippocampus, where the gamma oscillation is seen when rats and mice navigate a maze, gamma band activity has not previously been systematically linked to perception or attention in rodent cortex. Further we found that this rhythm is positively correlated with task performance, as predicted by the allocation of this dynamic with attention in primate studies.

These finding disagree with the emerging view from primate primary visual neocortex that gamma expression in V1 does not contribute to or correlate with perceptual success. There are many similarities between barrel cortex of rodent and primary visual cortex of primates—primate V1 and barrel neocortex are the primary representation of the dominant high-resolution sensory modality for that species, primate V1 and barrel neocortex are both show multiple well-organized feature maps (Andermann et al., 2004; Andermann and Moore, 2006; Kremer et al., 2011) (a property not observed, for example, in mouse V1), primate V1 and barrel neocortex are the largest single neocortical areas in the respective brains of those animals, and primate V1 and barrel neocortex are both show strong differentiation of metabolic activity indicators across the neocortical sheet (e.g., cytochrome oxidase). <u>We therefore suggest that our finding may be in real contradiction to the primate V1 findings, not simply a cross-species or cross-area difference.</u>

Our data directly disagree with the view that alpha and gamma are in an inherent inverse relationship with respect to their dynamics. These rhythms show more subtlety in their cross-frequency relationship to detection (**Figure 6A-B**), they co-vary in their expression (**Figure 7**) and induction of gamma does not impact alpha expression (**Figure 8**). Thus, while we agree with the primary (and most important) hypothesis presented by Jensen and

Mazaheri (2010)—that alpha predicts decreased capability and gamma predicts success—we disagree with the coupling between these two rhythms postulated by those authors.

3.7 References

Andermann ML, Ritt J, Neimark MA, Moore CI. Neural correlates of vibrissa resonance; band-pass and somatotopic representation of high-frequency stimuli. Neuron. 2004 May 13;42(3):451-63.

Andermann, M.L. and C.I. Moore, A somatotopic map of vibrissa motion direction within a barrel column. Nat Neurosci, 2006. 9(4): p. 543-51.

Berger, H. (1929). Über das Elektroenkephalogramm des Menschen. Arch. Psychiatr. Nervenkr. 87, 527–570.

Börgers, C. & Kopell, N. J. Gamma oscillations and stimulus selection. Neural Comput 20, 383-414 (2008).

Burns SP, Xing D, Shapley RM. Is gamma-band activity in the local field potential of V1 cortex a "clock" or filtered noise? J Neurosci. 2011 Jun 29;31(26):9658-64.

Buzsàki G, Eidelberg E. Phase relations of hippocampal projection cells and interneurons to theta activity in the anesthetized rat. Brain Res. 1983 May 5;266(2):334-9.

Buzsáki, G. Rhythms of the Brain (Oxford Univ Press, Oxford, 2006).

Cardin, J. A., Carlén, M., Meletis, K., Knoblich, U., et al. Driving fast-spiking cells induces gamma rhythm and controls sensory responses. Nature 459, 663-667 (2009).

Chalk M, Herrero JL, Gieselmann MA, Delicato LS, Gotthardt S, Thiele A. Attention reduces stimulus-driven gamma frequency oscillations and spike field coherence in V1. Neuron. 2010 Apr 15;66(1):114-25.

Dang-Vu TT, McKinney SM, Buxton OM, Solet JM, Ellenbogen JM. Spontaneous brain rhythms predict sleep stability in the face of noise. Curr Biol. 2010 Aug 10;20(15):R626-7.

Fanselow, E.E. and M.A. Nicolelis, Behavioral modulation of tactile responses in the rat somatosensory system. J Neurosci, 1999. 19(17): p. 7603-16.

Fanselow, E.E., et al., Thalamic bursting in rats during different awake behavioral states. Proc Natl Acad Sci U S A, 2001. 98(26): p. 15330-5.

Fries, P., Reynolds, J. H., Rorie, A. E. & Desimone, R. Modulation of oscillatory neuronal synchronization by selective visual attention. Science 291, 1560-1563 (2001).

Fries, P., Womelsdorf, T., Oostenveld, R. & Desimone, R. The effects of visual stimulation and selective visual attention on rhythmic neuronal synchronization in macaque area V4. J Neurosci 28, 4823-4835 (2008).

Hamada Y.,E. Miyashita, and H. Tanaka. Gamma-band oscillations in the "barrel cortex" precede rat's exploratory whisking. Neuroscience. 1999;88(3):667-71.

Jensen, O., and Mazaheri, A. (2010). Shaping functional architecture by oscillatory alpha activity: gating by inhibition. Front. Hum. Neurosci. 4:186.

Jones SR, Pritchett DL, Sikora MA, Stufflebeam SM, Hämäläinen M, Moore CI (2009) Quantitative analysis and biophysically realistic neural modeling of the MEG mu rhythm: rhythmogenesis and modulation of sensory-evoked responses. J Neurophysiol 102:3554 –3572.

Jones SR, Pritchett DL, Stufflebeam SM, Hämäläinen M, Moore CI (2007) Neural correlates of tactile detection: a combined MEG and biophysically based computational modeling study. J Neurosci 27:10751–10764.

Knoblich, U., Siegle, J. H., Pritchett, D. L. & Moore, C. I. What do we gain from gamma? Local dynamic gain modulation drives enhanced efficacy and efficiency of signal transmission. Front Hum Neurosci 4, 1-12 (2010).

Kremer Y, Léger JF, Goodman D, Brette R, Bourdieu L. Late emergence of the vibrissa direction selectivity map in the rat barrel cortex. J Neurosci. 2011 Jul 20;31(29):10689-700.

Linkenkaer-Hansen K, Nikulin VV, Palva S, Ilmoniemi RJ, Palva JM (2004) Prestimulus oscillations enhance psychophysical performance in humans. J Neurosci 24:10186 – 10190.

Nguyen, D. P., Layton, S. P., Hale, G., et al. Micro-drive array for chronic in vivo recording: tetrode assembly. J Vis Exp 26 (2009).

Nicolelis M.A., Fanselow E.E. Dynamic shifting in thalamocortical processing during different behavioural states. Philos Trans R Soc Lond B Biol Sci. 2002 Dec 29;357(1428):1753-8.

Nicolelis, M.A. and E.E. Fanselow, Thalamocortical [correction of Thalamcortical] optimization of tactile processing according to behavioral state. Nat Neurosci, 2002. 5(6): p. 517-23.

Palva S, Linkenkaer-Hansen K, Naatanen R, Palva JM. (2005) Early neural correlates of conscious somatosensory perception. J Neurosci 25: 5248– 5258.

Pfurtscheller G (1992) Event-related synchronization (ERS): an electrophysiological correlate of cortical areas at rest. Electroencephalogr Clin Neurophysiol 83:62– 69.

Ray, S. & Maunsell, J. H. Differences in gamma frequencies across visual cortex restrict their possible use in computation. Neuron 67, 885-896 (2010).

Siegle, J. H. Combining optical stimulation with extracellular electrophysiology in behaving mice. In Fellin, T. & Halassa, M. M., Eds. Neuronal Network Analysis (Humana Press, New York, 2012).

Swadlow, H. A. & Gusev, A. G. The impact of 'bursting' thalamic impulses at a neocortical synapse. Nat. Neurosci. 4, 402–408 (2001).

Tiesinga P., Sejnowski T.J. Cortical enlightenment: are attentional gamma oscillations driven by ING or PING? Neuron. 2009 Sep 24;63(6):727-32.

Wiest, M.C. and M.A. Nicolelis, Behavioral detection of tactile stimuli during 7-12 Hz cortical oscillations in awake rats. Nat Neurosci, 2003. 6(9): p. 913-4.

Womelsdorf T, Fries P, Mitra PP, Desimone R (2006) Gamma-band synchronization in visual cortex predicts speed of change detection. Nature 439:733–736

3.8 Figures

Figure Legends
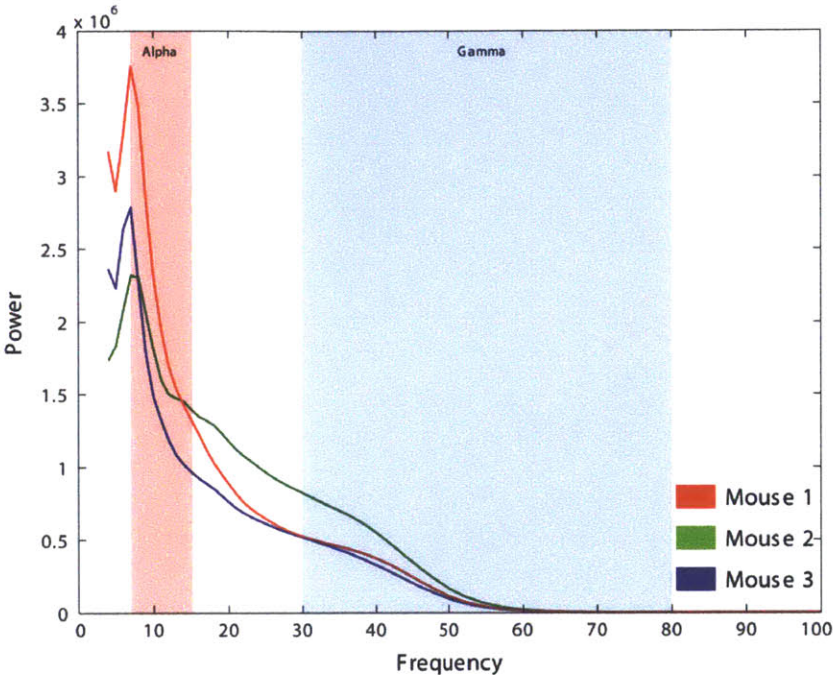
Figure 1 | Power Spectral Density for Individual Mice Spectra were taken for all electrodes that showed a significant vibrissa-driven response and then averaged within each mouse used for the data analysis in this Chapter (N = 3).
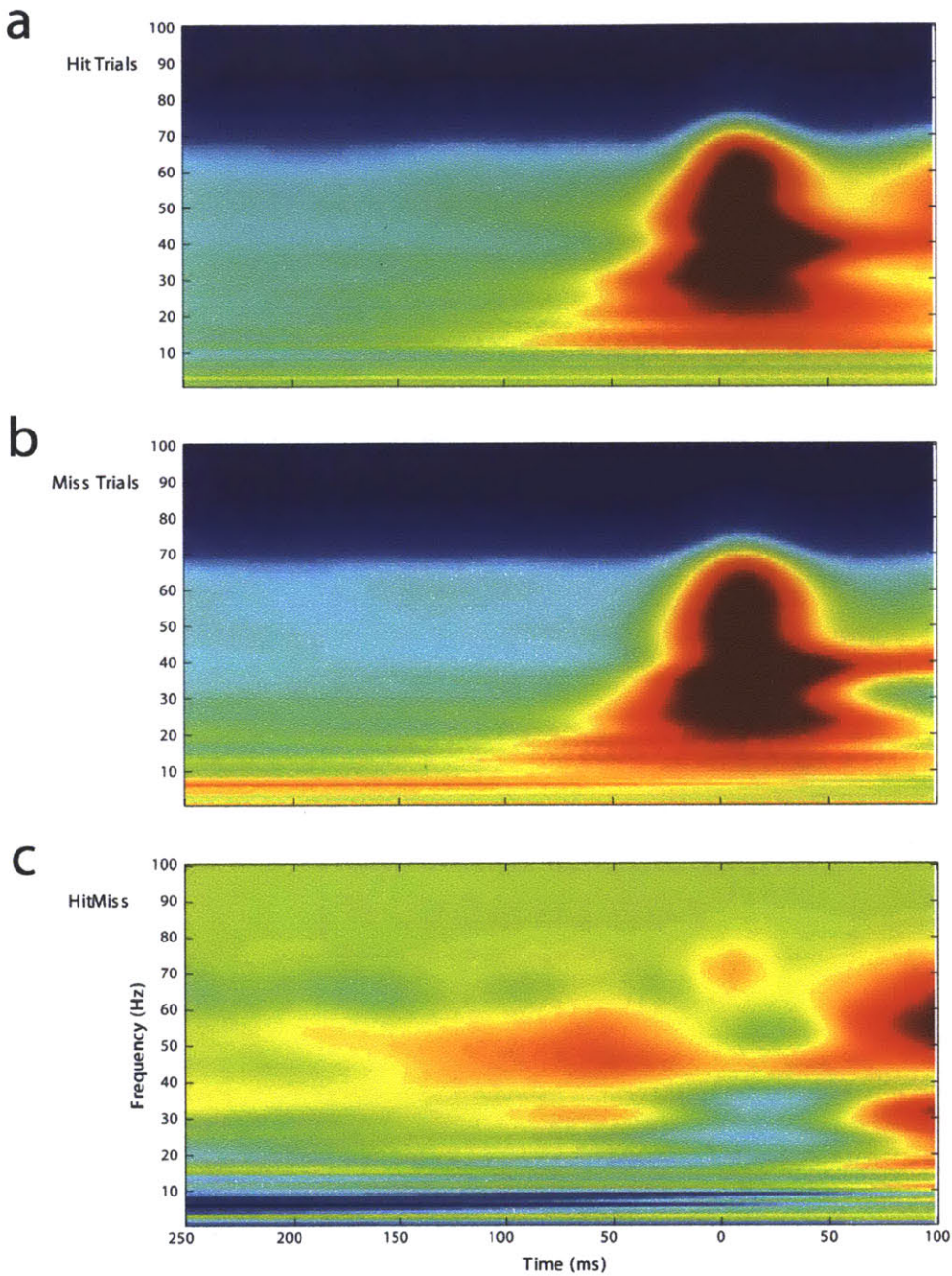
Figure 2 | Spectrograms of LFP Power During Task Performance a. Averaged across N = 3 mice, the mean spectrogram for all hit trials. Data were averaged across individual electrodes within each mouse prior to averaging across the group. b. Spectrogram for all miss trials calculated in the same fashion. c. Spectrogram of differences between hit and miss trials. Subtractions were conducted within-mouse prior to averaging across the group.
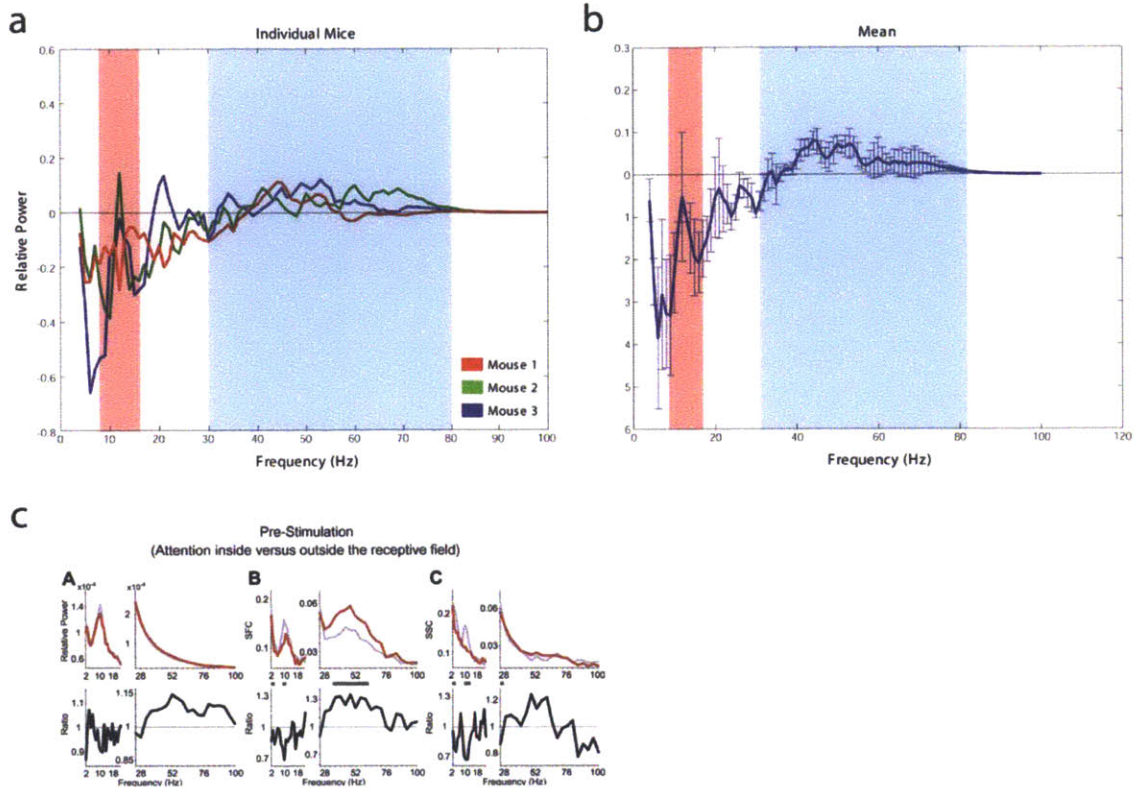
Figure 3 | Difference in the Power Spectral Density for the Time Period -250 to 0 milliseconds Before Tactile Stimulus Presentation Between Hit and Miss Trials a. Each animal, color code and analysis as in **Figure 1**. b. Mean across mice. c. Figure 5 from Fries et al. 2008, Figure 5. Attentional modulation of synchronization in the prestimulus period. The format is the same as in Figure 3, but showing the LFP power (A), SFC (B), and SSC (C) during the prestimulus interval, with attention directed inside (red) or outside (blue) the RF (top row) and the ratio between attentional conditions (bottom row).
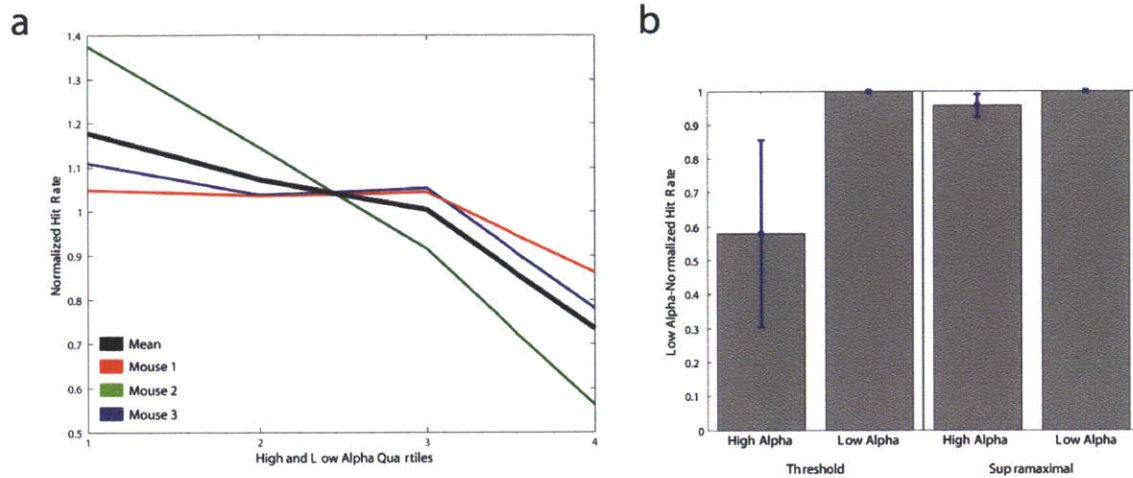
Figure 4 | Relation Between Pre-Stimulus Alpha Power and Stimulus Detection . For each mouse, the distribution of observed alpha power values for the period -250 to 0 milliseconds was broken into quartiles, and then the hit rate plotted for each. Thin lines show each mouse, thick line shows the mean. b. Following the general analysis scheme employed by Wiest and Nicolelis (2003), the hit rate for high (top 50% of values) and low alpha were measured for supramaximal sensory stimuli (two bars of right of figure). Values were normalized to the hit rate for low alpha (further right bar). The two bars on the left of the figure show the same analysis applied to threshold level tactile stimuli.

a

b
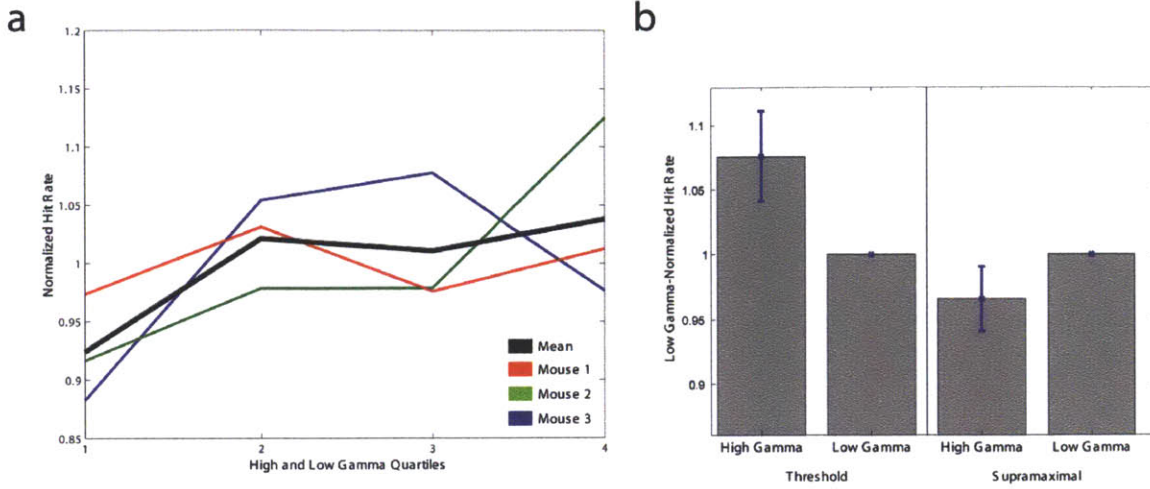
Figure 5 | Relation Between Pre-Stimulus Gamma Power and Stimulus Detection a.
Relation between quartile-sorted gamma power values and hit rate, as in Figure 4. b.
Relation between high and low gamma power values and hit rate, as in Figure 4B.

60
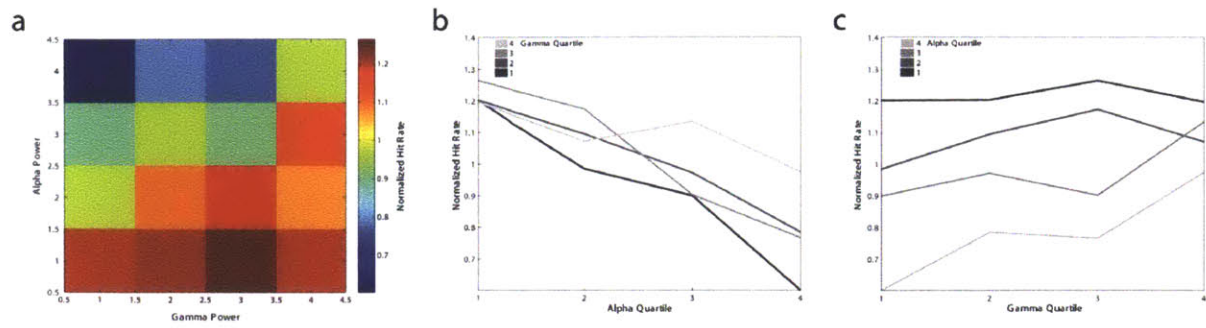
Figure 6 | Hit Rate as a Function of Alpha and Gamma Co-Expression A. Plot of the hit rate in trials that showed a combinations of alpha and gamma, segmented into the quartiles described above (please see text for full description). Hot colors indicate relatively higher hit rates for that bin. B. The hit rate as a function of gamma quartile, each line representing a different quartile alpha power level. Darker colors indicate lower alpha power values. C. The hit rate as a function of alpha quartile, each line representing a different quartile gamma power level. Darker colors indicate lower gamma power values.
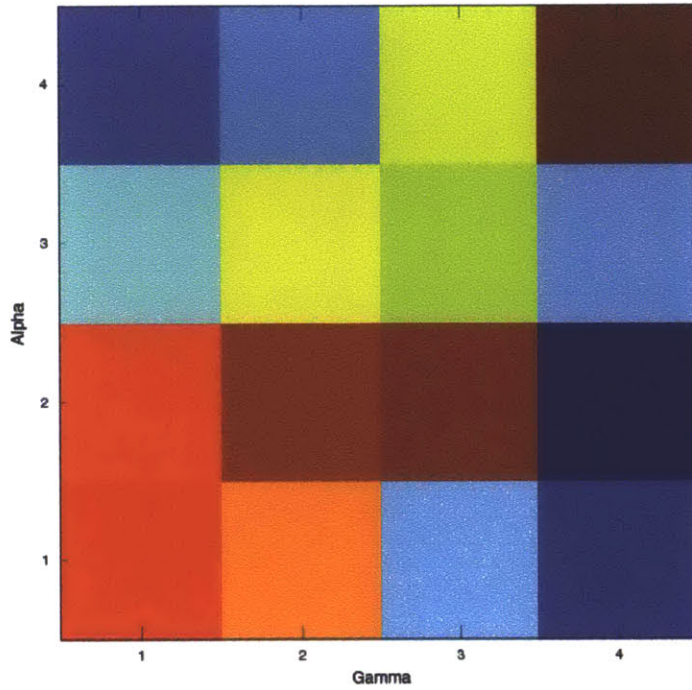
Figure 7 | The Probability of Alpha-Gamma Co-Expression at Different Power Levels
This plot shows the probability of a given trial falling into the bins that were used to show the relative conjoint impact of co-expression across these two frequencies on detection rate in **Figure 6A**.
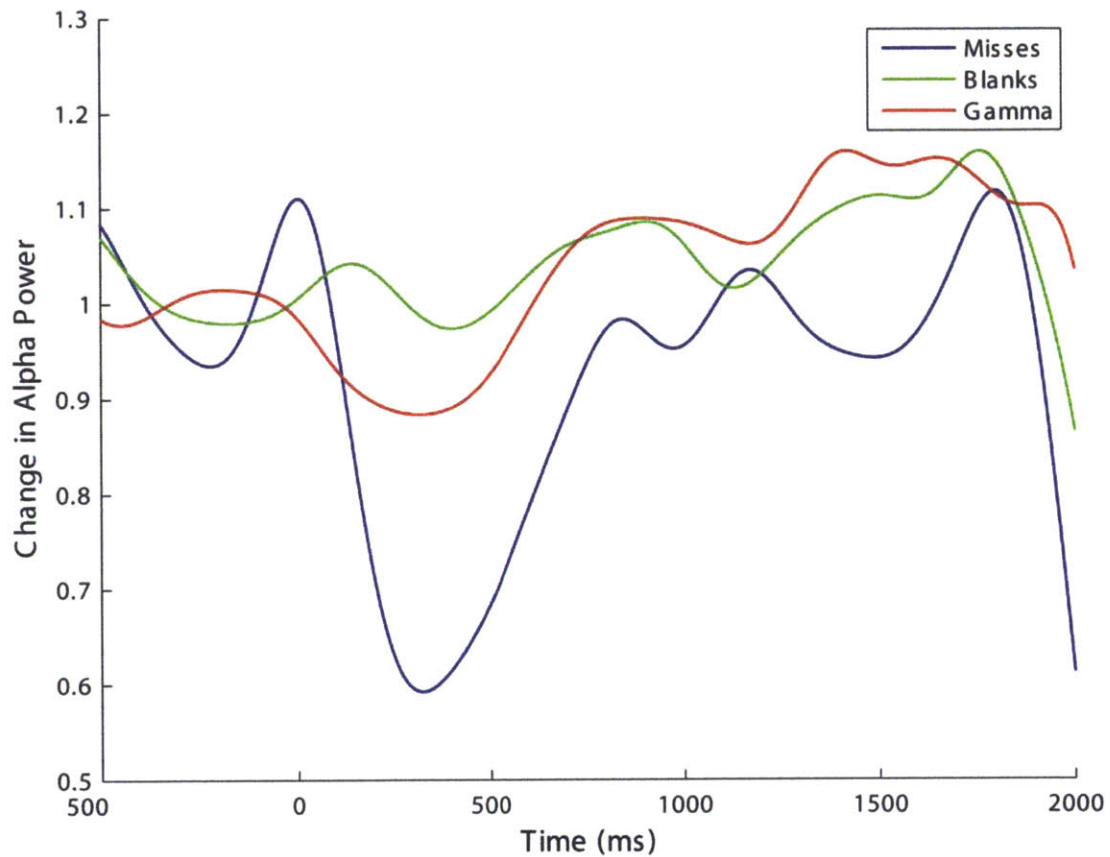
Figure 8 | The Impact of Optogenetic Gamma Induction and Subliminal Tactile Stimulation on Alpha Power Levels The *red* trace shows the impact on alpha power of fast-spiking neuron activation at 40 Hz for 600 milliseconds starting aligned to time zero. The *blue* trace shows the impact of a subliminal threshold level "missed" stimulus on alpha power, onset of sensory stimulation for 400 milliseconds aligned to time zero. The red trace shows natural fluctuations in alpha power on blank trials. Data were taken from the electrode in each mouse that showed the strongest optogenetic gamma induction and then averaged across animals.

Chapter 4

**Entraining Gamma Oscillations in Primary
Somatosensory Neocortex Enhances Tactile Detection**

4.1 Author Contributions

J.H.S., D.L.P., and C.I.M. designed the experiments. J.H.S. designed the implants and performed the viral injections. D.L.P. designed the behavioral rig and oversaw training. J.H.S. and D.L.P. analyzed the data and made the figures. J.H.S., D.L.P, and C.I.M. wrote the manuscript.

Siegle JH*, Pritchett DL*, and Moore CI [Manuscript submitted]

4.2 Abstract

Gamma oscillations (30-100 Hz) are hypothesized to enhance signal processing in the brain, an assertion that has generated significant debate. To test whether gamma can benefit perception, we used selective optogenetic drive of parvalbumin-positive, fast-spiking interneurons to generate 40 Hz oscillations in barrel cortex of mice performing a tactile detection task. Here, we show that gamma oscillations can enhance the detection of a sensory stimulus. This improvement was only observed when the temporal alignment between the entrained inhibition and sensory-evoked excitatory drive mimicked transformations that occur during attentional allocation. Subtly shifted stimulation patterns that did not produce these effects had no impact or led to a decrement in performance. Behavioral improvements did not result from changes in arousal, as entrained gamma did not benefit behavior at all phases of stimulus alignment, and the false-alarm rate did not change with optogenetic stimulation. Gamma-dependent perceptual enhancement was also observed for naturalistic tactile stimuli, but 20 Hz optogenetic drive did not facilitate detection. These results provide causal evidence that gamma in primary sensory neocortex can benefit perception in a mammalian model system.

4.3 Introduction

Gamma oscillations have been observed in multiple species across a diverse array of brain regions, and have been correlated with a variety of functional states, from memory consolidation to attention (Buzsáki 2006). The network-level mechanisms underlying gamma oscillations, which depend on rhythmic volleys of excitation and inhibition (Atallah and Scanziani 2009), suggest several ways they could benefit processing: through local gain modulation (Fries et al. 2001, Cardin et al. 2009, Knoblich et al. 2010), by mediating inter-areal communication (Gregoriou 2009, Colgin et al. 2009), or by feature binding (Singer 2008). In sensory neocortex, spiking becomes more tightly phase-locked to gamma oscillations with the allocation of attention, an effect that occurs without a decrement in stimulus-evoked firing rates (Fries et al. 2001, Womelsdorf and Fries 2007). This

65

transformation could benefit processing by making sensory responses more temporally compact, thereby increasing the impact of cell assemblies on downstream targets through a variety of potential mechanisms (Cardin et al. 2009, Knoblich et al. 2010, Steinmetz et al. 2000, Salinas and Sejnowski 2000, Azouz and Gray 2003, Börgers and Kopell 2008, Sohal et al. 2009). However, the prediction that neocortical gamma can enhance perception—by any mechanism—is a topic of substantial debate (Shadlin and Movshon 1999). Recent studies have concluded that the spatiotemporal dynamics of neocortical gamma are inappropriate for enhancing sensory processing, and that gamma expression is likely an epiphenomenal consequence of network drive (Ray and Maunsell 2010, Burns et al. 2011).

Optogenetic activation of fast-spiking interneurons can produce naturalistic gamma oscillations in the neocortex of anesthetized mice (Cardin et al. 2009). Under these experimental conditions, sensory responses to (vibrissal) stimulation showed effects emulating those occurring in response to the allocation of attention (Fries et al. 2001, Fries et al. 2008): the temporal distribution of evoked spikes was sharpened without decreasing overall firing rates (Supplementary Fig. 1). This transformation was only observed when stimuli were presented at a specific phase within the gamma cycle, likely because this phase aligned the 8-10 ms transmission time from the periphery to barrel cortex (Moore and Nelson 1998, Brecht and Sakmaann 2003, Brecht et al. 2003) with the recovery from optogenetically induced, synchronous inhibition (Cardin et al. 2009, Knoblich et al. 2010). To causally test the prediction that this transformation of the neocortical sensory signal benefits sensory perception, we entrained gamma oscillations in barrel cortex while mice performed a tactile detection task. Our manipulation increased inhibition in the neocortex and had no increase in firing rate. Using traditional spike counting analysis methods, this manipulation would not predict enhanced behavioral response, via enhanced transmission.

4.4 Methods

Custom fiber-optic–electrode implants were constructed from a plastic body, an electrode interface board, hand-cut polyimide and stainless steel tubing, twisted-wire stereotrodes or tetrodes, and a fiber-optic cable. During the implant surgery, 1 μL of virus (AAV DIO ChR2–mCherry) was injected at a rate of 0.05 μL/min at a depth of 450 μm beneath the cortical surface, at coordinates of -1.5 mm posterior and -3.5 mm lateral from bregma (Supplementary Fig. 2). The implant was placed slightly anterior to the viral injection site and sealed in place with dental acrylic. Finally, a custom head post made from durable plastic was affixed to the skull. Following a recovery period, mice were restricted to 1 mL/d of water, then trained on the tactile detection task. Vibrissae were secured with a silk suture loop and deflected by piezoelectric wafers. Task structure was controlled by a custom LabVIEW interface and analog circuitry. Once performance reached a plateau, we

added 40 Hz laser stimulation on a subset of trials. The light stimulus was delivered through a 200 μm fiber-optic cable connected to a 473 nm laser. Light power at the surface of the cortex was estimated to be 1 mW, or 30 mW/mm^2. Spikes and local field potentials were captured using a Plexon data acquisition system and saved for offline analysis in Matlab. All animals were perfused and tissue sectioned to measure the extent of mCherry expression in barrel cortex. All numbers are given as mean ± s.e.m., except where otherwise noted.

4.5 Results

Mice demonstrated high-quality psychophysical performance

We trained head-fixed mice to respond to 400 ms trains of 40 Hz vibrissae deflections. If mice licked a reward spout within 500 ms of deflection onset, a drop of water was delivered (Fig. 1a–b). Mice often displayed task knowledge on the first day and were proficient after ≤3 weeks of training. In the first two mice trained, we delivered stimuli of 10 different amplitudes to construct psychophysical response curves (Fig. 1c). Based on these curves, we determined the appropriate stimulation amplitude necessary for ~50% detection rates. In subsequent mice, we randomly interleaved these "threshold" stimuli (to test performance) and maximum-amplitude stimuli (to maintain animal engagement). Data from the first two animals demonstrated that mice sustain performance of the detection task consistently over weeks to months (Fig. 1d), with an average of 559 ± 7.0 and 528 ± 21.5 trials per session for each mouse (last 10 days of training).

Gamma entrainment in awake mice

As in previous studies, we gained causal control over fast-spiking interneurons by expressing the gene for channelrhodopsin-2, a light-gated cation channel, in parvalbumin-positive cells in the upper layers of the neocortex (Cardin et al. 2009, Sohal et al. 2009, Carlén et al. 2011). To test whether 40 Hz, millisecond-long light pulses enhanced gamma power in the barrel cortex of behaving mice, we used chronically implanted multi-wire electrodes (Supplementary Fig. 3). We found that local field potentials showed robust gamma entrainment (Fig. 2a). On certain electrodes, low latency light-evoked action potentials from fast-spiking cells were observed (Fig. 2b). We refer to these effects as "entrained" gamma oscillations for two reasons: the network impact of these oscillations is qualitatively similar to physiological gamma *in vivo* (Hasenstaub et al. 2005) and optogenetic stimulation of this type can be used to phase-reset ongoing gamma oscillations (Cardin et al. 2009).

To determine the impact of the relative timing between entrained gamma and sensory drive, we presented 40 Hz vibrissal deflections at 5 distinct phase offsets to the 40 Hz optogenetic stimulus (Fig. 3a). Because our electrodes did not provide enough well-isolated

single units to measure spike parameters, we quantified the stimulus-evoked potential (SEP) to examine the impact of stimulus phase offsets on the cortical response (Fig. 2c–d). In agreement with the previous study (Cardin et al. 2009), SEPs at phase 3 were more temporally compact (as indicated by the width of the response and its rise time). We also observed enhancement in SEP peak height (Fig. 2d).

Entrained gamma enhanced tactile detection

In N = 4 mice, we quantified the impact of entrained gamma on detection. To ensure that all trials were drawn from epochs in which animals were attentive, we set a d' threshold of 1.25 on trials from 14 consecutive test sessions (Fig. 1d–e; Supplementary Fig. 6a). In the remaining trials, we analyzed the response to threshold trials only, and eliminated trials in which mice licked during a 1-second interval before trial onset. We calculated three measures of perceptual acuity: hit rate, d', and reaction time (Fig. 3b).

All three measures revealed that processing was enhanced at phase 3, a phase that showed enhanced phase-locking (Cardin et al. 2009) and sharpening of the stimulus-evoked potential (Fig. 2d). On these trials (green dots), hit rate was higher than baseline for 3/4 animals and in the average (mean ratio to baseline = 1.16 ± 0.07, P = 0.035; one-tailed permutation procedure; see Supplementary Fig. 6b). Similarly, d' was higher than baseline for 4/4 animals and in the mean (mean ratio to baseline = 1.32 ± 0.08, P = 0.029). This effect was consistent across blocks of sessions (Supplementary Fig. 4b). In contrast, at a phase in which diminished phase-locking was observed[4] (phase 5, purple dots), hit rate and d' were lower than baseline for all 4 animals (hit rate mean ratio to baseline = 0.889 ± 0.016 , P = 0.035; d' mean ratio to baseline = 0.745 ± 0.144, P = 0.047). Reaction times showed the predicted inverse relationship to these measures, with a non-significant trend toward decreased response latency at phase 3 and a significant increase in response latency at phase 5 (P = 0.040).

The benefit of entrained gamma was not due to a simple arousal effect

An important question is whether the effects observed were due to heightened arousal driven by our optogenetic stimulus. Two findings contradict this idea. First, at 4/5 phases of stimulus-to-gamma alignment, synchronous inhibition had no impact on behavior or produced a behavioral deficit. Shifting entrained gamma oscillations by merely 10 ms (the temporal difference between phase 3 and phase 5) led to dramatic variation in task performance. Second, the rate of false alarms when no light stimulus was present was indistinguishable from the rate with light stimulus alone (0.1167 ± 0.0109, no light; 0.1170 ± 0.0122, with light). While we cannot say whether or not the mice detected the physiological impact of light presentation, it is clear that they did not associate it with reward delivery, as in previous studies (Huber et al. 2008).

Recruitment of fast-spiking interneurons at 20 Hz did not enhance detection

As another test of whether generally increasing inhibitory tone enhances detection, and/or whether detection of sustained and predictable (oscillatory) stimuli is enhanced by parallel entrainment of inhibition, mice were also trained to detect 20 Hz stimulation. If either prediction were true, then 20 Hz stimulation—outside the gamma range—should benefit perception. We tested 20 Hz stimuli on 3 animals that showed robust 40 Hz enhancement and observed behavioral effects of a much lower magnitude for all 6 phases presented within the 20 Hz cycle (Fig. 3d). False-alarm rates were also unchanged for the condition of 20 Hz laser stimulation (0.1467 ± 0.010 no laser vs. 0.1419 ± 0.019 with laser). However, the phase predicted to give maximal enhancement, 12.5 ms prior to stimulus onset (37.5 ms post-stimulus), was not used in this study.

Entrained gamma enhanced detection of naturalistic stimuli

The data described thus far provide causal evidence that gamma can enhance perception. However, the stimuli employed are unlikely to occur during natural sensing. Internally generated gamma is not typically aligned with sensory drive, nor is sensory stimulation periodic in the gamma range. The biomechanical properties of rodent vibrissae generate high-frequency micro-motions well above 40 Hz (Neimark et al. 2003, Ritt et al. 2008) and whisking frequency is below 20 Hz (Voigts et al. 2008). To test whether gamma-dependent enhancement occurred for naturalistic stimuli, we recorded velocity profiles from an *ex vivo* B2 vibrissa contacting a textured, rotating surface (Fig. 4a). An animal trained with periodically aligned 40 Hz stimuli was subsequently tested with these naturalistic velocity profiles while performing the same detection task. In this condition five different naturalistic stimuli were given either without any entrained gamma (50% of trials), or with entrained gamma from one of the 5 phase offsets, as defined from stimulus onset (10% of trials for each phase offset). On trials that included entrained gamma, there was a 34.8% enhancement in d', approximately the same enhancement observed for optimal phase alignment of a periodic stimulus (n = 235 trials from 1 mouse). This benefit for natural stimulus presentation was due to both enhanced hit rate (6.8%) and, in contrast to the 40 Hz condition, a reduction in false alarms (43.9%). A benefit in hit rate and d' was observed for 4 out of 5 naturalistic stimuli used (Fig. 4b), and is therefore unlikely to be a consequence of chance optimal phase alignment on a subset of trials.

4.6 Conclusion

By taking advantage of the temporal precision of light-gated ion channels (Boyden et al. 2005, Yizhar et al. 2011), we have shown that entrained gamma oscillations can enhance perception. Importantly, performance was only improved when the temporal relationship between inhibition and excitatory signals mimicked that observed across studies of attention (Fries et al. 2001, Fries et al. 2008). While our data do not indicate whether such a mechanism is employed under natural conditions, they do show that gamma could be

used to facilitate detection. We emphasize that our results do not speak to the importance of gamma's role in binding or discrimination (Singer 1999, Edden et al. 2009). Instead, they support a more basic hypothesis: that local gamma oscillations can facilitate the propagation of stimulus-evoked spikes, thereby improving detection processes. We also emphasize that we cannot determine the precise mechanisms by which entrained gamma enhanced perception. That said, perceptual benefits occurred at the phase that showed increased precision in spiking (Cardin et al. 2009) and in the stimulus-evoked potential (Fig. 2d). This suggests that the augmented synchrony that results from physiological gamma can enhance the probability of driving downstream targets and, ultimately, the detection of behaviorally relevant stimuli.

4.7 References

Atallah, B. V. & Scanziani, M. Instantaneous modulation of gamma oscillation frequency by balancing excitation with inhibition. *Neuron* **62,** 566-577 (2009).

Azouz, R. & Gray, C. M. Adaptive coincidence detection and dynamic gain control in visual cortical neurons in vivo. *Neuron* **37,** 513-523 (2003).

Börgers, C. & Kopell, N. J. Gamma oscillations and stimulus selection. *Neural Comput* **20,** 383-414 (2008).

Boyden, E. S., Zhang, F., Bamberg, E., Nagel, G. & Deisseroth, K. Millisecond-timescale, genetically targeted optical control of neural activity. *Nat Neurosci* **8,** 1263-1268 (2005).

Brecht, M. & Sakmann, B. Dynamic representation of whisker deflection by synaptic potentials in spiny stellate and pyramidal cells in the barrels and septa of layer 4 rat somatosensory cortex. *J Physiol* **543,** 49-70 (2002).

Brecht, M., Roth, A. & Sakmann, B. Dynamic receptive fields of reconstructed pyramidal cells in layers 3 and 2 of rat somatosensory barrel cortex. *J Physiol* **553,** 243-265 (2003).

Burns, S. P., Xing, D. & Shapley, R. M. Is gamma-band activity in the local field potential of V1 cortex a "clock" or filtered noise? *J Neurosci* **31,** 9658-9664 (2011).

Buzsáki, G. *Rhythms of the Brain* (Oxford Univ Press, Oxford, 2006).

Cardin, J. A., Carlén, M., Meletis, K., Knoblich, U., *et al.* Driving fast-spiking cells induces gamma rhythm and controls sensory responses. *Nature* **459,** 663-667 (2009).

Carlén, M., Meletis, K., Siegle, J. H., Cardin, J. A., *et al.* A critical role for NMDA receptors in parvalbumin interneurons for gamma rhythm induction and behavior. *Mol Psychiatry* (2011).

Colgin, L. L., Denninger, T., Fyhn, M., Hafting, T., *et al.* Frequency of gamma oscillations routes flow of information in the hippocampus. *Nature* **462,** 353-357 (2009).

Edden, R. A. E., Muthukumaraswamy, S. D., Freeman, T. C. A. & Singh, K. D. Orientation

discrimination performance is predicted by GABA concentration and gamma oscillation frequency in human primary visual cortex. *J Neurosci* **29**, 15721-15726 (2009).

Fries, P., Reynolds, J. H., Rorie, A. E. & Desimone, R. Modulation of oscillatory neuronal synchronization by selective visual attention. *Science* **291**, 1560-1563 (2001).

Fries, P., Womelsdorf, T., Oostenveld, R. & Desimone, R. The effects of visual stimulation and selective visual attention on rhythmic neuronal synchronization in macaque area V4. *J Neurosci* **28**, 4823-4835 (2008).

Gregoriou, G. G., Gotts, S. J., Zhou, H. & Desimone, R. High-frequency, long-range coupling between prefrontal and visual cortex during attention. *Science* **324**, 1207-1210 (2009).

Hasenstaub, A., Shu, Y., Haider, B., Kraushaar, U., *et al.* Inhibitory postsynaptic potentials carry synchronized frequency information in active cortical networks. *Neuron* **47**, 423-435 (2005).

Huber, D., Petreanu, L., Ghitani, N., Ranade, S., *et al.* Sparse optical microstimulation in barrel cortex drives learned behaviour in freely moving mice. *Nature* **451**, 61-64 (2008).

Knoblich, U., Siegle, J. H., Pritchett, D. L. & Moore, C. I. What do we gain from gamma? Local dynamic gain modulation drives enhanced efficacy and efficiency of signal transmission. *Front Hum Neurosci* **4**, 1-12 (2010).

Moore, C. I. & Nelson, S. B. Spatio-temporal subthreshold receptive fields in the vibrissa representation of rat primary somatosensory cortex. *J Neurophysiol* **80**, 2882-2892 (1998).

Neimark, M. A., Andermann, M. L., Hopfield, J. J. & Moore, C. I. Vibrissa resonance as a transduction mechanism for tactile encoding. *J Neurosci* **23**, 6499-6509 (2003).

Ray, S. & Maunsell, J. H. Differences in gamma frequencies across visual cortex restrict their possible use in computation. *Neuron* **67**, 885-896 (2010).

Ritt, J. T., Andermann, M. L. & Moore, C. I. Embodied information processing: vibrissa mechanics and texture features shape micromotions in actively sensing rats. *Neuron* **57**, 599-613 (2008).

Salinas, E. & Sejnowski, T. J. Impact of correlated synaptic input on output firing rate and variability in simple neuronal models. *J Neurosci* **20**, 6193-6209 (2000).

Shadlen, M. N. & Movshon, J. A. Synchrony unbound: a critical evaluation of the temporal binding hypothesis. *Neuron* **24**, 67-77, 111-25 (1999).

Singer, W. Neuronal synchrony: a versatile code for the definition of relations? *Neuron* **24**, 49-65, 111-25 (1999).

Sohal, V. S., Zhang, F., Yizhar, O. & Deisseroth, K. Parvalbumin neurons and gamma rhythms enhance cortical circuit performance. *Nature* **459**, 698-702 (2009).

Steinmetz, P. N., Roy, A., Fitzgerald, P. J., Hsiao, S. S., *et al.* Attention modulates synchronized neuronal firing in primate somatosensory cortex. *Nature* **404**, 187-190 (2000).

Voigts, J., Sakmann, B. & Celikel, T. Unsupervised whisker tracking in unrestrained behaving animals. *J Neurophysiol* **100**, 504-515 (2008).

Womelsdorf, T. & Fries, P. The role of neuronal synchronization in selective attention. *Curr Opin Neurobiol* **17**, 154-160 (2007).

Yizhar, O., Fenno, L. E., Davidson, T. J., Mogri, M. & Deisseroth, K. Optogenetics in neural systems. *Neuron* **71**, 9-34 (2011).

4.8 Figures
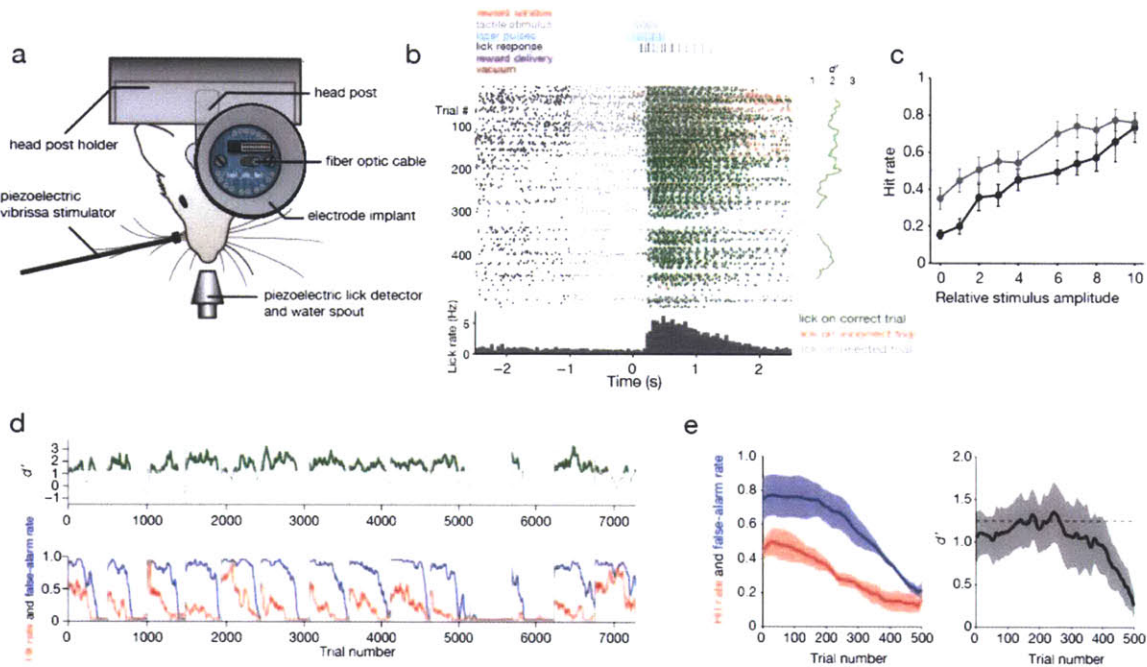
Figure 1 | Performance on the tactile detection task. a, Overview of the behavioral setup. **b,** Trial structure (top), lick raster (middle), and lick histogram (bottom). d' for 50-trial blocks is shown to the right of the raster plot, with a threshold of 1.25 indicated. **c,** Hit rate as a function of stimulus amplitude for two animals, averaged over 10 days of training. Gray dotted line indicates 50% hit rate, and gray box indicates amplitude chosen for "threshold" stimuli. Error bars indicate s.e.m. **d,** Hit rate (blue), false-alarm rate (red), and d' (black and green) for all trials from a representative animal. Values are from blocks of 50 trials, slid in 1-trial intervals. Vertical gray lines indicate the start of each session. Horizontal dashed line indicates d' threshold of 1.25. **e,** Hit rate (blue), false-alarm rate (red), and d' (black) as a function of trial number within a session, averaged over the 4 animals used in Figure 3b (mean ± s.e.m.).
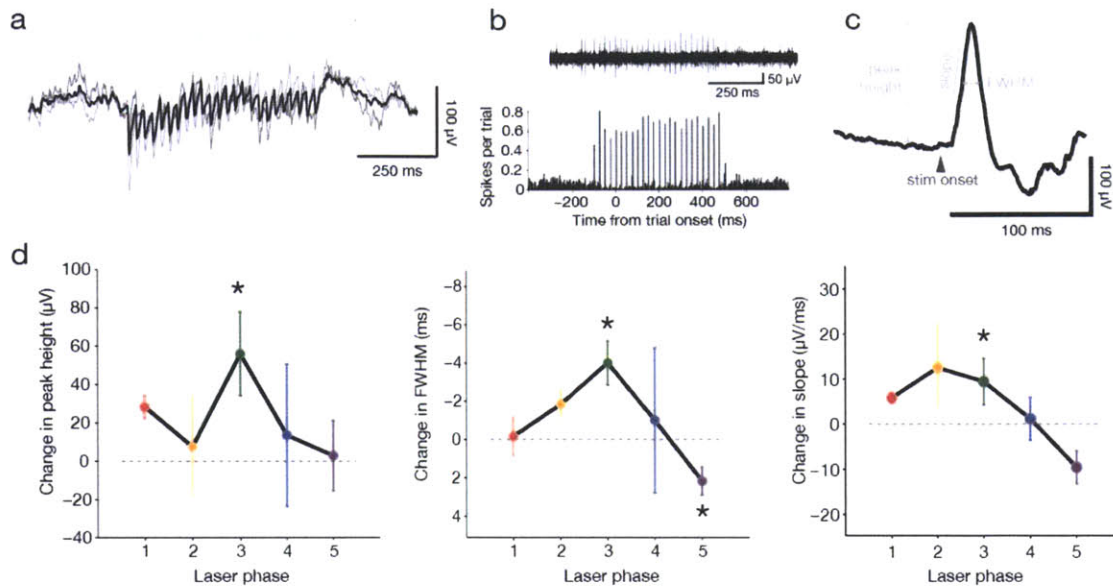
Figure 2 | Combining optogenetically entrained gamma oscillations and electrophysiology. a, Mean (thick line) and individual (thin lines) light-evoked response for three animals. Vertical blue lines indicate 1 ms laser pulses. **b**, Light-evoked spikes in an FS interneuron from a single trial (top) and the average of 96 trials from a single session (bottom). Vertical blue lines indicate 1 ms laser pulses. **c**, Structure of the stimulus-evoked potential (SEP) to the first vibrissae deflection in a 40 Hz train. Peak height, slope, and full-width-at-half-max (FWHM) are illustrated. **d**, Change in peak height, FWHM (note inverted y-axis), and slope of SEPs for 5 different phase offsets between 40 Hz laser pulses and 40 Hz vibrissae deflections, relative to baseline (no laser) trials (see Fig. 3a for an illustration of the 5 phases). Error bars, mean ± s.e.m. for 3 animals. * = $P < 0.05$ (phase-randomizing permutation test, Supplementary Fig. 6b). Error bars indicate s.e.m.
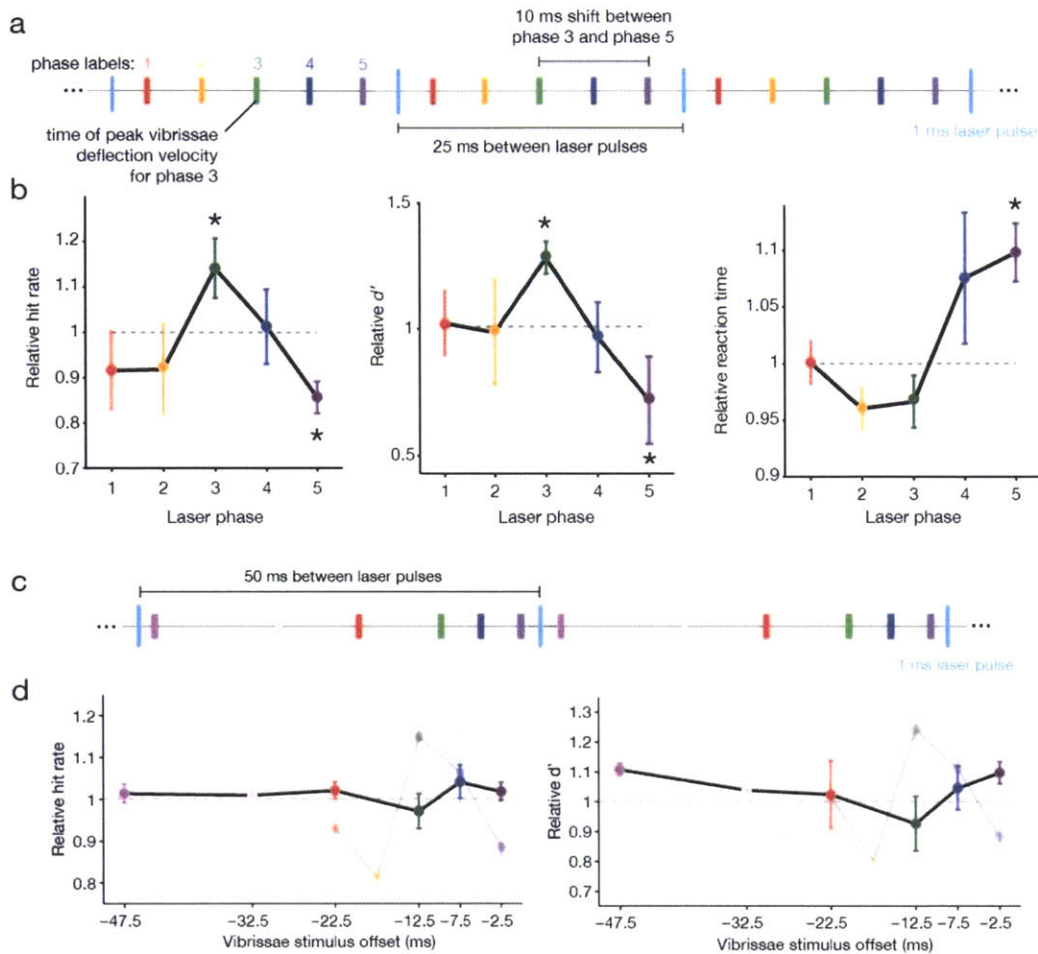
Figure 3 | Impact of entrained gamma on behavioral performance. a, Temporal relationship between 40 Hz vibrissae deflections and 40 Hz laser pulses at each of five phases. **b,** Relationship between laser phase and three measures of performance: hit rate (left), d' (middle), and reaction time (right). Bottom three plots display the baseline-normalized mean of the four individual mice in the top plots. For all three measures, performance is enhanced at phase 3 and impaired at phase 5. * = $P < 0.05$ (phase-randomizing permutation test, Supplementary Fig. 6b). Error bars indicate s.e.m., or standard-error above the median, in the reaction-time figure. **c,** Temporal relationship between 20 Hz laser pulses and 20 Hz vibrissae deflections at each of six vibrissae–laser offsets. **d,** Mean hit rate and d' for six vibrissae–laser offsets in the 20 Hz condition (black line) overlaid with data from the same animals from the 40 Hz condition (gray line) ($N = 3$ mice). Error bars indicate s.e.m.
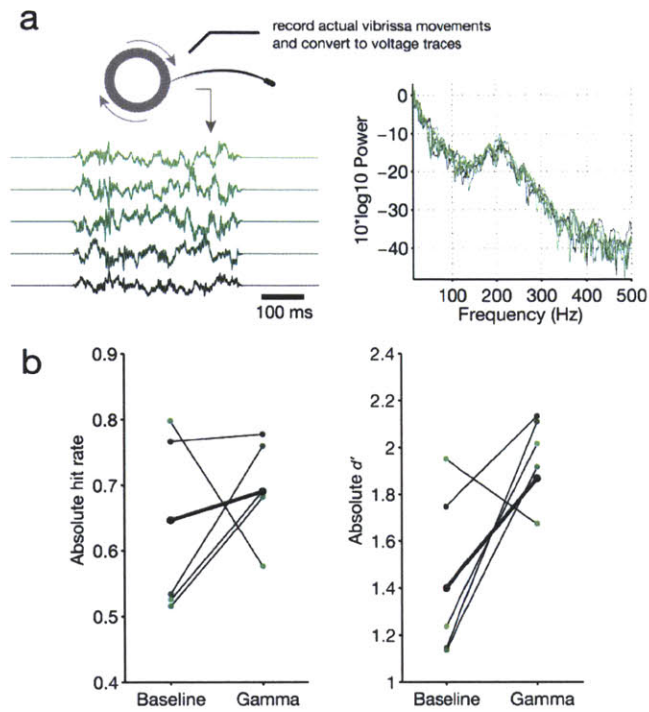
Figure 4 | Gamma enhances detection of naturalistic stimuli. a, Schematic of the data capture procedure for naturalistic stimuli, plus raw traces and power spectra for the five stimuli used in the experiment. **b,** Change in hit rate and d' between baseline and entrained-gamma conditions for five individual stimuli (thin lines) and for the mean across stimuli (thick lines).

4.9 Supplementary Figures
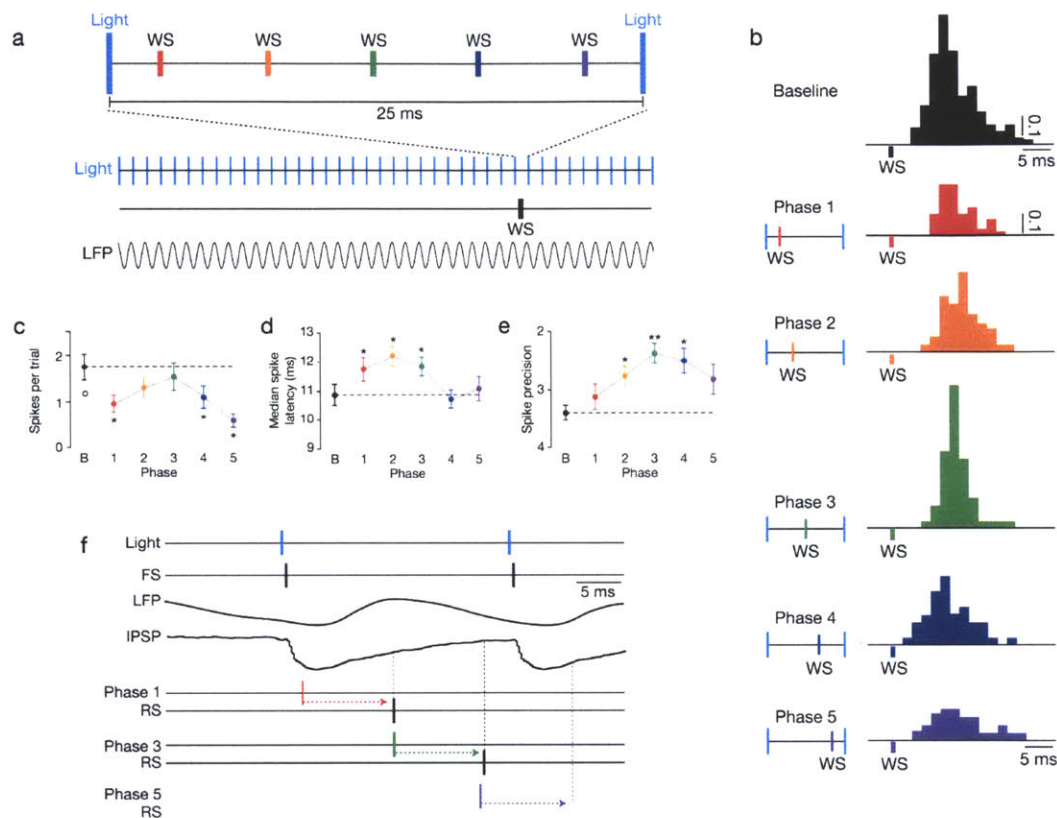
Figure S1 | Gamma oscillations gate sensory responses of excitatory neurons (adapted from Cardin et al., 2009[4]). a, In each trial, FS-PV+ inhibitory interneurons were activated at 40 Hz and a single vibrissa deflection (whisker stimulus, WS) was presented at one of five phases. **b,** Baseline response of one layer 4 RS cell to single vibrissa deflections, shown in units of spikes per trial (top). Responses of the same cell when the vibrissa was deflected at each of five temporal phases relative to the induced gamma oscillation (bottom 5 plots). **c,** Average spikes evoked per trial under each condition. Dotted line indicates baseline responses. **d,** Timing of the RS spike response, measured as a median spike latency. **e,** Spike precision of the RS responses. **f,** Schematic model of the gating of sensory responses by gamma oscillations. IPSP and LFP examples are averaged data traces. *$P <$ 0.05, **$P <$ 0.01; error bars, mean ± s.e.m.

a

AAV DIO *ChR2-mCherry*

b

200 µm
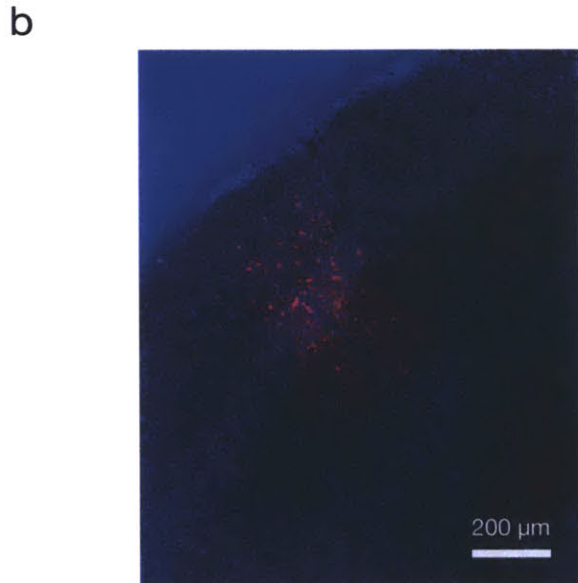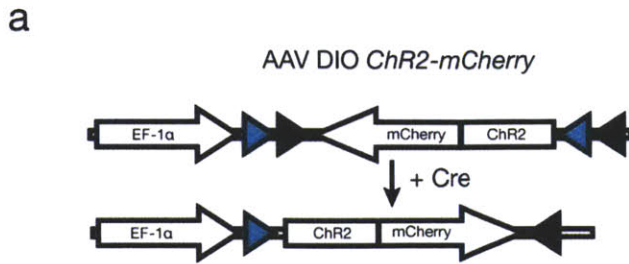
Figure S2 | AAV and histology. a, Schematic of the viral vector, which interacts with Cre in parvalbumin-positive cells to induce expression of *ChR2-mCherry*. **b**, Example histological section, showing viral expression primarily in the upper layers of barrel cortex. Expression was typically distributed over 1-2 barrels (300-500 µm medial–lateral spread, 500-1000 µm anterior–posterior spread). Blue = DAPI stain, red = mCherry fluorescence.

a

b

40-Hz, 400 ms
stimulus waveform

stimulus-evoked spikes

250 µV

250 ms

initial
deflection
at ~8 ms

synchronization
of LFP by stimulus

10 ms
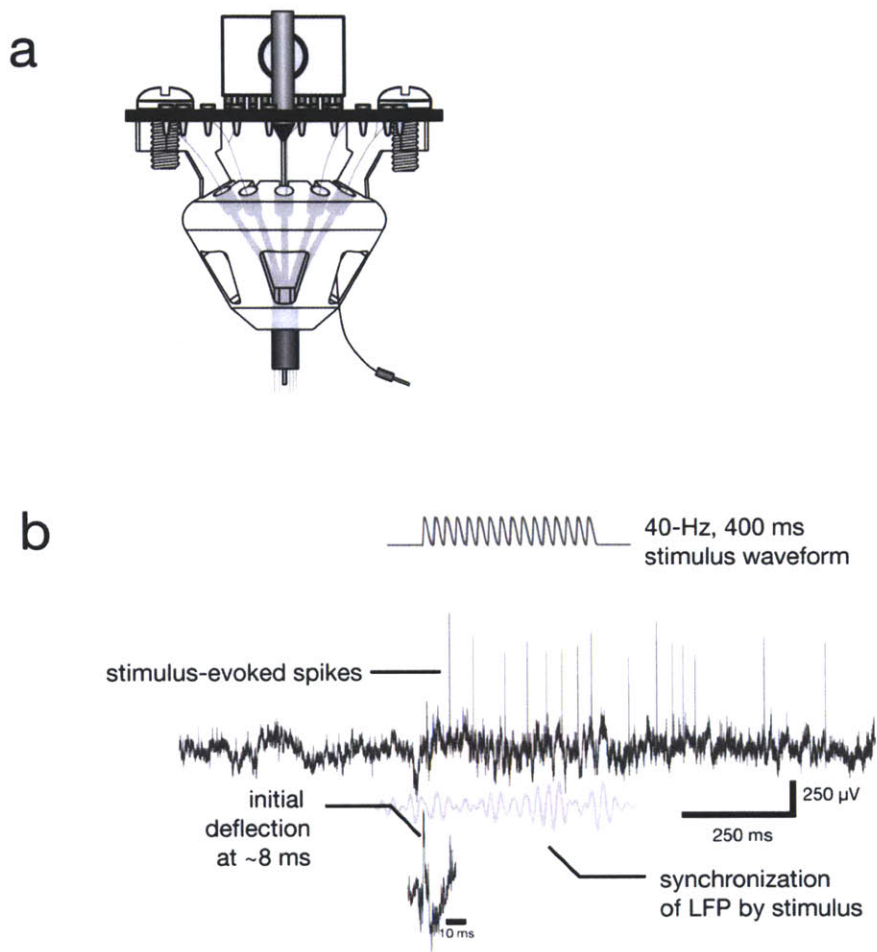
Figure S3 | Barrel cortex electrophysiology. a, Illustration of the fiber-optic–electrode implant used in experiments. **b**, Single-trial example of the evoked response. Inset shows latency between vibrissae deflections and onset of the stimulus-evoked potential.
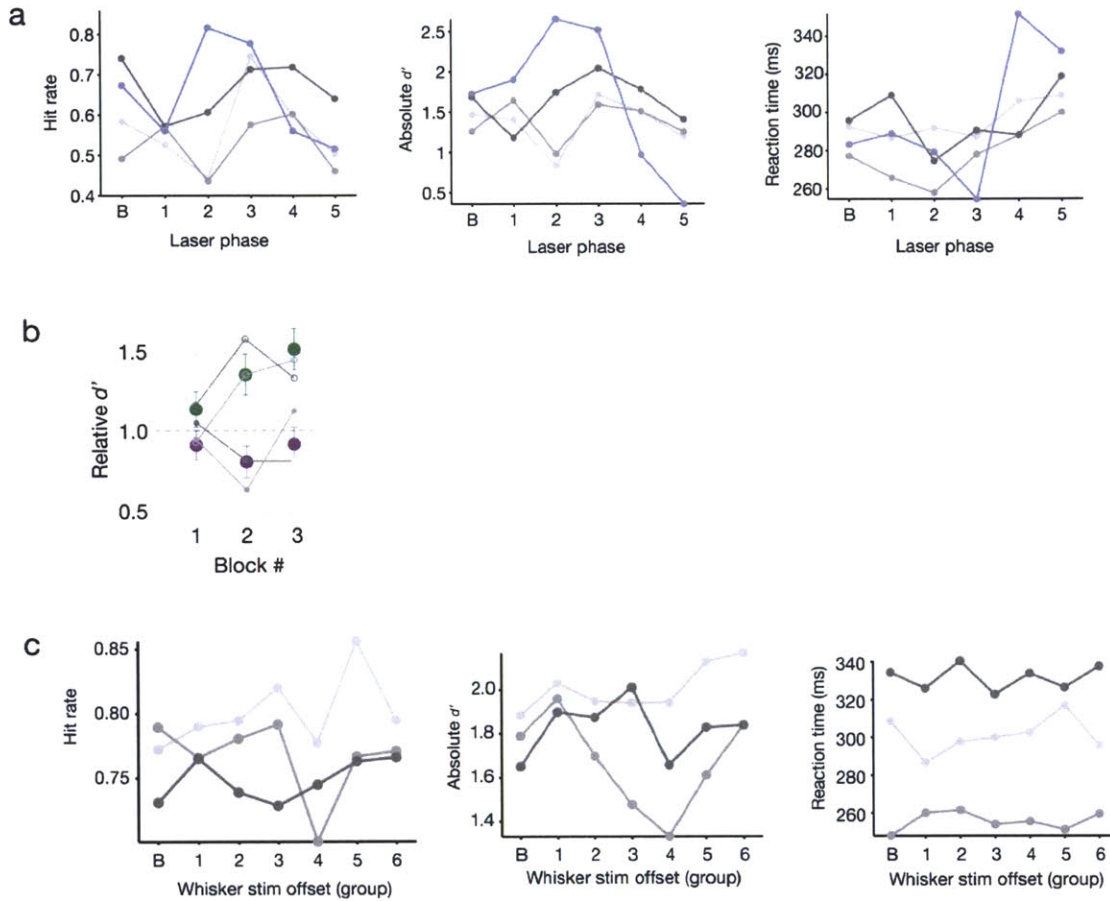
Figure S4 | Data for individual animals. a, Data from four animals (individual colored lines) that contributed to Fig. 3b (40 Hz stimulation). *B* = baseline (no laser) condition, 1-5 indicate the five phases of laser stimulation (see Fig. 3a for an illustration). **b,** d' statistics calculated for all animals (excluding animal 4, whose behavior was too variable to include), grouped into blocks of 6 sessions each. Note that d' values for phase 3 (green) are consistently above baseline, whereas d' values for phase 5 (purple) are consistently below baseline. Error bars indicate s.e.m. **c,** Data from the three animals (individual colored lines) that contributed to Fig. 3d (20 Hz stimulation).

80

a

inverse of Gaussian distribution

hit rate: 0.7
false alarm rate: 0.3

0.95
0.7
0.3

$d' \approx 1$

$d' \approx 2$

0.7
0.05

$d' \approx 2$

b

Randomize phase labels
(assume the laser has no impact)

$d'_1 = 1.25$
$d'_2 = 1.87$
$d'_3 = 0.89$
$d'_4 = 2.14$
$d'_5 = 3.31$

Recompute statistics

Repeat 10000x

Compute probability of original
statistic, given the
distribution derived from
the permutations for each animal

$p = 0.133$ $p = 0.107$ $p = 0.115$ $p = 0.128$

Combine probabilities from
each animal using Fisher's method
to yield the final P-value

$$X^2 = -2 \sum_{i=1}^{k} \ln(p_i)$$

Figure S6 | Statistical methods. a, Illustration of the d' statistic, which is influenced by both hit rate and false-alarm rate. A high value of d' ensures that the animal is licking consistently and accurately by penalizing false alarms. **b,** Permutation procedure for calculating P-values.

4.10 Supplementary Methods

[Same methods from Chapter 3]

Animals

All mice were male parvalbumin-Cre (PV-Cre) heterozygotes, derived from PV-Cre knock-in mice back-crossed into a C57BL/6J line (gift from S. Arber, now available as Jackson Laboratory strain B6;129P2-$Pvalb^{tm1(cre)Arbr}$). Mice were 8-10 weeks old at the time of initial surgery. Animals were individually housed and maintained on a 12-hour light/dark cycle (lights out at 9:00 PM). All experimental procedures and animal care protocols were approved by the Massachusetts Institute of Technology Institutional Animal Care and Use Committee and were in accordance with NIH guidelines.

AAV vectors

ChR2 fused to the fluorescent protein mCherry was cloned in the antisense direction into pAAV-MCS (Stratagene) to create AAV DIO *ChR2-mCherry* (Fig. S2). *ChR2-mCherry* was flanked by a pair of canonical loxP sites and a pair of mutated lox2272 sites. A woodchuck hepatitis B virus post-transcriptional element was placed in sense direction 5′ of the poly(A). Adeno-associated viral particles of serotype 2 were produced by the Vector Core Facility at UNC Chapel Hill.

Fiber-optic–electrode implants

Implants (Siegle 2012) were constructed around a custom plastic base, designed in SolidWorks (Dassault Systems, Waltham, MA) and printed via stereolithography in Accura 55 plastic (American Precision Prototyping, Tulsa, OK). The plastic base held 8 electrodes around a central fiber optic cable (Doric Lenses, Quebec, Canada). Electrodes were made from 12.5 μm polyimide-coated nichrome wire (Kanthal, Halstahammar, Sweden), twisted and heated to form tetrodes or stereotrodes (Nguyen et al. 2009). In three animals, the electrodes were stationary. In two animals, electrodes were fixed to laser-cut plastic springs (Pololu, Las Vegas, NV) individually driven by miniature screws. Electrodes were attached to a custom electrode interface board (Sunstone, Mulino, OR) with gold pins (Neuralynx, Bozeman, MT). Individual electrodes were gold plated to an impedance of 200-400 kΩ. The fiber optic cable had an inner diameter of 200 μm and a cladding diameter of 260 μm, and was terminated with a 1.25 mm metal ferrule (Fig. S3).

Surgical procedure

Mice were anesthetized with isofluorane gas anesthesia (0.75-1.25% in 1 L/min oxygen) and secured in a stereotaxic apparatus. The scalp was shaved, wiped with hair removal cream, and cleaned with iodine solution and alcohol. Following IP injection of Buprenex (0.1 mg /kg, as an analgesic) and dexamethasone (4 mg/kg, to prevent tissue swelling) and local injection of lidocaine, the skull was exposed with an incision along the midline. After the skull was cleaned, two small stainless steel watch screws were implanted in the frontal skull plates, one of which served as ground. Next, a ~1.5 mm-diameter craniotomy was drilled over barrel cortex of the left hemisphere (1.5 mm posterior to bregma and 3.5 mm lateral to the midline). Virus was delivered through a

glass micropipette attached to a Quintessential Stereotaxic Injector (Stoelting). The glass micropipette was lowered through the dura to a depth of 450 μm below the cortical surface. A bolus of 1 μl of virus (AAV DIO ChR2-mCherry; 2×10^{12} viral molecules per ml) was injected into the cortex at 0.05 μl/min. After the injection, the pipette was held in place for 10 min at the injection depth and 10 min at a depth of 200 μm before being fully retracted from the brain. The fiber-optic–electrode implant (Fig. S3a) was aligned with the craniotomy at an angle of 15º from vertical and lowered to the surface of the cortex, centered approximately 200 μm anterior to the injection site. If anything more than a small amount of bleeding resulted from electrode implantation, the surgery was cancelled. Once the implant was stable, a small ring of dental acrylic was placed around its base. A drop of surgical lubricant (Surgilube) prevented dental acrylic from contacting the cortical surface. A custom head post made from durable plastic (APProto) was then affixed to the skull with adhesive luting cement (C&B Metabond). Once the cement was dry, the scalp incision was closed with VetBond (3M), and mice were removed from isoflurane. Mice were given 3-10 days to recover prior to the start of water restriction.

Stimulus delivery and behavioral control
Vibrissae were stimulated by computer-controlled movements of piezoelectric wafers (Noliac, Kvistgård, Denmark). Stimulations consisted of high-speed deflections in the dorsal direction with a raised cosine velocity profile (5 ms duration). Vibrissae were held with a silk suture loop fed through a 4 mm, 21-gauge stainless steel cannula, which was attached to the piezoelectric wafer via a glass capillary tube (0.8 mm outer diameter). As many vibrissae as possible were secured, centered around the C2 vibrissa, and gripped approximately 5 mm from the mystacial pad. Mice were photographed from above at the start of each session to confirm which vibrissae were being stimulated. For maximum-amplitude deflections, vibrissae moved approximately 1 mm at the point of contact. Water delivery was based on gravitational flow controlled by a solenoid valve (Lee Co., Westbrook, CT) connected with Tygon tubing. Mice received distilled water through a plastic tube mounted on a piezoelectric wafer with epoxy. This "lick tube" was positioned near the animal's mouth using a micromanipulator. The water volume was controlled by the duration of valve opening (30-60 ms), calibrated to give ~8 μl per opening. Individual licks were detected by amplifying and thresholding the output of the piezoelectric wafer using a custom circuit board.

The light stimulus was delivered through a jacketed fiber-optic cable 200 μm in diameter and 2.5 m long (Doric Lenses, Quebec, Canada) connected to a 473 nm laser (Opto Engine, Salt Lake City, UT). Laser light passed through an adjustable neutral-density filter and a collimator (Thorlabs PAF-X-15-PC-A) before entering the fiber. The 2.5 m fiber was connected to the animal's head via two mating metal ferrules sheathed in a zirconia sleeve. Light loss for this connection was measured for each implant prior to surgery, and was usually around 50%. The amplitude of the light stimulus was calibrated daily with an optical power meter (Thorlabs PM100D with S120C sensor). Light power at the surface of the cortex was estimated to be ~1 mW, or 30 mW/mm².

All behavioral events, piezoelectric control, reward delivery, laser stimulation, and lick measurements were monitored and controlled by custom software written in LabVIEW and interfaced with a PCI DIO board (National Instruments, Austin, TX).

Trial structure

On each trial, vibrissae were stimulated for 400 ms at a single amplitude, varying between 0 ("blank" trials) and 1 mm ("maximal" trials). Amplitude did not vary within a given trial. For any given session, all stimuli consisted of either 40 Hz, 20 Hz, or "naturalistic" deflections. On laser-stimulation trials, 1 ms light pulses were delivered at 40 Hz for 600 ms. Vibrissae deflections began after the fourth light pulse. The precise timing of the vibrissae deflections relative to the light pulses was varied across five phases, but remained consistent within individual trials. For all sessions, inter-trial intervals were uniformly distributed between 4 and 6 s.

If mice licked the reward spout at any point up to 500 ms after the onset of the vibrissae stimulus, a drop of water was delivered. After a slight delay, any remaining water was removed via vacuum suction. This prevented mice from receiving reward that was not immediately preceded by a vibrissae stimulus.

Behavioral training

Training began after at least 3 days of post-operative recovery and at least 7 days of water restriction (1 ml /d). At the beginning of each session, mice were secured to the head post apparatus with their bodies placed inside a Falcon tube. Initial training sessions lasted approximately 5 minutes, to allow mice to accommodate to head fixation. At first, all trials were maximal, with no blank trials. On successive days, training time was gradually increased to 45 minutes. Blank stimuli (up to 10%) were randomly interleaved and the probability of non-maximal stimuli was increased to 30%. Before moving to the next stage of training, each mouse had to perform two sessions in which it performed with an overall d' of 1.25.

After reaching criterion on the training task, laser light stimulation was added on a subset of trials. Laser stimulation was given ~100 ms preceding tactile stimulation for a duration of 600 ms (100 ms post stimulation) at ~1 mW power on the cortical surface. 50% of trials were at a single threshold value ranging from 20-40% of the maximum stimulus amplitude, with the same duration to peak amplitude (5 ms). 30% of trials were blank, with the remaining 20% of trials at max amplitude, to keep the animals engaged. On half of all trials, laser stimulation was presented at one of 5 temporal offsets (Figure 3a).

Mice that did not consume 1 ml of water during the training sessions were supplemented with water in their home cage several hours after the experiment finished.

Electrophysiology

Spikes and local field potentials were recorded using stereotrodes or tetrodes integrated into a custom implant[31] (Fig. S3). Recording electrodes were either

84

implanted 300–400 µm from the surface of the cortex during surgery, or lowered to the same depth over the course of several days. Throughout the recording session, broadband signals referenced to ground and digitized at 40 kHz (Recorder/64, Plexon, Dallas, TX). Electrophysiology data was synchronized with behavioral data via TTL pulses at the start of each trial.

Histology

At the end of training, electrodes sites were lesioned with 15 µA of current for 10 s. Mice were transcardially perfused with 100 mM PBS followed by 4% formaldehyde in PBS. Brains were post-fixed for at least 18 h at 4 °C. 60 µm sections were mounted on glass slides with Vectashield (Vector Laboratories), coverslipped, and imaged with an upright fluorescent microscope (Fig. S2). Viral expression was confirmed in all animals. Expression was generally limited to the upper layers of barrel cortex (II-IV). In one animal, expression was also observed in the lower layers (V and VI). Ventral/medial and anterior/posterior spread of the virus ranged between 0.5 and 1.5 mm, encompassing 1-3 barrel columns.

Data analysis

Data analysis was performed in Matlab (Mathworks, Natick, MA). Raw data from LabVIEW was converted to event times for behavioral analysis. Trials were first filtered based on d' according to the following procedure: (1) hit rate and false alarm rates were calculated for blocks of 50 trials, slid in 1-trial intervals. A negative offset was added to the hit rate and an equal-but-opposite offset was added to false alarms, to prevent d' saturation. An offset of 0.04 was used for all analyses, except the natural stimulation condition, where an offset of 0.025 was used to include more trials. Hit rate was capped at a minimum value equivalent to the offset and false alarm rate was capped at a maximum value equivalent to 1 minus the offset. (2) d' was calculated as Z(hit rate) – Z(false alarm rate), where Z stands for the inverse of the Gaussian distribution function (Fig. S6a). (3) For any blocks with d' above a threshold value of 1.25, the middle trial (trial 25) was included in the analysis. After d' filtering, trials with pre-stimulus licks within one second of trial onset were also eliminated. Trials were selected from the remaining subset based on the parameters of the vibrissae and laser stimuli. Hit rate, d', and median reaction time were calculated for each animal for each set of parameters.

P-values were obtained using the following permutation procedure (Fig. S6b): To test the null hypothesis that the laser had no impact on SEPs or behavior, the phase labels (including the "blank," or laser-free, phase) for all trials were randomized, and relevant statistics were computed on the shuffled data (Efron and Tibshirani 1993). This procedure was repeated 10,000 times (behavioral data) or 250 times (SEP data), to yield a distribution for each statistic. Thus, for each animal, we were able to compute a probability that each actual statistic would be greater or less than the values computed under the null hypothesis. Probabilities for each animal were combined using Fisher's method (Little and Folk 1971) to yield a final P-value. Statistical tests were only performed on phases in which at least 3 out 4 animals showed the same trend.

Continuous electrophysiological data from the Plexon system was either low-pass filtered (3rd-order Butterworth) and downsampled to 2 kHz or filtered between 600 and 6000 Hz (acausal FIR filter) and thresholded to extract spikes. Stimulus-evoked potential statistics were calculated on the mean SEP for each animal, taken from an electrode with clear vibrissae and laser responses. One animal had electrophysiology that was contaminated with 60 Hz line noise, and was therefore not included in the analysis.

References

Efron, B. & Tibshirani, R. *An introduction to the bootstrap* (Chapman & Hall, London, 1993).

Little, R.C. & Folk, J. L. Asymptotic optimality of Fisher's method of combining independent tests. *J Amer Stat Assoc* **66**, 802-806 (1971).

Nguyen, D. P., Layton, S. P., Hale, G., et al. Micro-drive array for chronic in vivo recording: tetrode assembly. *J Vis Exp* **26** (2009).

Siegle, J. H. Combining optical stimulation with extracellular electrophysiology in behaving mice. In Fellin, T. & Halassa, M. M., Eds. *Neuronal Network Analysis* (Humana Press, New York, 2012).

Chapter 5

Conclusions

5.1 Conclusions

In this thesis I asked three important questions on how ongoing brain states matter for perception, a topic that is still hotly debated. 1) Is the alpha/mu rhythm predictive of perception? 2) Is the gamma rhythm important for perception? And 3) Are these indicative of different cortical "states,"? Put another way are alpha, beta, and gamma just manifestations of the same underlying cortical processes?

Is the alpha/mu rhythm predictive of perception?

Much of the evidence from EEG and MEG in humans points to alpha operating as "idle" or disengaging rhythm. Our work shows high power in the alpha is indicative of lower stimulus detection rates in both human and in the mouse (**Chapter 2 and 3**). This is in direct contrast to hypotheses in the barrel corticex literature, which suggest that high power of alpha is beneficial to perception (Nicolelis and Fanselow 02). Further, MEG results in our lab and elsewhere have shown higher alpha power with distracting stimuli, as if the high alpha power suppresses perception of the distracting stimulus (Jones et al. 10; Foxe and Worden 02). Both pieces of data suggest the alpha oscillation is correlated with the behavioral percept and may be selectively engaged in attention.

To probe this hypothesis we used human MEG because it offers a better solution to the inverse problem allowing us to more accurately localize the source of the signal to primary SI. Further, because MEG is constrained to the sulci and apical dendrites as the putative source of the signal, MEG is a viable candidate for biophysical modeling (Jones et al. 07). This allows us to pose questions about the circuit and test them in vivo using a rodent model system (a key model system used to inform most biophysically plausible models. See Nicolelis and Fanselow 2002, for counter-hypothesis).

From this work, we show data suggesting that at the level of MEG, primary somatosensory cortex should have a neural correlate of detection. A major cortical oscillation observed in EEG/MEG studies, the alpha/mu oscillation, showed the predicted power distribution: on average, when comparing trials when the participant detected the stimulus and trials when the participant did not detect the stimulus, there was higher alpha power for miss trials than hit trials.

Next, we wanted to extend our findings from the human MEG work into rodent barrel cortex. First it was required that we successfully replicate the results in a rodent model system. Despite the similarities of rodent cortex, (e.g. 6 layered, same distributions of excitatory to inhibitory cell type), the opposite hypothesis existed in the barrel cortical field about the relevance of the alpha oscillation. First, rodents whisk (move their whiskers) at the alpha frequency (~8 Hz). This is thought to beneficial for increasing discriminability of objects, occurring through increased bursting in the thalamus, which would operate via increase the efficiency cortically. That a thalamic burst would generate multiple thalamic spikes per sensory event would be advantageous because if the first spike did not elicit a

cortical response, then the second or third spike was more likely to get through (Swadlow et al. 01).

This hypothesis was in direct conflict with the EEG observations that during periods of high alpha, which is thought to be generated by bursting in the thalamus, activity in the cortex would be in a state that would not permissive to detecting the thalamic activity, i.e. high inhibition in the cortex. To resolve this conflict, we therefore recorded form rodents performing simple detection tasks.

We show that as in previous observations, rodents do in fact express an alpha oscillation that behaves similar to human alpha oscillation. We see in our mice local field potential recordings an alpha/mu oscillation, similar to human, and a gamma band oscillation, not seen in our human recordings, but similar to monkey physiology (Fries et al. 01; Fries et al. 08).

However, contrary to what was proposed by Nicolelis, with rodents in our task detecting a liminal stimulus, increased alpha actually leads to suppression of behavioral response, just as we observed in human subjects. Further, in our human task we saw a linear correlation of power in the alpha and beta bands and task performance in a detection task. In our mice, we observe this same relationship in both the alpha and beta bands. The last piece of evidence against the Nicolelis hypothesis is that we observed that suppression of alpha on a strong sensory stimulus (nearly 100% detected) is small and does not reach significance, which argues the phenomena observed in the Weist and Nicolelis (2003) paper was the result of using supramaximal stimuli.

Is the gamma rhythm predictive of perception?

One advantage to using a rodent model to probe state-dependence of cortical response in primary sensory cortices is that the use of the extracellular technique lets us resolve micro-circuits that are only debatably observed using human MEG. One such oscillation is the gamma band oscillation observed primarily in primates and in the hippocampus in rodents. The gamma oscillation has been observed in states that also express low levels of alpha power (Fries et al. 08, Jensen and Mazaheri 10). This even led to the hypothesis that these two oscillations are anti- correlated (Jensen and Mazaheri 10), or that the alpha oscillation is somehow artifactual to the cortex not expressing gamma (unnamed critique).

Using our mouse behavioral prep, we first asked whether we see expression of the gamma oscillation in rodents performing our task. During task performance, when comparing detected trials to undetected trials, we see that trials where the mouse detected the stimulus had, on average, a higher power in the gamma (30-60 Hz, in this case) range. These are the same trials that showed lower average power in the alpha band, as predicted by the Jensen hypothesis.

Effect of Causal Manipulation of a Gamma Frequency Oscillation
In the last set of experiments used optogenetics to causally entrain a gamma oscillation to understand the benefit of the gamma oscillation on behavioral perception. In a previous

experiment, (Cardin et al. 09) we showed a phasic relationship of the timing of the inhibitory gamma, the amplitude and the timing of the evoked sensory response. We showed that the phase determined by the arrival of sensory information in the cortex with minimal inhibition, and showed enhanced spike timing (i.e. most of the spikes occurred in a tighter temporal window) (Cardin et al. 09, Knoblich et al. 10). This led to the prediction that the packeting of spikes would drive enhancement of downstream cortical response through enhanced synaptic drive. This should further drive increased behavioral benefit, but this should be phasically modulated by the overall inhibition.

We saw that in mice trained to perform a simple detection task, performance of the mouse was phasically dependent on the phase of the entrained gamma oscillation, and that the phase was predicted by our anesthetized physiology, as having the highest increase precision and no difference in overall firing rate. Further, when we used a naturalistic stimulus, one that does not have any predictable relationship to our entrained gamma oscillation, we saw the overall effect of behavioral enhancement.

These results indicate that an entrained gamma oscillation is sufficient to recapitulate the behavioral enhancement often seen associated with enhanced gamma power or gamma spike field coherence (Fries et al. 01; Fries et al. 08). This is consistent with many modeling studies that suggest that the interaction of FS inhibition and excitatory neurons are responsible enhancement of downstream response through increased synaptic drive. (Knoblich et al. 10; Börgers 08)

Do alpha, beta, and gamma represent separate and distinct cortical states?

Alpha and Beta in Mu
The mu oscillation is compromised of 2 distinct oscillations: the alpha rhythm and the beta rhythm (Tiihonen et al. 1989). To our knowledge, no study has examined their co-occurrence to determine whether these oscillations are parts of the same cortical state, or if there could be two independent oscillators that both have the same impact on perception. We show in SI, both alpha and beta are negatively correlated with perception, but independently (**Chapter 2**, Jones et al. 10), this was also seen in mouse barrel cortex (**Chapter 3**). Further, we show that although there are instances when alpha and beta co-occur, the distribution is not predictive of some simple frequency harmonic (**Chapter 2**), and modeling revealed the possibility of two separate oscillators (Jones et al. 09).

Alpha and Gamma Inverse Correlation
One common observation of alpha and gamma is that the oscillations are inversely correlated (Fries et al. 01; Fries et al. 08). Jensen and Mazaheri 2010 suggested that this correlation was due alpha blocking the gamma expression. We wanted to explore the relation of alpha to gamma directly by looking at the single trial dynamics instead of the average performance on a trial by trial basis. To do this we assigned every trial a number for the quartile of alpha and for gamma independently and then we looked at the performance in each bin. If alpha and gamma where truly coupled, one would expect all trials to lie along the negative diagonal of high alpha to high gamma. However, we found

that for any given alpha power, any given power of gamma is expressed, but it is the combination of both the power in the alpha and gamma bands that will be predictive of the overall hit rate. Where high versus low alpha would be the major determinate and gamma power adding to the overall detection rates.

The second way we explored this alpha gamma coupling is through optogenetics. Recall that an ongoing alpha oscillation can be desynchronized via peripheral sensory stimulation. We reasoned that if fast-spiking interneurons were playing a role in the generation of both the alpha and gamma oscillation, then activation of this cell type should cause a desynchronization of the alpha oscillation. This is plausible if there is an interaction of the alpha and the gamma frequency (Jensen and Mazaheri 10), and we already expected a role for inhibition in generating a behavioral suppression of response during high alpha activity.

When we turned on fast spiking interneuron activity during ongoing alpha what we saw is that this manipulation did not change the power of the alpha oscillation. This indicates to use that either, alpha generated on our electrodes is upstream of our manipulation (i.e. thalamic), and/or FS cells do not play a role in the generation of this oscillation. Further, the manipulation we used was one that is known to entrain a cortical gamma oscillation, thus another point arguing against the inverse correlation of the gamma and alpha oscillation, as the entrained gamma oscillation did not affect the overall power in the alpha band.

Remaining questions

Multi unit activity and/or single unit activity, synaptically tagged inhibition during gamma or alpha episodes One possible experiment would be to use channelrhodopsin in SOM+ interneron type, as they may be a candidate for inhibition during the slow alpha oscillation (Veirling-Classen et al. 10). Further, we could use channelrhodopsin to synaptically tag different interneuron types. We can then look at the active neurons during alpha and/or gamma, and then use a laser stimulus to select the sub-population that is tagged with channelrhodopsin, and compare this activity to periods of high power alpha and/or gamma activity. Further, we can use halorhodopsin in both populations to inactivate them to see the effect on alpha/gamma.

Single trial analysis Decile analysis is close to being able to predict on a single trial, but it may have better predictive power using both alpha/gamma simultaneously on a trial by trial basis. Simply put, we need more trials, and animals, for this type of predictive analysis

Spatial alpha/gamma deployment. Recent evidence from EEG/MEG show that correlates of this permissive/not state can be read out on the surface of cortex. Is this due to calcium currents in the cortex in intrinsically bursting layer V cells (Agmon and Connors 92; Bullimanta et al. 08) or driven from thalamus to layer IV? (Swadlow et al. 11, Nicolelis and Fanselow 02). Recent work from Swadlow indicates it could be both (Bereshpolova 2011). The open question is what is the spatial scale of this oscillation? Swadlow's work suggests that this is really a global event (they measure state in hippocampus), work in humans suggests that alpha can be at least as specific as modalities or hemispheric. One possible constraint on the specificity is that the mechanism that ends the non-permissive alpha

state, for example, acetylcholine from the reticular formation has less of control of spatial scale versus a more top-down mechanism such as attention driving local inhibition Parikh and Sarter 08, Tiesinga and Sjenowski 09).

Moreover, the evoked sensory responses under an active cortex lead to a more focal spread of activity in barrel cortex (Ferezou et al. 07). This is seen most dramatically using imaging of the surface of the cortex as sensory stimuli are given to untrained mice, who are either sitting quiescently or actively whisking using voltage sensitive dyes (See Figure 3, from Ferezou et al. 07).

A complimentary dataset from the thalamus indicates that as the animal goes from quiet wakefulness, to whisker twitching, to whisking, that membrane potential of relay neurons in the thalamus go from a -55mv, to -70 mv (which leads to bursting in the thalamus at 7-12 Hz), to a more depolarized level (Gentet et al. 10). This leads to the hypothesis that response variability size of the evoked response, mean and standard deviation, may be dependent on alpha amplitude (Jones et al. 09). Phase-phase coupling, phase-amplitude coupling not explored at all in this thesis (Palva et al. 12). However, I predict that the larger amplitude response seen in the model and in the MEG and LFP data is due to larger variability of response during alpha perhaps due to input arriving at different phases in an alpha cycle.

Further, we can then use the VGAT mouse, channelrhodopsin in all inhibitory neurons so that when light stimulation is restricted to the thalamus we can cause spindle-alpha oscillations (Halassa et al. 11), to then reliably give the input at a fixed phase relationship and see the output on evoked response and behavior of the animal, where now the power in the alpha band is constant.

Final Thoughts

Can you vary number of stimuli relative to frequency of entrained gamma? Why not just use paired pulse stimulation? Do you need a rhythm, or is this multiply aligned biophysical realities? In the entrained gamma study, we show that the phasic manipulation enhances behavior when used a 40 Hz gamma entrainment, and not at the 20 Hz manipulation, while we have yet to use the laser phase that gave the enhanced benefit prestimulus. One open question is if this manipulation requires multiple instances of prestimulus inhibition, or if a single pulse enough?

We are actively investigating these questions, but one short-coming is in the behavioral design. To train mice to perform quickly and accurately a 400 ms stimulus was used to give the mice enough time to integrate the stimulus over. This does not allow for pairing of a single stimulus with either single or multiple epochs of flanking inhibition (Knoblich et al. 10).

However, we favor the hypothesis that a single inhibitory pulse pre-stimulus should enhance the onset response (rise to peak response), and that a single inhibitory pulse post-stimulus would remove spikes that would have the smallest effect downstream, i.e. increase efficiency. A rhythm at the gamma frequency offers multiple instances of enhancement from pre/post inhibition pairing, at the fastest rate possible.

When trying to synchronize the sensory input to the entrained gamma oscillation, are we doing something that never happens with the phase alignment? Results from the naturalistic stimulus condition suggest that under optimal condition, seen with the phasic manipulation, enhancement is on par with the enhancement under naturalistic conditions. Further, the naturalistic stimuli where given with all the phase alignments used in the optimal alignment condition. This strongly suggests that when there is not opportunity for the stimulus to be aligned to the ongoing gamma oscillation, that gamma offers multiple "windows of opportunity" for enhancement to occur, and when a high velocity stimulus is aligned with one of the "windows" enhanced transmission occurs.

Is gamma is just reflecting local alertness, reduced low frequency oscillations? No, we are seeing that they are not directly correlated (**Chapter 3**). But however because the same state that favors both high alpha and low gamma, or vice versa, maybe indicative that there could correlated with alertness possibly due modulation via a neural modulator, such as acetylcholine.

How can you test mechanistically what the gamma is doing? How could you probe its downstream impact? Can you use thalamus as the downstream area? Inherently the use of the thalamus as a downstream area raises the question about how these oscillations are expressed in different cell layers. The projection to the thalamus is via layer V and VI (depending on to what part of thalamus) and it has also been shown that deep cortical layers do not express gamma without superficial cortex (Roopun et al. 08), so perhaps the appropriate read out would be cortical, maybe SII or MI.

A similar question has to do with the laminar specificity of the Alpha oscillation. Putative mechanisms for the alpha oscillation are: 1) via bursting in the thalamus, which is read out as a cortical input into layer IV and the apical dendrites of layer V, or 2) intrinsically bursting neurons and SOM+ interneurons in layer V, both of which show a low-pass response to frequency driven stimulation at around the frequencies of alpha (Silva et al. 91, Fanselow et al. 08).

Important for the question of downstream readout, one of the putative mechanisms of alpha through layer 5 bursting neurons in to the thalamus, thus the alpha oscillation may be limited to the thalamocortical input/output structures (wildly, speculative), while gamma oscillation may be a permissive mechanism for largely cortical-cortical interactions, as seen in Gregoriou et al. 09.

References

Agmon, A. and Connors B.W., Correlation between intrinsic firing patterns and thalamocortical synaptic responses of neurons in mouse barrel cortex. J Neurosci, 1992. 12(1): p. 319-29.

Bereshpolova Y., Stoelzel C.R., Zhuang J., Amitai Y., Alonso J.M., Swadlow H.A. Getting drowsy? Alert/nonalert transitions and visual thalamocortical network dynamics. J Neurosci. 2011 Nov 30;31(48):17480-7.

Börgers C., Epstein S., N.J. Kopell. Gamma oscillations mediate stimulus competition and attentional selection in a cortical network model. Proc Natl Acad Sci U S A. 2008 Nov 18;105(46):18023-8.

Cardin J.A., M. Carlén, K. Meletis, U. Knoblich, F. Zhang, K. Deisseroth, L.H. Tsai, C.I. Moore. Driving fast-spiking cells induces gamma rhythm and controls sensory responses. Nature. 2009 Jun 4;459(7247):663-7.

Crochet S., Poulet J.F., Kremer Y., Petersen C.C. Synaptic mechanisms underlying sparse coding of active touch. Neuron. 2011 Mar 24;69(6):1160-75.

Crochet, S. and C.C. Petersen, Correlating whisker behavior with membrane potential in barrel cortex of awake mice. Nat Neurosci, 2006. 9(5): p. 608-10.

Fanselow, E.E. and M.A. Nicolelis, Behavioral modulation of tactile responses in the rat somatosensory system. J Neurosci, 1999. 19(17): p. 7603-16.

Fanselow, E.E., et al., Thalamic bursting in rats during different awake behavioral states. Proc Natl Acad Sci U S A, 2001. 98(26): p. 15330-5.

Fanselow E.E., Richardson K.A., Connors B.W.. J Neurophysiol. Selective, state-dependent activation of somatostatin-expressing inhibitory interneurons in mouse neocortex. 2008 Nov;100(5):2640-52.

Ferezou I., Haiss F., Gentet L.J., Aronoff R., Weber B., Petersen C.C. Spatiotemporal dynamics of cortical sensorimotor integration in behaving mice. Neuron. 2007 Dec 6;56(5):907-23.

Fries P. Neuronal gamma-band synchronization as a fundamental process in cortical computation. Annu Rev Neurosci. 2009;32:209-24.

Fries P., Reynolds J.H., Rorie A.E., and R. Desimone. Modulation of oscillatory neuronal synchronization by selective visual attention. Science. 2001 Feb 23;291(5508):1560-3.

Gentet L.J., Avermann M., Matyas F., Staiger J.F., Petersen C.C. Membrane potential dynamics of GABAergic neurons in the barrel cortex of behaving mice. Neuron. 2010 Feb 11;65(3):422-35.

Gentet L.J., M. Avermann, F. Matyas, J.F. Staiger, and C.C. Petersen. Membrane potential dynamics of GABAergic neurons in the barrel cortex of behaving mice. Neuron. 2010 Feb 11;65(3):422-35.

Gregoriou G.G., Gotts S.J., Zhou H., Desimone R. Long-range neural coupling through synchronization with attention. Prog Brain Res. 2009;176:35-45.

Hayut I., Fanselow E.E., Connors B.W., Golomb D. LTS and FS inhibitory interneurons, short-term synaptic plasticity, and cortical circuit dynamics. PLoS Comput Biol. 2011 Oct;7(10):e1002248.

Jensen, O., et al., Oscillations in the alpha band (9-12 Hz) increase with memory load during retention in a short-term memory task. Cereb Cortex, 2002. 12(8): p. 877-82.

Jones S.R., Kerr C.E., Wan Q., Pritchett D.L., Hämäläinen M., Moore C.I. Cued spatial attention drives functionally relevant modulation of the mu rhythm in primary somatosensory cortex. J. Neurosci. 2010 Oct 13;30(41):13760-5.

Jones S.R., Pritchett D.L., Stufflebeam S.M., Hämäläinen M., Moore C.I. Neural correlates of tactile detection: a combined magnetoencephalography and biophysically based computational modeling study. J. Neurosci. 2007 Oct 3;27(40):10751-64.

Jones, S.R., et al., Alpha-frequency rhythms desynchronize over long cortical distances: a modeling study. J Comput Neurosci, 2000. 9(3): p. 271-91.

Knoblich U., Siegle J.H., Pritchett D.L., and Moore C.I. What do we gain from gamma? Local dynamic gain modulation drives enhanced efficacy and efficiency of signal transmission. Front. Hum. Neurosci. 2010 4:185.

Nicolelis M.A., Fanselow E.E. Dynamic shifting in thalamocortical processing during different behavioural states. Philos Trans R Soc Lond B Biol Sci. 2002 Dec 29;357(1428):1753-8.

Nicolelis, M.A. and Fanselow E.E., Thalamocortical [correction of Thalamcortical] optimization of tactile processing according to behavioral state. Nat Neurosci, 2002. 5(6): p. 517-23.

Parikh V., Sarter M. Cholinergic mediation of attention: contributions of phasic and tonic increases in prefrontal cholinergic activity. Ann N Y Acad Sci. 2008;1129:225-35.

Roopun A.K., Kramer M.A., Carracedo L.M., Kaiser M., Davies C.H., Traub R.D., Kopell N.J., Whittington M.A.. Period concatenation underlies interactions between gamma and beta rhythms in neocortex. Front Cell Neurosci. 2008;2:1.

Silva, L.R., Y. Amitai, and B.W. Connors, Intrinsic oscillations of neocortex generated by layer 5 pyramidal neurons. Science, 1991. 251(4992): p. 432-5.

Swadlow, H.A., Efferent neurons and suspected interneurons in S-1 vibrissa cortex of the awake rabbit: receptive fields and axonal properties. J Neurophysiol, 1989. 62(1): p. 288-308.

Tiesinga P., Sejnowski T.J. Cortical enlightenment: are attentional gamma oscillations driven by ING or PING? Neuron. 2009 Sep 24;63(6):727-32.

Wiest, M.C. and M.A. Nicolelis, Behavioral detection of tactile stimuli during 7-12 Hz cortical oscillations in awake rats. Nat Neurosci, 2003. 6(9): p. 913-4.

Vierling-Claassen D., Cardin J.A., Moore C.I., Jones S.R. Computational modeling of distinct neocortical oscillations driven by cell-type selective optogenetic drive: separable resonant circuits controlled by low-threshold spiking and fast-spiking interneurons. Front Hum Neurosci. 2010 Nov 22;4:198.